PERFORMANCE OF NONSTRUCTURAL COMPONENTS IN TRIPLE FRICTION PENDULUM BASE-ISOLATED BUILDINGS

by

Göktuğ Tüfekçi

B.S., Civil Engineering, Kocaeli University, 2017

Submitted to the Institute for Graduate Studies in
Science and Engineering in partial fulfillment of
the requirements for the degree of
Master of Science

Graduate Program in Civil Engineering

Boğaziçi University

2021

To my family

ACKNOWLEDGEMENTS

I would like to wholeheartedly thank my advisor and thesis supervisor Prof. Serdar Soyöz. for his support, thoughtfulness, and kindness throughout this research. I have the deepest appreciation for his mentorship. His patience and guidance assisted me in further study in my research.

I would like to express my infinite gratitude to Prof. Hilmi Luş for his supportive attitude towards me during my studies. I would also like to thank Assoc. Prof. Ufuk Yazgan for serving as a member of my thesis committee.

I owe a tremendous amount of gratitude to Assoc. Prof. Seval Pınarbaşı Çuhadaroğlu for encouraging me throughout my undergraduate and graduate studies.

I would also like to thank my friend, colleague, Muhammet Çalayır, for our countless hours of collaborative work during graduate studies. Our work in a tandem approach and unconditional support for each other has been a great motivation in our individual research.

Last, but most of all, I would like to thank my family: my parents Meyrem and Halil, and my sisters Gökçem and Şevval. Their unconditional love and support have been the source of comfort and strength that made it all possible during the COVID-19 pandemic.

ABSTRACT

PERFORMANCE OF NONSTRUCTURAL COMPONENTS IN TRIPLE FRICTION PENDULUM BASE-ISOLATED BUILDINGS

Recent earthquakes indicated that poorly performing nonstructural components cause the majority of consequential injuries, economic losses, and disruption of structural functionality, especially in critical facilities. This research investigates the seismic behavior of nonstructural components in a triple friction pendulum (TFP) base-isolated medical facility under three dimensional (3D) earthquakes. A hypothetical four-story reinforced concrete TFP base-isolated hospital building was created in SAP2000 to examine the performance of its nonstructural components when subjected to 3D ground motions. The base-isolated building model was analyzed to obtain floor accelerations for a suite of 11 ground motion pairs including their vertical components. These floor accelerations in the vertical and horizontal directions were then employed as excitations for the rocking response of rigid blocks, corresponding to different unanchored acceleration-sensitive building contents. The rigid blocks with various slenderness and size were compared to study their rocking response when subjected to horizontal only and horizontal-vertical (H-V) floor accelerations. Additionally, the slab center absolute vertical accelerations were compared for classification in terms of their peak acceleration values associated with nonstructural damage.

The Horizontal-Vertical coupling effect in the floor accelerations due to 3D ground motions had a substantial effect on the rocking response of the nonstructural contents in comparison to the horizontal only floor accelerations. Although the relatively larger and stockier blocks were clearly less influenced, the comparably small and slender contents were greatly affected by the H-V coupling response in terms of their rocking, toppling, and jumping behavior. Consequently, the H-V coupling effect needs to be carefully evaluated for critical facilities, especially the friction pendulum-type base-isolated buildings, regarding the assessment of their seismic performance of nonstructural components.

ÖZET

EĞRİ ÜÇ YÜZEYLİ SÜRTÜNMELİ TABAN YALITIMLI BİNALARDA YAPISAL OLMAYAN ELEMANLARIN PERFORMANS ANALİZİ

Son zamanlardaki depremler kritik öneme sahip yapılardaki yapısal olmayan elemanlarının hasar almaları nedeniyle dolaylı şekilde yaralanmalara, ekonomik kayıplara ve bu kritik yapıların işlevselliğinin bozulmasına sebep olduğunu göstermiştir. Bu araştırma, üç boyutlu depremler altında, tabandan eğri üç yüzeyli sürtünmeli yalıtım sistemi izole edilmiş tıbbi bir tesisin içindeki yapısal olmayan bileşenlerin sismik davranışını araştırmaktadır. Yapısal olmayan bileşenlerin performansını incelemek için tabandan eğri üç yüzeyli sürtünmeli yalıtım sistemi izole edilmiş varsayımsal dört katlı betonarme bir hastane binası SAP2000 yapı analizi programında oluşturulmuştur. Tabandan izole edilmiş bina modeli, düşey bileşenleri de dahil olmak üzere 11 yer hareketi çiftinden oluşan bir grup altında kat ivmelerini elde etmek için analiz edilmiştir. Sonrasında, düşey ve yatay yönde elde edilen bu kat ivmeleri sabitlenmemiş ivmeye duyarlı farklı geometrik özelliklere sahip binada bulunan elemanlara karşılık gelen rijit blokların sallanma tepkisi için uyarılar olarak kullanıldı. Çeşitli narinlik ve boyutlara sahip rijit bloklar, yalnızca yatay ve yatay-düşey kat ivmelerine maruz kaldıklarında sallanma tepkilerini incelemek için karşılaştırıldı. Ek olarak, döşeme merkezinden elde edilen mutlak düşey ivmeleri, en yüksek düşey tepe ivme değerleriyle ilişkili yapısal olmayan hasar açısından sınıflandırma bölgeleriyle karşılaştırılmıştır.

3 boyutlu yer hareketlerinden kaynaklanan kat ivmelerindeki Yatay-Düşey bağlantı etkisi, sadece yatay kat ivmelerine kıyasla yapısal olmayan içeriklerin sallanma tepkisi üzerinde önemli bir etkiye neden olmuştur. Nispeten daha büyük ve bodur bloklar açıkça daha az etkilenmiş olsa da, nispeten küçük ve narin içerikler, sallanma, devrilme ve sıçrama davranışları açısından Yatay-Düşey bağlantı tepkisinden büyük ölçüde etkilenmiştir. Sonuç olarak, kritik tesisler için, özellikle sürtünmeli sarkaç tipi tabandan izole edilmiş binalar için, yapısal olmayan bileşenlerin sismik performanslarının değerlendirilmesine ilişkin olarak, Yatay-Düşey bağlantı etkisinin dikkatli bir şekilde değerlendirilmesi gerekir.

TABLE OF CONTENTS

ACKNOWLEDGEMENTS iv
ABSTRACT v
ÖZET vi
LIST OF FIGURES ix
LIST OF TABLES xv
LIST OF ACRONYMS/ABBREVIATIONS xvi
LIST OF SYMBOLS xviii
1. INTRODUCTION 1
1.1. General 1
1.2. An Introduction to Rocking Response 2
1.3. Full-Scale Base-isolated Building Experiments in Literature 6
1.3.1. General 6
1.3.2. Full-scale base-isolated four-story reinforced concrete hospital building experiment at E-Defense 7
1.3.2.1. Near-fault and long-duration ground motions 8
1.3.2.2. Vertical ground motions 9
1.3.3. Full-scale base-isolated five-story steel moment frame hospital building experiment at E-Defense 11
1.3.4. Full-scale structural and nonstructural building system performance during earthquakes at the University of California, San Diego (UCSD) Network for Earthquake Engineering Simulation (NEES) (NEES@UCSD) facility 13
1.4. Rocking Response of Contents on an Isolated Base 16
1.5. Scope and Objectives 17
1.6. Thesis Outline 18
2. SEISMIC PERFORMANCE OF A TRIPLE FRICTION PENDULUM BASE-ISOLATED BUILDING 19
2.1. Introduction 19
2.2. Building Description 19
2.3. Structural Modeling Assumptions and Details 20
2.4. Isolation System Design and Modeling 22

2.5. Building Modal Response 28
2.6. Ground Motion Selection and Scaling 30
2.7. Structural Response 32
2.7.1. Horizontal and Horizontal-Vertical Coupling Response 36
2.7.2. Vertical Slab Response 41
3. SEISMIC PERFORMANCE OF FREESTANDING CONTENTS 45
3.1. Introduction 45
3.1.1. Review of the Rocking Response of a Rigid Block 45
3.1.2. Coefficient of Restitution 49
3.1.3. Derivation of Vertical Reaction Force on Rocking Response 50
3.2. Freestanding Contents Rocking Response 51
3.3. Effect of High Frequency Oscillations in Trigonometric Excitation 51
3.3.1. Effect of Horizontal- Vertical Coupling on Rocking Response 61
3.3.2. Effect of Story Level 70
3.4. Freestanding Rigid Block Jumping Response 71
4. CONCLUSIONS AND RECOMMENDATIONS 72
4.1. Summary 72
4.2. Recommendation and Future Study 73
REFERENCES 74
APPENDIX A: 85
APPENDIX B: 86
APPENDIX C: 87
APPENDIX D: 88
APPENDIX E: 89
APPENDIX F: 90

LIST OF FIGURES

Figure 1.1. Nonstructural damage: (a) fallen ceiling tiles at the San Carlos Hospital and (b) content damage in Talca court house (Miranda et al., 2012) permission in APPENDIX B. 2

Figure 1.2. Building overview (a) physical experiment (b) room types 8

Figure 1.3. Bearings (a) natural rubber bearing and (b) U-shaped steel damper (Sato et al., 2011) permission in APPENDIX D. 9

Figure 1.4. Plan and accelerometer placements, a1 and a2, near columns and slab centers respectively (Furukawa et al., 2013) permission in APPENDIX C. 10

Figure 1.5. Observed damages sustained as a result of vertical floor excitations include (a) an overturned container placed on shelves and (b) a machine block related to heart-lung diseases (Furukawa et al., 2013) permission in APPENDIX C. 11

Figure 1.9. Building overview (a) façade, (b) residential area and (c) laboratory on the second floor, (d) electronical devices room on the third floor, (e) intensive care unit on the fourth, and (f) operating theater on the fifth floor. Yellow arrows show the direction of the excitations. Units in meters (Chen et al., 2016) permission in APPENDIX E. 14

Figure 1.10. Disruption to equipment and nonstructural contents on the second floor (a) motion of unanchored objects, (b) movement of the unanchored refrigerator after test BI-7, (c) overturning of a bookshelf after test for the

fixed base (FB) building (Pantoli et al., 2016a) permission in APPENDIX F.....15

Figure 1.11. Damage in medical contents at the fifth floor: (a) damage state based on PFA, (b) overturning of the patient bed at the FB building, (c) damage to the cabinet due to the movement of the patient bed at the FB, (d) overturning of contents on the 4th floor (Pantoli et al., 2016a) permission in APPENDIX F.....16

Figure 2.1. Building location and source-to-site distance (AFAD, 2021).....19

Figure 2.2. Building: (a) elevation view, (b) plan view. 20

Figure 2.3. Drawing of TFP isolation. 23

Figure 2.4. Normalized hysteresis loop of the TFP bearing system at the DD-1 level. .26

Figure 2.5. Mode 1: *T* = 2.706 s (Isolation mode in the Y direction).....29

Figure 2.6. Mode 3: T = 2.419 s (Isolation mode in the RZ direction). 29

Figure 2.7. Mode 4: T = 0.311 s (1st structural mode in the Y direction).....30

Figure 2.8. Mode 7: T = 0.125 s (1st vertical mode).....30

Figure 2.9. Selected ground motion response spectra in the horizontal direction.....31

Figure 2.10. Selected ground motion response spectra in the vertical direction. 32

Figure 2.11. X and Y-direction hysteresis loops for the center bearing.....33

Figure 2.12. X and Y-direction hysteresis loops for the center bearing. 34

Figure 2.13. X and Y-direction hysteresis loops for the center bearing. 35

Figure 2.14. X and Y-direction hysteresis loops for the center bearing. 36

Figure 2.15. Absolute mean peak responses: (a_1) X-direction floor acceleration, (a_2) Y-direction floor acceleration, (b_1) X-direction floor displacement, (b_2) Y-direction floor displacement, (c_1) X-direction floor velocity, (c_2) Y-direction floor velocity. 37

Figure 2.16. Floor response spectra in the Y direction at the roof level under the horizontal ground motions only. 39

Figure 2.17. Floor response spectra in the Y direction at the roof level under the horizontal and vertical ground motions. 39

Figure 2.18. Floor response spectra in the Y direction: (a) 4th, (b) 3rd, (c) 2nd, (d) 1st 40

Figure 2.19. Three slabs having different adjacents on the plan view. 41

Figure 2.20. Mean values of vertical peak Slab (1) center accelerations under the 11 ground motion pairs. 42

Figure 2.21. Mean values of vertical peak Slab (2) center accelerations under the 11 ground motion pairs. 43

Figure 2.22. Mean values of vertical peak Slab (3) center accelerations under the 11 ground motion pairs. 43

Figure 2.23. Vertical PFA values on the roof: (a) Slab (1), (b) Slab (2), (c) Slab (3). 44

Figure 3.1. Drawing of a rigid block under pure planar rocking motion for two rotational directions: (a) $\theta > 0$, (b) $\theta < 0$. 46

Figure 3.2. Rocking response of a relatively small rigid block ($\alpha = 10°$, b = 0.093 m, h = 0.528 m, $p \approx 5.2$ rad/s) subjected to: (a) horizontal excitations and (b) highly fluctuated horizontal excitations with vertical components.....52

Figure 3.3. Rocking response of a relatively large rigid block ($\alpha = 10°$, b = 0.372 m, h = 2.113 m, $p \approx 2.6$ rad/s) subjected to: (a) horizontal excitations and (b) highly fluctuated horizontal excitations with vertical components.....53

Figure 3.4. Rocking response of a relatively small rigid block ($\alpha = 8.5°$, b = 0.08 m, h = 0.535 m, $p \approx 5.2$ rad/s) subjected to: (a) horizontal excitations and (b) highly fluctuated horizontal excitations with vertical components.....55

Figure 3.5. Rocking response of a relatively large rigid block ($\alpha = 8.5°$, b = 0.318 m, h = 2.114 m, $p \approx 2.6$ rad/s) subjected to: (a) horizontal excitations and (b) highly fluctuated horizontal excitations with vertical components.....56

Figure 3.6. Rocking response of a relatively small rigid block ($\alpha = 12°$, b = 0.113 m, h = 0.53 m, $p \approx 5.2$ rad/s) subjected to: (a) horizontal excitations and (b) highly fluctuated horizontal excitations with vertical components.....57

Figure 3.7. Rocking response of a relatively large rigid block ($\alpha = 12°$, b = 0.448 m, h = 2.1 m, $p \approx 2.6$ rad/s) subjected to: (a) horizontal excitations and (b) highly fluctuated horizontal excitations with vertical components.....58

Figure 3.8. Rocking response of a relatively small rigid block ($\alpha = 15°$, b = 0.142 m, h = 0.53 m, $p \approx 5.2$ rad/s) subjected to: (a) horizontal excitations and (b) highly fluctuated horizontal excitations with vertical components.....59

Figure 3.9. Rocking response of a relatively large rigid block (α = 15°, b = 0.558 m, h = 2.1 m, $p \approx 2.6$ rad/s) subjected to: (a) horizontal excitations and (b) highly fluctuated horizontal excitations with vertical components.....60

Figure 3.10. Rocking response of a relatively small rigid block (α = 10°, b = 0.093 m, h = 0.528 m, $p \approx 5.2$ rad/s) subjected to: (a) horizontal and (b) the H-V coupled floor accelerations induced by the 1999 Kocaeli, Iznik earthquake. 62

Figure 3.11. Rocking response of a relatively large rigid block (α = 10°, b = 0.372 m, h = 2.113 m, $p \approx 2.6$ rad/s) subjected to: (a) horizontal and (b) the H-V coupled floor accelerations induced by the 1999 Kocaeli, Iznik earthquake. 63

Figure 3.12. Rocking response of rigid blocks: (a) 8.5° and (b) 10° under the Horizontal-Vertical coupling and Horizontal only floor accelerations due to the 1999 Kocaeli, Iznik earthquake.....65

Figure 3.13. Rocking response of rigid blocks: (a) 12° and (b) 15° under the Horizontal-Vertical coupling and Horizontal only floor accelerations due to the 1999 Kocaeli, Iznik earthquake.....66

Figure 3.14. Rocking response of rigid blocks with a slenderness of 15° under the Horizontal-Vertical coupling and Horizontal only floor accelerations due to the 2010 Darfield, SPFS earthquake. 67

Figure 3.15. Rocking response spectra of the two rigid block types (a) 8.5° and (b) 10° subjected to 10 earthquakes with and without horizontal-vertical (H-V) coupling effect.....68

Figure 3.16. Rocking response spectra of the two rigid block types (a) 8.5° and (b) 10° subjected to 10 earthquakes with and without horizontal-vertical (H-V) coupling effect. 69

Figure 3.17. Comparison of the rigid blocks with slenderness of 12° under the horizontal and vertical coupled floor accelerations. 70

Figure 3.18. Jumping response of the rigid blocks with slenderness of 12° on the various slabs. 71

LIST OF TABLES

Table 1.1. Peak ground accelerations, velocity, displacements, duration of earthquakes and spectral acceleration for the BI building (Chen et al., 2016) permission APPENDIX E. 15

Table 2.1. TFP bearing properties. 25

Table 2.2. SAP2000 modeling parameters. 27

Table 2.3. Seven modes (out of 100) of the TFP base-isolated building. 28

Table 2.4. Amplification factor for X-direction horizontal acceleration due to the vertical component of ground motions at each floor. 38

Table 2.5. Amplification factor for Y-direction horizontal acceleration due to the vertical component of ground motions at each floor. 38

Table A.1. Ground motions for scaling according to TBSC (2018) 85

LIST OF ACRONYMS/ABBREVIATIONS

2D	Two Dimensional
3D	There Dimensional
AFAD	Afet ve Acil Durum Yönetimi Başkanlığı
ASCE	American Society of Civil Engineers
BI	Base-isolated
CLB	Cross-linear bearing
CSI	Computers and Structures, Inc.
DCDT	Direct Current Differential Transformer
DD-1	Deprem Yer Hareketi Düzeyi-1
EPS	Earthquake Protection Systems
FB	Fixed base
FEMA	Federal Emergency Management Agency
FNA	Fast nonlinear analysis
H-V	Horizontal-vertical
IO	Immediate Occupancy
LRB	Lead rubber bearing
MCE	Maximum Considered Earthquake
NEES	Network for Earthquake Engineering Simulation
NLRHA	Nonlinear response history analysis
ODE	Ordinary Differential Equations
PEER	Pacific Earthquake Engineering Research Center
PFA	Peak floor acceleration
PGA	Peak ground acceleration
PGD	Peak ground displacement
PGV	Peak ground velocity
SDOF	Single Degree of Freedom
SRSS	Square Root Sum of Squares
TBSC	Turkish Building Seismic Code
TFP	Triple friction pendulum

TS	Turkish Standards
UCSD	University of California, San Diego

LIST OF SYMBOLS

b	Base width of rocking block
D	Over strength factor
D_M	DD-1 level maximum displacement of bearing
D_y	Yield displacement of the isolation system
d_i	*i*th slider displacement capacity of TFP
d_{slider}	Slider diameter
e	Coefficient of restitution
e_{max}	Maximum coefficient of restitution
E_c	Tangent modulus of elasticity of concrete
E_{loop}	Energy dissipated in each cycle of isolator
f_{ck}	Characteristic compressive strength of concrete
$\overline{f}_y$	Normalized vertical force of rigid block
G_c	Shear modulus of concrete
g	Gravity constant
h	Height of the rocking block
h_i	Half the height of *i*th TFP slider
I_O	Rigid body moment of inertia around point *O*
K_v	Compressive stiffness of isolator
$k_{\text{eff,M}}$	Effective stiffness of isolation system at DD-1 level displacement
L_i	*i*th effective pendulum length
$\mathbf{M}_O$	Total moment about point *O*
m	Mass of block
$m_j^{(s)}$	Seismic mass at node *j*
p	Frequency parameter
p_b	Friction pendulum bearing pressure
R	Structural behavior factor
R_b	Distance from corner to rigid block's center
R_i	Radius of inner slider surface *i*th

R_{JB}	The Joyner-Boore distance
$S_{ae}^{(DD-1)}$	Horizontal spectral acceleration at DD-1 level with 5% damping
S_{D1}	Design spectral acceleration at 1s period
S_{DS}	Design spectral acceleration at short period
S_{M1}	DD-1 level spectral acceleration at 1s period
$T_{\text{eff,M}}$	Effective period of isolation system at DD-1 level displacement
T_i	Building period at *i*th mode
T_v	Vertical period of isolation
u_2	Second stage bearing displacement
u_3	Third stage bearing displacement
$\ddot{U}_f^x$	Horizontal floor acceleration at base of block
$\ddot{U}_f^y$	Vertical floor acceleration at base of block
V	Base shear
V_{s30}	Shear wave velocity for top 30 m of soil
W	Weight
$w_j^{(s)}$	Seismic weight at node j
$w_{G,j}^{(s)}$	Seismic weight at node j from dead loads
$w_{Q,j}^{(s)}$	Seismic weight at node j from live loads
$\mathbf{y}(\mathbf{x}, t)$	ODE state vector

α	Slenderness
θ	Rotation of rocking block
$\dot{\theta}_1$	Angular velocity before impact
$\dot{\theta}_2$	Angular velocity after impact
$\ddot{\theta}$	Angular acceleration
$\bar{\theta}$	Mean rotation of rocking blocks
$\zeta_{\text{eff,M}}$	Effective isolation damping ratio at DD-1 level displacement
η_{M}	Damping scaling at DD-1 level displacement
μ_i	Friction coefficient of *i*th TFP sliders
v_c	Poisson's ratio of concrete
B_M	Effective damping of isolation system

1. INTRODUCTION

1.1. General

Nonstructural components are the contents and parts of a building that do not resist gravity, earthquake, wind, and other loads (FEMA 2012). These components consist of architectural, mechanical, electrical, plumbing systems, and contents. Despite having less attention, earthquake-induced nonstructural damage has an equivalent significance in performance-based earthquake engineering as structural damage. The failure of the nonstructural components in buildings, especially critical facilities (e.g., hospitals, fire stations, government buildings, and advanced computing centers), can pose a risk to life safety, property, and functionality during and after seismic events. While ensuring the structural integrity of these facilities is essential, their continued functionality is necessary during seismic excitations within the performance-based design.

Recent earthquakes showed that poorly performing nonstructural components led to the majority of consequential injuries, economic losses, and disruption of structural functionality (Soong, 1990; Soong, Chen, et al., 1993; Reitherman and Sabol, 1995; Phipps, 1997; Kircher, 2003; Miranda, Mosqueda et al., 2012). In addition to threats to life safety, Kircher (2003) reported that nonstructural damage due to the 1994 Northridge earthquake caused roughly $9 billion, which corresponds to half of the total economic losses. Nonstructural components usually account for at least 80% of a building's overall cost (Taghavi and Miranda, 2003). Miranda et al. (2012) highlighted that the earthquake in Chile on February 27, 2010, led to serious nonstructural damage for almost all types of buildings. Although a small percentage of the hospitals underwent severe structural damage, the cause of the evacuation order for these hospitals was the extreme disruption in nonstructural components after the earthquake (Miranda et al., 2012). Fallen objects and the overturning of shelves were the most prevalent cause of nonstructural damage as shown in Figure 1.1. Additionally, another recent strong ground motion, the 2011 off the Pacific coast of Tohoku earthquake, followed by many aftershocks, caused extreme damage in nonstructural components, which resulted in deaths in several cases. The major cause for the loss of human

life stemming from nonstructural damage was that ceiling boards performed poorly and fell due to their weak strength under vertical excitations (Motosaka and Mitsuji 2012).



Figure 1.1. Nonstructural damage: (a) fallen ceiling tiles at the San Carlos Hospital and (b) content damage in Talca court house (Miranda et al., 2012) permission in APPENDIX B.

Therefore, it is imperative to design nonstructural components properly to avoid injury, fatalities, economic losses, and functional interruption in critical facilities subjected to earthquakes. The inherent uncertainty and complexity associated with nonstructural components behavior under excitations are the main reasons that this field received relatively less attention. Nevertheless, nonstructural contents' behavior during a seismic event is classified that building contents can rock, overturn, jump, slide, twist, or perhaps a mix of these. This thesis particularly assesses the rocking, overturning, and jumping response of building contents in a triple friction pendulum base-isolated building subjected to earthquakes. It is critical to correctly determine these responses in order to quantify unanchored contents' damage and decrease uncertainty within the performance-based earthquake engineering framework.

1.2. An Introduction to Rocking Response

Understanding and predicting the rocking behavior of rigid blocks stimulated the interest of researchers from the late 1800s (Perry, 1881). Milne (1885) first put overturning

hypotheses to the test and made the approach practical. Under certain constrained conditions, Milne concluded that the peak horizontal acceleration, as an overturning threshold, can be obtained by the taking moment equilibrium about the pivoting point and stated that the columns topple as the ground acceleration goes beyond the value of the width to height ratio multiplied by gravity. After Milne's (1885) work, Kirkpatrick (1927) conducted research on the seismic stability of rocking columns. This research introduced the column size effect and the duration of the excitation period on the stability of freestanding columns in addition to the effect of the peak ground acceleration. His analyses revealed that increasing the period of the excitation causes overturning of freestanding columns even under lower accelerations.

In 1963, Housner (1963) published his paper regarding the rocking response of rigid blocks. He analyzed the free and forced vibration responses due to rectangular and half-sine pulse excitations. Following Kirkpatrick's (1927) size-frequency scale effect, through an energy approach, Housner (1963) emphasized that smaller columns with a similar geometric ratio are more prone to overturn than bigger ones. His research also showed that when two accelerations have the same amplitude, the one with a longer duration is more likely to cause overturning. Since Housner's (1963) work, a substantial amount of research has been conducted on the rocking response of rigid and flexible rocking objects (Aslam et al., 1980; Yim et al., 1980; Shenton, 1996; Makris and Roussos, 2000; Makris and Konstantinidis, 2003a; Dimitrakopoulos and DeJong, 2012; Klaboe et al., 2018).

Aslam et al. (1980) performed shaking table and analytical studies on the rocking and overturning of rectangular blocks of different sizes, as well as aspect ratio, in order to better understand the behavior of solid concrete blocks employed as radiation shields in particle accelerator laboratories. The rocking response of blocks due to seismic motion was found to be consistent with the findings gained from single pulse excitations. This research also emphasized overturning is highly sensitive to minor changes in the boundary conditions, coefficient of restitution, and earthquake characteristics.

Yim et al. (1980) used a probabilistic technique to develop numerical analyses through simulated ground motions to study the sensitivity of the rocking and overturning response. This research highlighted that with the growing size or reducing aspect ratio, the stability of the block does not necessarily rise monotonously under a certain excitation. It

was, however, concluded that when the rocking response of rigid blocks is analyzed from a probabilistic perspective with the ground motion described as a random process, predictable trends occur.

Spanos and Koh (1984) examined the rocking response of unanchored blocks under harmonic steady-state excitation. They defined safe and unsafe regions and created analytical methods for determining fundamental subharmonic modes of the system.

Makris and Roussos (2000) studied the transient rocking response of a rigid block under trigonometric pulses and near-source earthquakes. They presented that Housner's (1963) assumption for the minimum half-sine pulse acceleration amplitude required to topple a rigid block is wrong. In actuality, a block overturns under a half-sine pulse throughout its free vibration regime, not at the time the pulse terminates, as Housner (1963) assumed. This research also concluded that although bigger blocks are more dependent on incremental ground velocity, smaller blocks are more susceptible to peak ground acceleration.

A freestanding block can topple in one of two modes: by demonstrating one or more impacts or without impacts (Zhang and Makris, 2001). It was concluded that the presence of this second mode implies that a block can withstand a pulse with an acceleration value greater than the minimum acceleration amplitude that is able to topple the block. This multivaluedness on the overturning acceleration spectrum complicates the already difficult process of measuring the peak acceleration of prior earthquakes by just examining the geometry of items that overthrown or withstood during these excitations.

The fundamental differences in the dynamical structure of two systems, a single-degree-of-freedom (SDOF) oscillator (regular pendulum) and a slender rigid block (inverted pendulum), were examined comprehensively by Makris and Konstantinidis (2003a). Their study found that an equivalent SDOF oscillator cannot substitute a rocking structure, as Priestley et al. (1978) assumed, and FEMA 356 (2000) accepted. They concluded that using equivalent SDOF oscillators are naturally incorrect and should be abolished, especially for smaller and less slender blocks.

Regarding the pure rocking response of a rigid block, Konstantinidis and Makris (2010) compared the findings obtained using the commercially available software Working Model to those found by using ODE solvers in MATLAB for integrating the equation of motion. (Makris and Roussos, 2000; Makris and Konstantinidis, 2003a; MATLAB, 2002). Notably, the software Working Model accurately estimates this response's multivaluedness in the range above the lowest toppling acceleration line.

Earlier research on developing numerical tools for simulating rocking behavior in response to earthquakes demonstrated that simulation outcomes are very parameter-dependent, and data from experimental studies are required to adjust these tools. Therefore, Klaboe et al. (2018) conducted 312 unanchored concrete block tests on a unidirectional earthquake simulator to determine the rocking behavior of blocks and to make that experimental data available online.

Nuclear standards, guidelines, and reports do not address the rocking response and overturning susceptibility of freestanding objects, with the exception of an approximate method offered in ASCE 43-05 for estimating the maximum rocking angle in place of nonlinear time history analysis (Dar et al., 2016). Dar et al. (2016) analyzed the approximate method used in ASCE 43-05 qualitatively first and then compared its estimates to those obtained from a range of nonlinear time history analyses. This research showed that the ASCE 43-05 approach produces very inaccurate, and in many instances imprecise, estimations of peak rocking rotation for various block shapes and excitation levels.

While considerable research has been conducted on the rocking response of rigid objects using recorded earthquakes or analytical pulse excitations for a range of items, studies employing floor accelerations to examine the toppling susceptibility of slender building contents are rare. Kamil and Tung (2001) investigated the rocking response of building objects in a five-story shear structure under simulated earthquake excitations in order to determine the validity of Housner's energy balance equation (1963). This research concluded that Housner's equation successfully captured the maximum of the resulting average pseudo-velocity spectrum at each floor. The findings implied that since the pseudo-velocity response spectrum is greater at the ground level than other floors, any block that remains stable at the base should be stable at any story from above, particularly for a stiff

building. Yet, the research did not explicitly examine the responses of objects at various floors under the same ground motion. Filiatrault et al. (2004) also used floor vibrations produced from nonlinear response history analysis of three- and six-story reinforced concrete structures exposed to simulated ground excitations to conduct a shaking-table test on bookcase–partition wall systems. They demonstrated that hitting the bookcases against the wall prevents the bookcases from toppling by eliminating unwanted resonance. Additionally, within the seismic performance of unanchored building contents, Bao and Konstantinidis (2020) examined the dynamics of rocking–sliding objects in the presence of nearby wall pounding. They concluded that when the peak floor acceleration demand on the content is relatively low, positioning it adjacent to a wall has a beneficial effect in rocking response, consistent with results that Filiatrault et al. (2004) found. Perhaps, the most comprehensive studies on the assessment of rigid blocks rocking at both fixed and isolated base structures using floor accelerations were conducted by Linde (2016). Linde et al. (2020) evaluated the rocking response of rigid blocks on a four-story concentrically braced frame structure. They showed that considering practical uses, the influence of vertical floor vibration on the maximum rocking response is found to be insignificant, particularly for slender elements. It was also concluded that the variation in rocking demands across floors is substantially greater for stocky contents than for slender ones.

1.3. Full-Scale Base-isolated Building Experiments in Literature

1.3.1. General

In the horizontal direction, seismic isolation has been shown to be an effective way of ensuring structural integrity during large earthquakes, except for some specific ground motion types (e.g., near-fault, long-duration ground motions). However, further research on base-isolated structures subjected to vertical ground motions is still needed within the performance-based earthquake engineering framework.

The amplitude of vertical floor responses becomes a significant criterion to determine the building functionality in seismically base-isolated structures because horizontal floor accelerations are considerably reduced in these structures. Consequently, the vertical component of earthquakes influences seismically base-isolated buildings in two ways (Kitayama et al., 2017):

1. It changes the response of the isolation and structural system in the horizontal direction.
2. It amplifies the vertical response of the structure above the bearings or transmits as it is.

Buildings with the friction pendulum bearing system experience an increase in horizontal seismic demands, including lateral forces, accelerations, and drift when subjected to the vertical earthquake combined with horizontal components of the ground motion. Vertical accelerations at columns' location are naturally transferred through the sliding bearings with little variation up to higher floors, unless there is uplift in the sliding bearing, since this system is vertically stiff. Furthermore, the vertical accelerations are amplified through globally vertically flexible elements (e.g., slabs, beams), increasing the likelihood of nonstructural component damage, especially in acceleration-sensitive components. These increases in seismic demand due to the vertical earthquake and its combination with horizontal ground motions cause nonstructural contents damage in terms of rocking, overturning, jumping, slide, twist, and possibly a combination of these. As a result, these phenomena stimulate researchers to create experimentally validated analytical models to study the performance of base-isolated critical facilities and to more accurately assess the demand on nonstructural components under strong ground motions.

1.3.2. Full-scale base-isolated four-story reinforced concrete hospital building experiment at E-Defense

Over the last decade, shake table tests have been conducted to investigate a variety of full-scale base-isolated and fixed-base medical facilities for their seismic performance of structural and nonstructural components (Sato et al., 2011; Soroushian et al., 2012; Ryan et al., 2016; Chen et al., 2016). While a few earthquakes and many experiments helped confirm that in terms of structural systems, base-isolated buildings behaved well (Çelebi, 1996; Bozorgnia et al., 1998; Nagarajaiah and Sun, 2000), questions exist over the true effectiveness of base isolation for various forms of ground motion, including near-fault earthquakes, the long-period ground motions, and the vertical component of earthquakes.

1.3.2.1. Near-fault and long-duration ground motions

To address the first question regarding the base-isolated building performance under near-fault and long-period ground motions, Sato et al. (2011) conducted a full-scale base-isolated four-story reinforced concrete building experiment on a shaking table at E-Defense, Japan, shown in Figure 1.2. Four earthquakes, including recorded near-fault ground motions, synthesized long-period and long-duration ground motions, were employed to analyze the performance of the base-isolated building. With the exception of the JMA Kobe earthquake, two horizontal components were used as input parameters for both near-fault and long-period ground motions at the same time. The base isolation system, designed as natural rubber bearings with a parallel U-shaped steel damper in Figure 1.3, effectively mitigated the floor acceleration response generated by the near-fault earthquake. However, the long-period ground motion resulted in movement of furniture and medical types of equipment supported by casters.

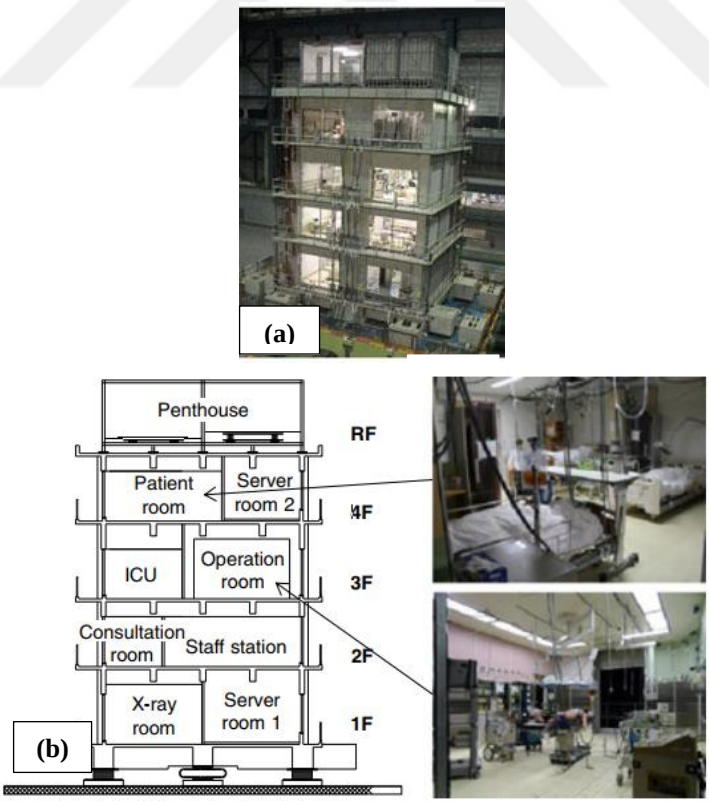

Figure 1.2. Building overview (a) physical experiment (b) room types (Furukawa et al., 2013) permission in APPENDIX C.

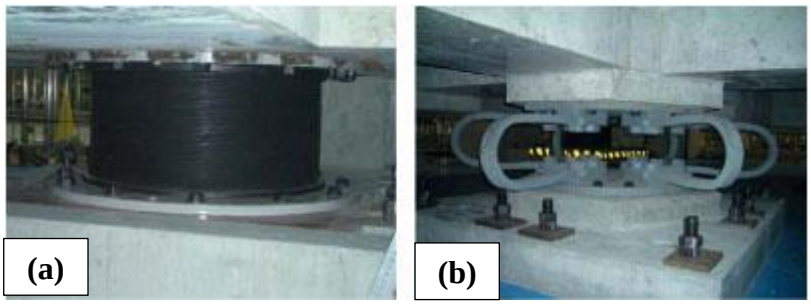

Figure 1.3. Bearings (a) natural rubber bearing and (b) U-shaped steel damper (Sato et al., 2011) permission in APPENDIX D.

1.3.2.2. Vertical ground motions

Vertical earthquakes are often in the frequency of between 7 and 20 Hz (Elnashai, 1997). These frequencies coincide with the range of the lowest vertical natural frequencies of building structures (Furukawa et al., 2013). Bozorgnia et al. (1997) studied the vertical response of twelve instrumented buildings recorded during the 1994 Northridge earthquake. According to this study, vertical natural frequencies varied between 5 and 13 Hz for the three base-isolated structures. Therefore, these vertical frequency ranges from earthquakes and base-isolated buildings show the likelihood of resonance and considerable amplification of vertical responses as a consequence.

With regard to the continuing project of Sato et al. (2012), Furukawa et al. (2013) carried out a series of full-scale shaking experiments to determine the influence of the vertical response on the same base-isolated building's nonstructural components. Although base isolation is a well-established technique shown to considerably lessen structural responses to horizontal ground excitations, this system-level experimental research reported that vertical accelerations were greatly amplified in some circumstances due to the rubber base isolation system. In general, the study concluded that the damage due to the vertical ground motions is not severe if the peak vertical accelerations are less than 2g, with following exceptions:

1. Tiny objects positioned on shelves slid or overturned.
2. Objects on nonrigid furniture lifted off that led to amplifying the acceleration response.

3. Vertically eccentric contents ended up rocking and lifting off.

Furukawa et al. (2013) measured floor accelerations at near columns (a1) and slab centers (a2) in the vertical direction as well as the horizontal floor accelerations indicated in Figure 1.4. The El Centro XYZ earthquake induced an absolute maximum vertical acceleration varying from 2.1 g (base) to 4.2 g (roof) at each floor of a2 locations in the base-isolated building. The vertical acceleration ratio between the columns (a1) at the roof and base floor was 3.9. Furthermore, the vertical acceleration ratio between the slab centers (a2) and the columns (a1) ranged from 2.1 to 3.7 at each floor. Under these ranges of accelerations generated by the given ground motions, medical equipment, such as the operating table, incubator and patient bed, lifted off. Between the acceleration values of 9 and 18 m/s^2, devices, including CT scan gantry, rocked. The containers dropped off the shelves when the absolute vertical acceleration exceeded 9 m/s^2. Figure 1.5 indicates the observed damage during the earthquakes.

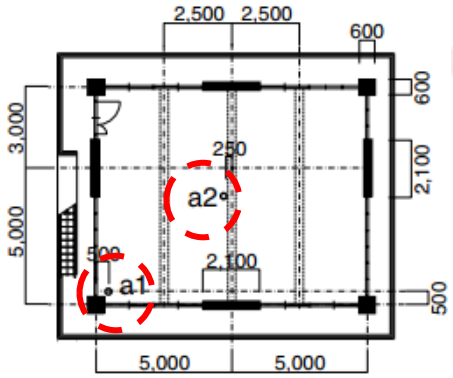

Figure 1.4. Plan and accelerometer placements, a1 and a2, near columns and slab centers respectively (Furukawa et al., 2013) permission in APPENDIX C.

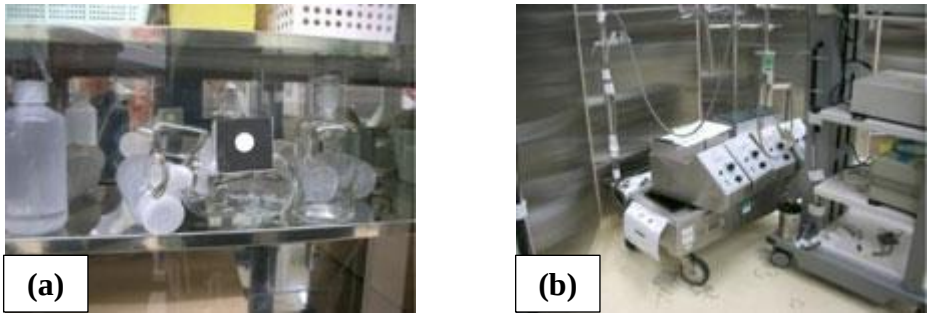

Figure 1.5. Observed damages sustained as a result of vertical floor excitations include (a) an overturned container placed on shelves and (b) a machine block related to heart-lung diseases (Furukawa et al., 2013) permission in APPENDIX C.

This full-scale experiment concludes information on nonstructural building contents under the vertical excitations as follows:

1. Freestanding items begin to jump when the vertical floor acceleration exceeds 1 g. Furthermore, the vertical ground motions can be destructive to the furniture, medical equipment, and other medical objects in the base-isolated system only if the absolute vertical floor acceleration is above 2 g.
2. Some furniture and medical equipment had noticeable responses when the peak floor accelerations were between 1 and 2 g. Small objects on shelves, tables, and pendants on the ceiling slid, overturned, or dropped down. Vertically eccentric equipment rocked and jumped.

1.3.3. Full-scale base-isolated five-story steel moment frame hospital building experiment at E-Defense

The main purpose of this full-scale experiment was to show the efficiency of base isolation in protecting not only the building structure but also its nonstructural components and contents during strong earthquakes (Ryan et al., 2012). On the 4th and 5th floors, the building in their studies was equipped with types of medical equipment and contents. Two isolation types, triple friction pendulum bearings and a hybrid of lead-rubber and cross-linear bearings were used in the seismic performance analyses of the building. The effect of vertical acceleration on the performance of seismically isolated structures was investigated using a

range of horizontal only and 3D excitations. The horizontal floor accelerations and story drifts considerably increased in the building response when the vertical component of the ground motion is included (K. L. Ryan et al., 2012).

This recent behavior was confirmed through analysis and was defined as the horizontal-vertical (H-V) coupling effect between the horizontal and vertical responses (Dao and Ryan 2014, Guzman ve Ryan 2018). In comparison to the fixed base and LRB/CLB designs, this H-V relation was substantially more pronounced in the tested building with TFP bearings. The evidence for considerable coupling in the TFPSEI system was found to be due to the friction mechanism in the sliding bearings (Ryan and Dao 2015).

Prior to this full-scale experimental research, some analytical studies indicated an increase in the response of friction pendulum isolated buildings under 3D motions compared to 2D ones. Early research (Lin and Tadjbakhsh 1986) demonstrated that when a single mass isolated by a pure-friction isolator is under harmonic motion with equivalent horizontal and vertical frequencies, the horizontal force and displacement increase significantly in comparison to horizontal vibrations only. Calvi et al. (2004) performed a numerical model of a bridge with single friction pendulum isolators. The study concluded that the bearing base shear and the response of bending, torsion, and shear of the piers increased with the inclusion of the vertical motion in the analyses. Khoshnoudian and Rabiei (2010) were among the first to introduce the increase of horizontal response at higher floors due to the amplification in the base shear of friction pendulum isolators under vertical motions. Another study (Politopoulos and Moussallam, 2012) indicated that increases in acceleration were caused by a coupling between the building's vertical and higher horizontal modes. This phenomenon was also observed by several other researchers (Almazan and De La Llera, 2002; Shakib and Fuladgar, 2003; Eröz and DesRoches, 2008; Panchal et al., 2010; Kitayama et al., 2017).

However, there are other studies showing that the vertical excitation effect on the horizontal responses is relatively small. Zayas et al. (1987) analyzed a single-story structure with single pendulum isolators. They indicated that the structure experienced a small effect in the horizontal responses due to the inclusion of the vertical motion. A rigid-frame bridge model with single sliding isolators was also investigated in the concern of the vertical

excitation effect (Mosqueda et al., 2004). The study resulted in the effect of the vertical motion on the response of the rigid model was little. Another test of a 6-story structure with multi-spherical sliding bearings was conducted to evaluate vertical shaking on the bearings and building response (Fenz and Constantinou, 2008). Although it was found that vertical excitation had a negligible effect, increases in horizontal base shear by up to approximately 25% and floor accelerations by up to a factor of 2.0 were observed. Morgan and Mahin (2011) also studied the vertical acceleration effect on isolators through the peak table vertical acceleration ranging from 0.15 to 0.3 g. They indicated no considerable contribution from the vertical motion to the bearing displacement, maximum base shear, and floor response spectra.

In addition to providing structural integrity, the main objective of the isolated structure is to maintain the building operational and protect sensitive contents from damage during and after earthquakes. As the amplification in both horizontal and vertical responses due to the vertical excitation, the performance of nonstructural components, particularly in critical facilities, needs to be analyzed considering the horizontal-vertical coupling effect.

1.3.4. Full-scale structural and nonstructural building system performance during earthquakes at the University of California, San Diego (UCSD) Network for Earthquake Engineering Simulation (NEES) (NEES@UCSD) facility

Another comprehensive experimental research on a full-scale building was conducted to improve comprehension of nonstructural system behavior during seismic events as indicated in Figure 1.6 (Chen, et al. 2016; Pantoli et al., 2016a; Pantoli et al., 2016b). The full-scale five story reinforced concrete building was equipped with a wide range of nonstructural components and systems (Chen, et al. 2016). The building's nonstructural components were arranged based on the design purpose of each floor. Throughout the testing period, the building with high damping rubber isolators were subjected to the ground motions summarized in Table 1.1, and the base-isolated building was quasi-linear elastic. Over the height of the building, the peak floor accelerations were relatively constant and below 0.4 g. Additionally, the peak interstory drift ratios were low below 0.5%. Damage states classification was identified in three main categories:

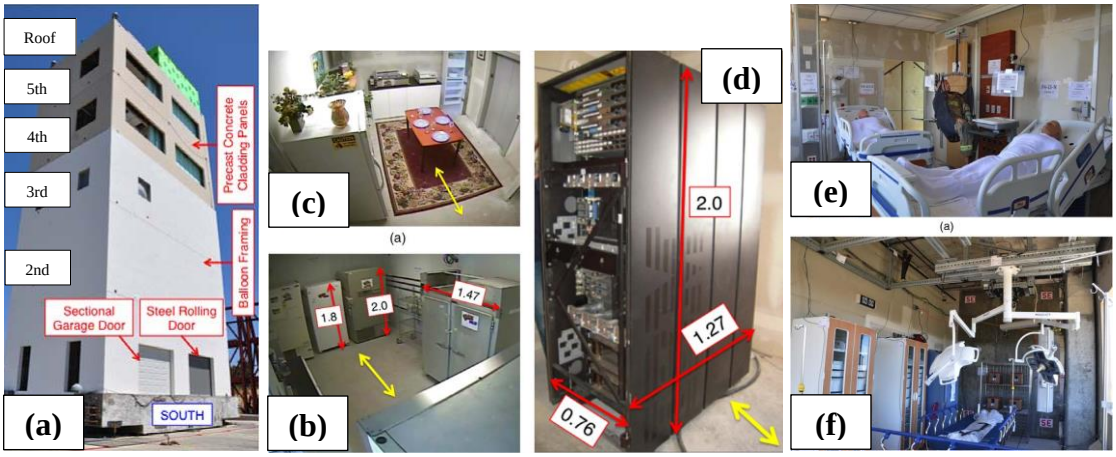

Figure 1.6. Building overview (a) façade, (b) residential area and (c) laboratory on the second floor, (d) electronical devices room on the third floor, (e) intensive care unit on the fourth, and (f) operating theater on the fifth floor. Yellow arrows show the direction of the excitations. Units in meters (Chen et al., 2016) permission in APPENDIX E.

1. Minor: Fundamentally superficial or easily repairable damage not causing threat to life safety. Cracks in wall panels, façade, or plywood ceilings that are readily repaired, and little movement of equipment that does not impair their operation.
2. Moderate: Disrepair to confirm the component or equipment operates optimally. However, it does not need the building to be evacuated and does not cause any harm to life safety.
3. Severe: Directly or indirectly represents a considerable risk to life safety. Instances are full detaching of gypsum boards from wall panels, severe tile damage, overturning of contents or equipment, total failure of door opening mechanisms, or full failure of crucial egress parts making them useless (Pantoli et al., 2016a).

Table 1.1. Peak ground accelerations, velocity, displacements, duration of earthquakes and spectral acceleration for the BI building (Chen et al., 2016) permission APPENDIX E.

Motion	Peak input acceleration (g)	Peak input velocity (mm/ s)	Peak input displacement (mm)	Strong motion duration (s)	Spectral acceleration at 2.5 s (g)
BI-I:CNPIOO	0.21	232.7	84.2	15	0.09
BI-2:LACIOO	0.22	244. I	89.3	20	0.1
BI-3:LACIOO	0.25	244.8	89.5	20	0.1
BI-4:SP100	0.52	348.7	82.7	80	0.09
BI-5:1CA50	0.17	223.2	47.6	130	0.11
BI-6:1CA100	0.32	425.9	94.6	128	0.21
BI-7:1CA140	0.5	625.9	129.2	97	0.29

Although the base isolated building experienced minor damage due to the peak floor acceleration of around 0.2 g, the fixed base structure was in the range of severe nonstructural damage due to the peak floor accelerations ranging from 0.3 g to 0.7 g shown in Figure 1.7. Similar behavior of different contents was also observed at the fifth floor in Figure 1.8. Therefore, exceeding the floor acceleration of around 0.3 g can cause nonstructural damage in the building.

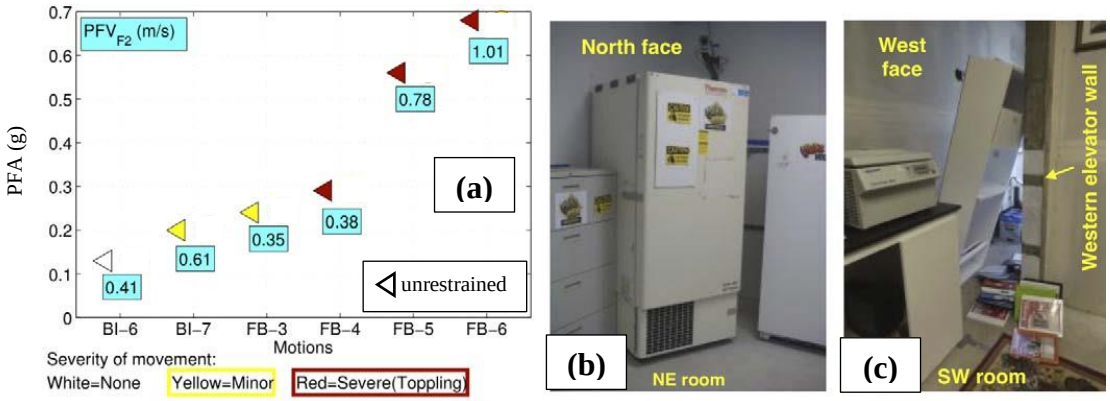

Figure 1.7. Disruption to equipment and nonstructural contents on the second floor (a) motion of unanchored objects, (b) movement of the unanchored refrigerator after test BI-7, (c) overturning of a bookshelf after test for the fixed base (FB) building (Pantoli et al., 2016a) permission in APPENDIX F.

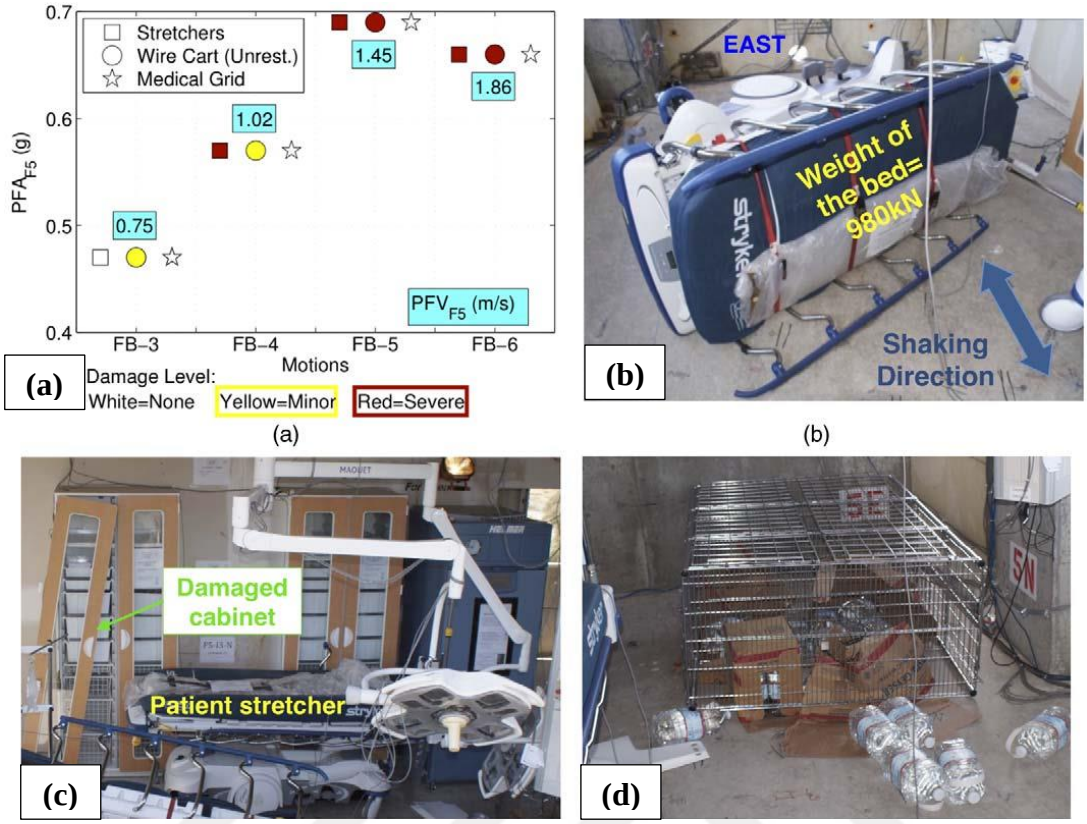

Figure 1.8. Damage in medical contents at the fifth floor: (a) damage state based on PFA, (b) overturning of the patient bed at the FB building, (c) damage to the cabinet due to the movement of the patient bed at the FB, (d) overturning of contents on the 4th floor (Pantoli et al., 2016a) permission in APPENDIX F.

1.4. Rocking Response of Contents on an Isolated Base

Although the concept of anchoring nonstructural components for seismic protection seems plausible, anchoring some elements is problematic due to their brittleness and potential for damage when fixed. Additionally, some objects are designed with mobility concerning the facility needs, so preventing these objects from their original function is undesirable (Dar et al., 2016). Therefore, base isolation is one of the alternative ways to mitigate earthquake demands on these objects. The majority of research on this subject has focused on the protection of statues and artworks in the literature (Caliò and Marletta, 2003; Roussis et al., 2008, Chiozzi et al., 2014). Vassiliou and Makris (2012) studied the rigid rocking blocks on viscoelastic bearings and single and double sliding isolators. They reported that isolation degrades the ability of blocks to be more stable when the frequency

of the excitation of the blocks rises as increasing the lowest ground acceleration necessary to generate overturning.

1.5. Scope and Objectives

Seismically base-isolated buildings, especially hospitals with friction pendulum bearings, have recently increased in earthquake-prone regions for the last decade (EPS, 2021). Additionally, the full-scale base-isolated building tests equipped with medical contents have been investigated through large shake tables for the last ten-year period. (Sato et al., 2011; Furukawa et al., 2013; Ryan et al., 2016). While much experimental and analytical research has been performed on the structural components of base-isolated buildings and the base isolation system itself, seismic performance assessment of nonstructural components in these structures is uncommon. Given the crucial nature of nonstructural components and their potentially serious consequences in critical facilities, this subject desperately requires more comprehensive research to better understand their behavior during seismic events.

In this research, seismic performance assessment of nonstructural components in a hypothetical four-story reinforced concrete triple friction pendulum base-isolated hospital building subjected to the three components of ground motions was investigated. For a base-isolated hospital building, probable nonstructural damage states due to the direct effect of vertical ground motions on slabs were indicated based on reported damage levels of the full-scale experimental studies conducted at E-Defense (Furukawa et al., 2013; Ryan et al., 2016). The response of unanchored acceleration-sensitive nonstructural contents in the base-isolated building was also investigated in terms of their rocking, toppling, and jumping response due to earthquake-induced floor accelerations. This research provides insight into the nonstructural damage of a generic base-isolated hospital building located in Istanbul, Turkey, prior to the expected Marmara earthquake strikes in the region.

1.6. Thesis Outline

This thesis consists of three chapters. The first chapter emphasizes the concept of nonstructural component behavior during seismic events, rocking response, full-scale base-isolated building experiments, and the combination of rocking response of contents on an isolated base in the literature. Chapter 1 also includes the thesis scope and objectives.

In Chapter 2, the base-isolated building model with triple friction bearings was created in a computer-aided structural analysis program (SAP2000, 2021). According to TBSC (2018), the seismic requirement for designing the TFP bearings was calculated, and the geometrical characteristics of the TFP bearings were determined developing an iterative MATLAB algorithm. The base-isolated building model was subjected to 11 ground motion pairs scaled per TBSC (2018) in order to determine the horizontal and vertical floor accelerations. The H-V coupling effect in the response was studied and compared to the scenario in which the base-isolated building model response was under the horizontal ground motions only.

The aim of Chapter 3 is to study the H-V coupling effect on the rocking response of acceleration-sensitive nonstructural components. Chapter 3 also examined the effect of story levels and jumping response by taking the H-V coupling effect into account. The acceleration-sensitive nonstructural components were modeled as symmetrical rigid blocks. Under trigonometric functions and floor accelerations obtained through the base-isolated building model in Chapter 2, the rigid blocks were solved using the numerical integration solver, ODE45, with Event Location in MATLAB.

2. SEISMIC PERFORMANCE OF A TRIPLE FRICTION PENDULUM BASE-ISOLATED BUILDING

2.1. Introduction

Nonstructural components failure in buildings, particularly critical facilities, potentially jeopardize life safety, property, and functioning both during and after earthquakes. These facilities' uninterrupted operation is crucial in addition to maintaining their structural integrity within performance-based earthquake engineering. Seismic isolation offers one of the most viable solutions to reducing the response of structures and thereby protecting their nonstructural components under seismic activity. Despite the current level of safety inherent in seismically isolated buildings, the uncertainty and complexity associated with the response of nonstructural components require further research on these buildings subjected to strong ground motions in the vertical and horizontal directions.

2.2. Building Description

A hypothetical four-story reinforced concrete triple friction pendulum base-isolated hospital building was created to study the performance of its structural and nonstructural components under earthquakes. The ground motion level was selected as Deprem Yer Hareketi Düzeyi-1 (DD-1) (TBSC, 2018), corresponding to Maximum Considered Earthquake (MCE) (ASCE7-16, 2016). The building is a critical medical facility located in Istanbul (latitude: 40.981065°, longitude: 29.162871°) on site class ZC soil (very dense/soft rock) with an S_{DS} and S_{D1} of 1.889 and 0.651, respectively, as indicated in Figure 2.1.



Figure 2.1. Building location and source-to-site distance (AFAD, 2021).

The structure has 4.5-meter-high stories and four 8-meter bays by six 8-meter bays as shown in Figure 2.2. The lateral load resisting system of the isolated superstructure was designed as reinforced concrete frames (considering the Immediate Occupancy (IO) performance level for base-isolated buildings) in accordance with TBSC (2018) and TS500, (2000). Beams have 600 mm x 700 mm cross-sections, and columns are in dimensions of 900 mm x 900 mm at each floor. The thickness of the floor slabs is 200 mm except for the base floor. In order to form a rigid bending connection to the friction pendulum bearings, the thickness of the base slabs was chosen 600 mm.

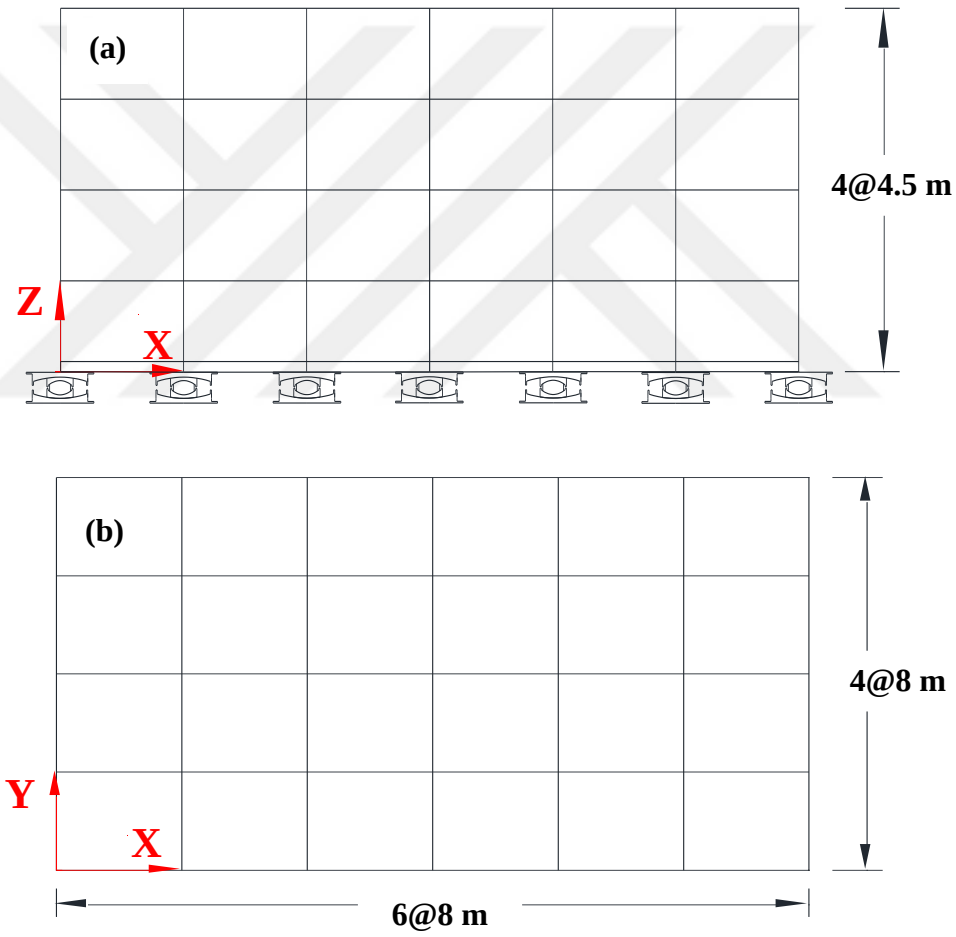

Figure 2.2. Building: (a) elevation view, (b) plan view.

2.3. Structural Modeling Assumptions and Details

A 3D modeling of the base-isolated building was developed and analyzed on the CSI software (SAP2000, 2021). The superstructure model was created assuming linear behavior in the structural members, and nonlinearity in the entire model was included through link

elements representing the sliding bearings (P-Δ effects were neglected). All beams and columns were modeled using frame elements joined at ends, whereas slabs were simulated through shell elements.

In SAP2000, there are two methods for Nonlinear Response History Analysis (NLRHA), which are Direct Integration and Fast Nonlinear Analysis (FNA) (Wilson, 2004). Direct Integration analyzes the coupled equations of motion at each time step iteratively. This approach is computationally demanding and thereby making it unsuitable for design. The FNA method relies on the modal decomposition of linear systems and considers the element's nonlinear response as unbalanced forces associated with external loads. This method can be used for structures having lumped nonlinear elements, such as base isolations and gap members (Wilson, 2004; CSI, 2017). Additionally, Sarlis and Constantinou (2010) demonstrated that FNA enables better control over the modal damping matrix and recommended that FNA be employed if link elements are utilized in conjunction with NLRHA for base isolation systems in SAP2000 (Giammona et al., 2015). Since well-suited for time-history analysis in terms of computational efficiency and other recommendations, FNA was applied with Ritz Vectors to analyze the TFP isolated building in the structural analysis software.

Columns and beams were designed using the C60 concrete grade, with a compressive strength of f_{ck} = 60 MPa. Slabs were designed with the C40 concrete grade, having a compressive strength of f_{ck} = 40 MPa. The unit weight, γ_c, and Poisson's ratio, ν_c, of the two concrete grades were taken 25 kN/m^3 and 0.2, respectively. The elastic and shear moduli of the concrete were calculated as (TS500, 2000)

$$E_c = 3250\sqrt{f_{ck}} + 14000 \tag{2.1}$$

$$G_c = \frac{E_c}{2(1+\nu_c)}. \tag{2.2}$$

The gravity loading is a superimposed dead load of 2 kPa (installments and infill/partition walls) and live load of 3.5 kPa (operating rooms) in addition to the unit-weight of the beams, columns, and slabs (TS498, 1997). In all translational directions, the mass in the analyses was derived from element self-weight and loads directly applied to shell

elements. Additionally, these loads were assigned quasi-statically, such that dynamically over an extended period (Scheller and Constantinous, 1999). The built-in ramp function in the structural analysis program was utilized with a duration of 5 sec build-up time and 5 sec constant loads. The oscillation problem was solved applying a modal damping ratio of 99%. In order to distribute the mass on the floors by interconnecting nodes, shell elements were discretized by 0.8 m x 0.8 m mesh size for each slab. According to TBSC (2018), the seismic mass is obtained by a linear combination of dead and live loads, with a scale factor. This scale factor, *n*, stemming from the less likelihood of the entire structure loaded with its full design live load, was taken 0.3 and used to calculate the seismic mass as follows:

$$w_j^{(s)} = w_{G,j}^{(s)} + n w_{Q,i}^{(s)} \tag{2.3}$$

$$m_j^{(s)} = \frac{w_j^{(s)}}{g}. \tag{2.4}$$

2.4. Isolation System Design and Modeling

TFP base isolators behave as a function of sliding on their four surfaces demonstrated in Figure 2.3. In this base isolation system, four sliding surfaces with restraining rims control displacements. The optimum design of the *i*th sliding bearings can be obtained through the radii, R_i, dimension of the surfaces, d_i, and also their friction coefficients, μ_i, (Becker, 2011). Since there is a thickness of each sliding surface, the effective pendulum length, L_i, is defined in Equation (2.5). This adjustment makes it possible to detect the displacements generated by movement on each sliding surface at the bearing center instead of at the sliding surface with the following expression:

$$L_i = R_i - h_i. \tag{2.5}$$

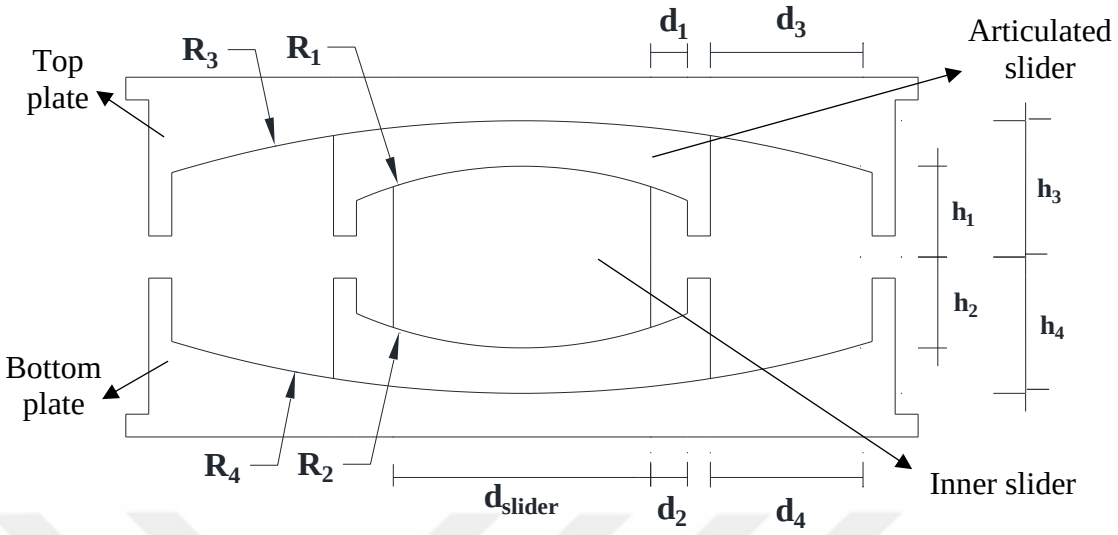

Figure 2.3. Drawing of TFP isolation.

The two outer surfaces were designed to have the same friction coefficient and radius in this study. Additionally, the two inner articulated sliders with the same friction coefficient and radius were chosen ($\mu_1=\mu_2$, $\mu_3=\mu_4$ and $R_1=R_2$, $R_3=R_4$). The TFP bearings were designed to withstand the ground motions at the DD-1 level per TBSC (2018). It is stated that the maximum displacement, D_M, under the DD-1 level is evaluated as (TBSC, 2018)

$$D_{\mathrm{M}} = 1.3\left(\frac{g}{4\pi^2}\right) T_{\mathrm{M}}^2 \eta_{\mathrm{M}} S_{\mathrm{ae}}^{(\mathrm{DD\text{-}1})}\left(T_{\mathrm{eff,M}}\right) \tag{2.6}$$

where

$$\eta_{\mathrm{M}} = \sqrt{\frac{10}{5+\zeta_{\mathrm{eff,M}}}} \tag{2.7}$$

and where η_{M} denotes the damping scaling coefficient.

In order to obtain the maximum displacement and other design parameters of the TFP bearings, a MATLAB code was written (MATLAB, 2019). This code iteratively determines the maximum displacement for the given spectral seismic demand ($S_{ae}^{(DD-1)}\left(T_{\mathrm{eff,M}}\right) = S_{M1}/T_M$), building weight, and the assumed radii by including the friction coefficient modification due to the pressure on the individual bearing. Based on the

friction pendulum bearing pressure, p_b, the friction coefficient modification was determined with the following expression (McVitty and Constantinou, 2015):

$$\mu_i = 0.122 - 0.01p_b \text{ (ksi)}. \tag{2.8}$$

This equation is valid at isolator pressures ranging from 13.8 to 55.2 MPa (2 to 8 ksi). Therefore, considering the building weight, we developed the bearings' geometry not only to meet the displacement capacity of the bearing surfaces but also to account for the stress range.

Additionally, the friction coefficient values obtained from Equation (2.8) need to be modified for a higher design velocity of the outer surfaces. (McVitty and Constantinou, 2015). Therefore, the friction coefficients of the outer surfaces were adjusted to reduce these coefficients by 0.015, and the friction coefficients of the inner surfaces were set to 0.03, as McVitty and Constantinou (2015) recommended. The effective period and stiffness were calculated as follows:

$$T_{\text{eff,M}} = 2\pi\sqrt{\frac{W}{gk_{\text{eff,M}}}} \tag{2.9}$$

where

$$k_{\text{eff,M}} = \frac{\mu_4 + \frac{1}{L_3 + L_4}(D_M - u_3)}{D_M}W \tag{2.10}$$

where

$$u_3 = u_2 + (\mu_4 - \mu_3)(L_3 + L_2) \tag{2.11}$$

and

$$u_2 = (\mu_3 - \mu_1)L_1 + (\mu_3 - \mu_2)L_2. \tag{2.12}$$

D_y was assumed 0.0005 m (Nikfar and Konstantinidis, 2019). The effective damping for the bearings was obtained with the energy dissipation through the following expressions:

$$\zeta_{eff} = \frac{E_{loop}}{2\pi k_{eff} D_M^2} \tag{2.13}$$

where

$$E_{loop} = 4(E_1 - E_2 - E_3 - E_4) \tag{2.14}$$

where

$$E_1 = \left(\mu_4 - \frac{1}{L_3 + L_4} u_3\right) D_M W \tag{2.15}$$

$$E_2 = \left(\frac{1}{L_2 + L_3} - \frac{1}{L_3 + L_4}\right) u_3^2 W \tag{2.16}$$

$$E_3 = \left(\frac{1}{L_1 + L_2} - \frac{1}{L_2 + L_3}\right) u_2^2 W \tag{2.17}$$

$$E_4 = \left(\frac{\mu_1}{D_y} - \frac{1}{L_1 + L_2}\right) D_y^2 W \tag{2.18}$$

and where ζ_{eff} denotes the effective damping. The displacement limits of the inner surfaces were taken 0.04 m. However, the displacement limits of the outer surfaces were calculated based on D_M (TBSC, 2018) as follows:

$$d_3 = 0.5(D_M - u_2). \tag{2.19}$$

Table 2.1 summarizes also the properties of the TFP isolations at the DD-1 level.

Table 2.1. TFP bearing properties.

Effective Period ($T_{eff,M}$)	2.63 s
Effective Damping ($\zeta_{eff,M}$)	15%
Design Displacement (D_M)	0.402 m
Inner Radii (R_1, R_2)	0.45 m
Outer Radii (R_3, R_4)	1.3 m
Height for Inner Surfaces (h_1, h_2)	0.09 m
Height for Outer Surfaces (h_3, h_4)	0.15 m
Inner Friction Coefficients (μ_1, μ_2)	0.012 (slow), 0.03 (fast)
Outer Friction Coefficients (μ_3, μ_4)	0.021 (slow), 0.052 (fast)
Slider Diameter (d_{slider})	0.28 m
Inner Displacement Capacity (d_1, d_2)	0.04 m
Outer Displacement Capacity (d_3, d_4)	0.191 m

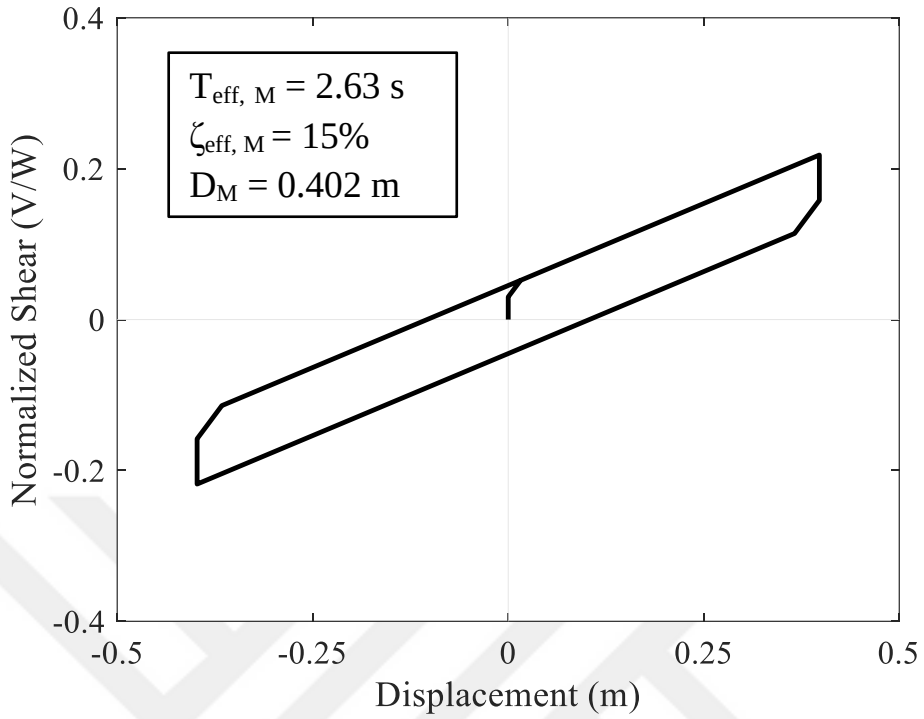

Figure 2.4. Normalized hysteresis loop of the TFP bearing system at the DD-1 level.

The triple friction pendulum bearings were modeled as link elements under each of the 35 columns in SAP2000. In addition to the horizontal parameters of the TFP bearings summarized in Table 2.1, the compressive stiffness, K_v, of the isolators was set at 12.5 Hz. Ryan and Polanco (2008) observed undesired damping at frequencies lower than the natural frequency of the superstructure due to the mass-proportional term in Rayleigh damping. This artificial dampening, also called damping leakage, prevents the first mode of the base-isolated building from existing in the response. Ryan and Polanco (2008) recommended that using stiffness-proportional damping be a way to apply minimal damping to the isolation modes of the building. Sarlis and Constantinou (2010) also studied damping leakage and compared various damping implementations for a base-isolated building model in SAP2000. They concluded that interpolated damping, Rayleigh damping with override, and constant damping with override resulted in similar outputs but different computational time. Giammona et. al. (2015) conducted research regarding the full-scale TFP base-isolated building tested at E-Defense. They compared the E-Defense experiment with their SAP2000 models. In their research, a constant damping ratio of 2% was used for all modes, with 0% damping in the first three isolation modes through FNA Modal Overrides in SAP2000.

Additionally, Guzman and Ryan (2018) and Guzman and Ryan (2020) investigated base-isolated structures subjected to the horizontal-vertical ground motions and modeled their lead rubber bearing base-isolated building in SAP2000 using 2.5 percent constant modal damping with a damping coefficient of 5% in the vertical mode. As a result, in our research's nonlinear time-history analyses, the stiffness damping approach, including a 2% damping ratio, was used with 3% modal damping override at the first vertical mode. Consequently, the structural and isolator modeling parameters are summarized in Table 2.2 motivated by (Giammona et al., 2015).

Table 2.2. SAP2000 modeling parameters.

Properties	Modeling Assumptions
Computational Procedures	Fast Nonlinear Analysis (FNA)
Model Members	Linear-elastic frame for beams and columns, shell elements for slabs, and nonlinear link elements for TFP bearings
Analysis and Ground Motions Directions	X-Y-Z
Damping	2% stiffness damping, with 3% damping in vertical mode via Modal Damping Overrides
Modes Number in Analyses	100
Global P-Δ effects	Not included
Gravity Loading	Applied to the structure using built-in ramp function
Rigid Diaphragm	Used for each floor level

2.5. Building Modal Response

Modal analyses of the base-isolated building were determined through Ritz Vectors. At the isolation level, the periods of the isolated building were calculated using a linear elastic spring and the effective stiffness of the isolators at the DD-1 level, which corresponds to $T_{M,eff}$ = 2.63 s and T_v = 0.08 s. Table 2.3 summarizes the first seven modes out of 100. The undeflected form is shown in gray for reference and modes in the structural analysis program in Figure 2.5 to Figure 2.8. The first mode (T_1 = 2.706 s), corresponding to the isolation mode, is indicated in Figure 2.5. This first mode was dominated by the existence of the TFP bearings. Mode 3 (T_3 = 2.419 s) represents the torsional behavior through the isolation system.

Table 2.3. Seven modes (out of 100) of the TFP base-isolated building.

Mode	Periods	Notes
1	2.706	Isolation modes in Y, X, RZ, respectively
2	2.703	
3	2.419	
4	0.311	1st Horizontal Structural Mode (Y)
5	0.303	2nd Horizontal Structural Mode (X)
6	0.276	3rd Horizontal Structural Mode (RZ)
7	0.125	1st Vertical Mode

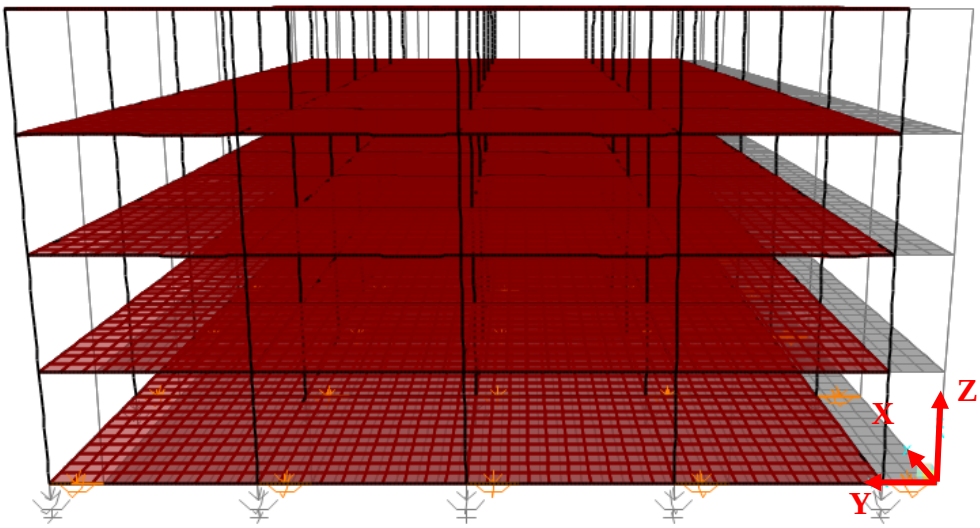

Figure 2.5. Mode 1: *T* = 2.706 s (Isolation mode in the Y direction).

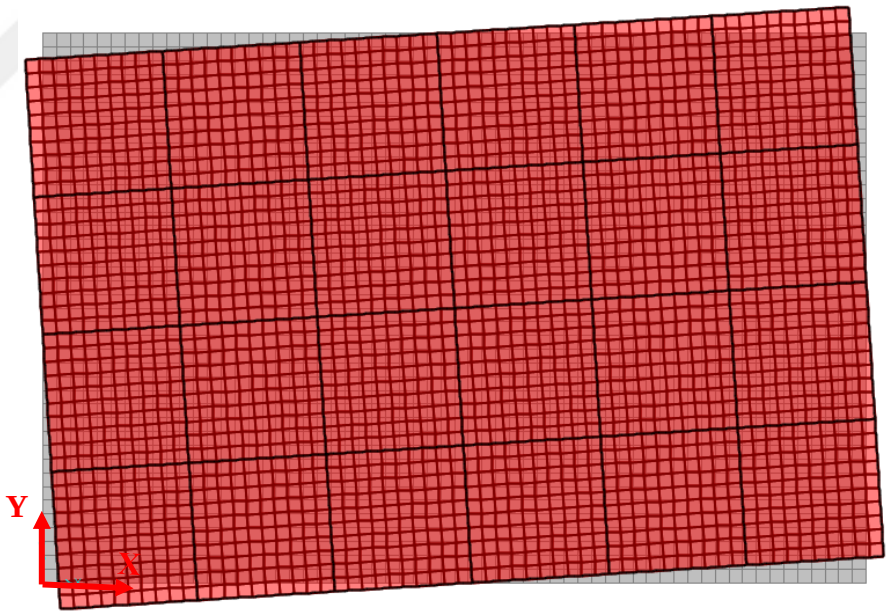

Figure 2.6. Mode 3: T = 2.419 s (Isolation mode in the RZ direction).

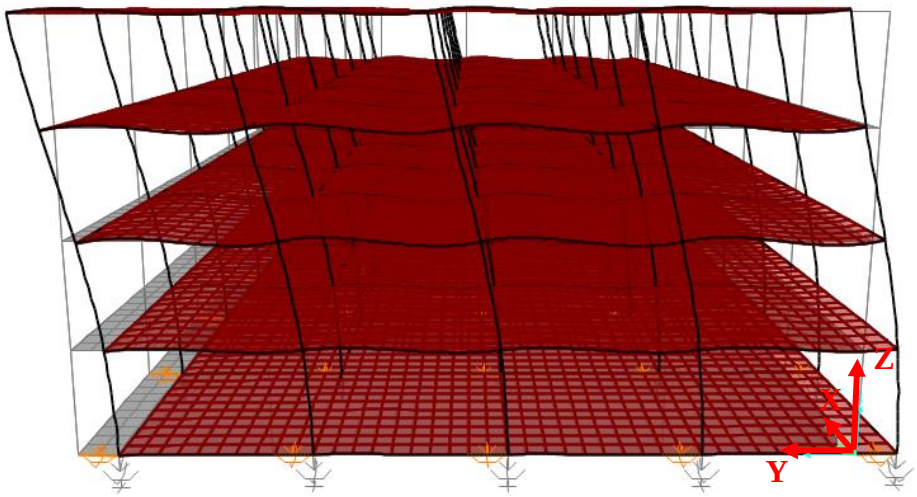

Figure 2.7. Mode 4: T = 0.311 s (1st structural mode in the Y direction).

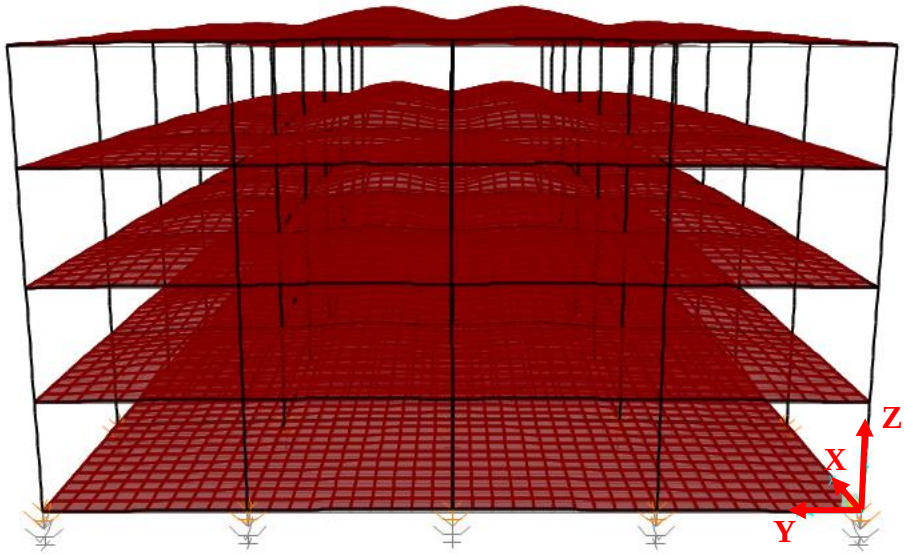

Figure 2.8. Mode 7: T = 0.125 s (1st vertical mode).

2.6. Ground Motion Selection and Scaling

Target spectra for the DD-1 level were calculated according to TBSC (2018). 11 ground motion pairs were chosen on the NGAWest2 Pacific Earthquake Engineering Research Center (PEER) website as follows (PEER 2021):

1. Fault type (Strike Slip)
2. Magnitude (7.0 – 7.5)

3. The Joyner-Boore distance, R_{JB}, (19 km – 60 km)
4. Shear wave velocity, V_{s30}, (360 m/s – 760 m/s)

The horizontal components of these 11 pairs were combined by the Square Root Sum of Squares (SRSS) method in Figure 2.9. According to TBSC (2018), ground motion scaling is performed within the period range between $0.5T_M$ (T_M is the effective period based on upper bound values of the friction coefficients under the DD-1 level.) and $1.25T_M$ (T_M is the effective period based on lower bound values of the friction coefficients under the DD-1 level.). The upper bound values were calculated using coefficients of 1.2 and 1.16 related to aging and contamination effects, as McVitty and Constantinou (2015) used.

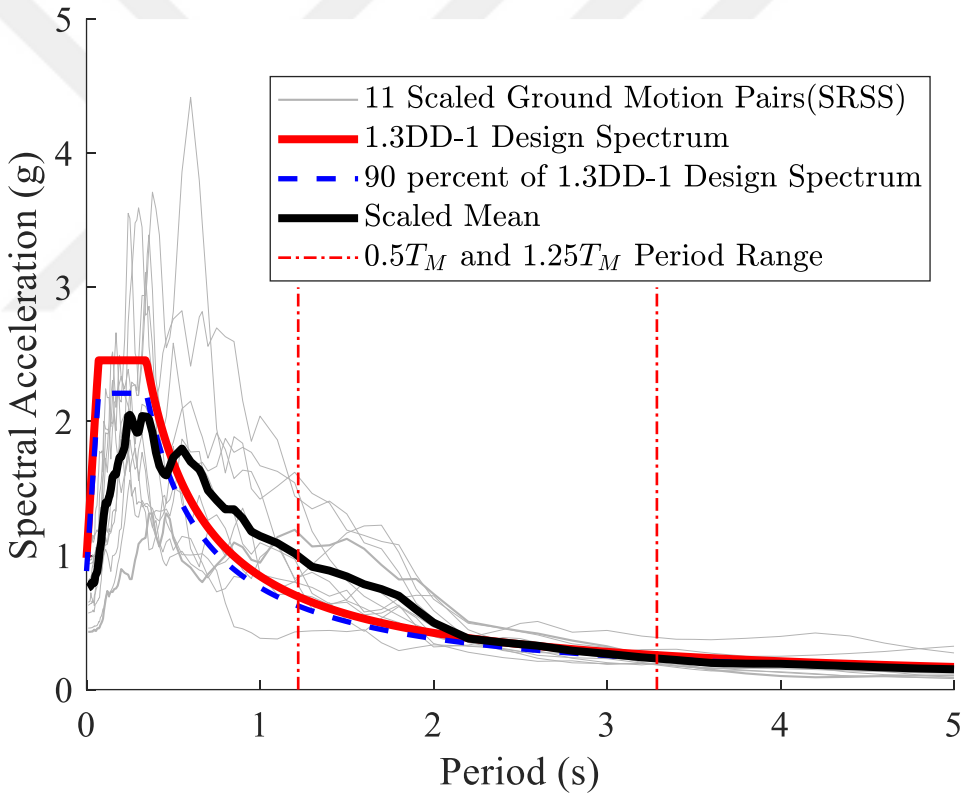

Figure 2.9. Selected ground motion response spectra in the horizontal direction.

Consequently, the response spectra of each ground motion were matched to the DD-1 level design spectrum by using the Amplitude Scaling method between the periods of 1.22 and 3.29 s with minimizing the sum of the square differences. As seen in Figure 2.10, the vertical components of the ground motion pairs were also scaled employing the same amplitude scaling factor obtained for the corresponding horizontal ground motions.

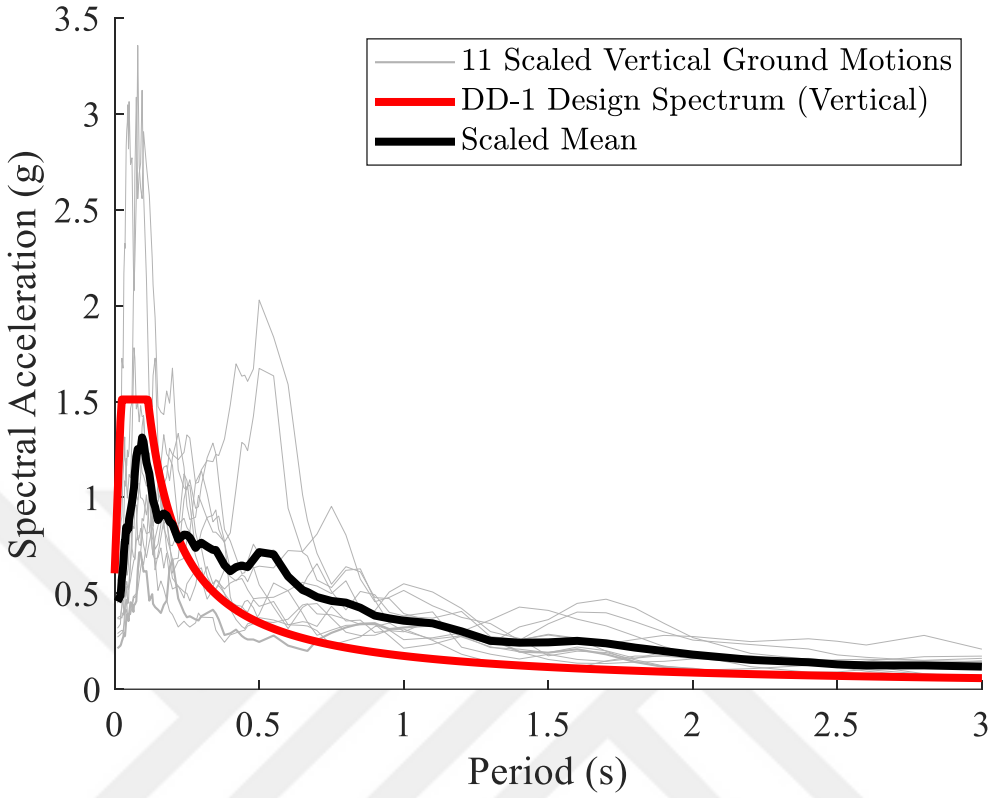

Figure 2.10. Selected ground motion response spectra in the vertical direction.

2.7. Structural Response

Figure 2.11 to Figure 2.14 indicate that the TFP bearing displacements due to the scaled ground motions in the X and Y directions are less than the theoretical bearing displacement based on the DD-1 level. since TBSC (2018) uses the value of S_{M1} to design the maximum bearing displacement when Equation (2.6) is employed for $S_{\mathrm{ae}}^{\mathrm{DD\text{-}1}}(T_{\mathrm{M}}) = S_{\mathrm{M1}}/T_{\mathrm{M}}$. This is also the case in ASCE 7-16 stated as (ASCE7-16, 2016):

$$D_M = \frac{gS_{M1}T_M}{4\pi^2 B_M}. \tag{2.20}$$

The hysteresis loops of the bearing at the center were shown in Figure 2.11 to Figure 2.14. It is important to note that the hysteresis loops may vary considerably in the two horizontal directions under the same ground motion.

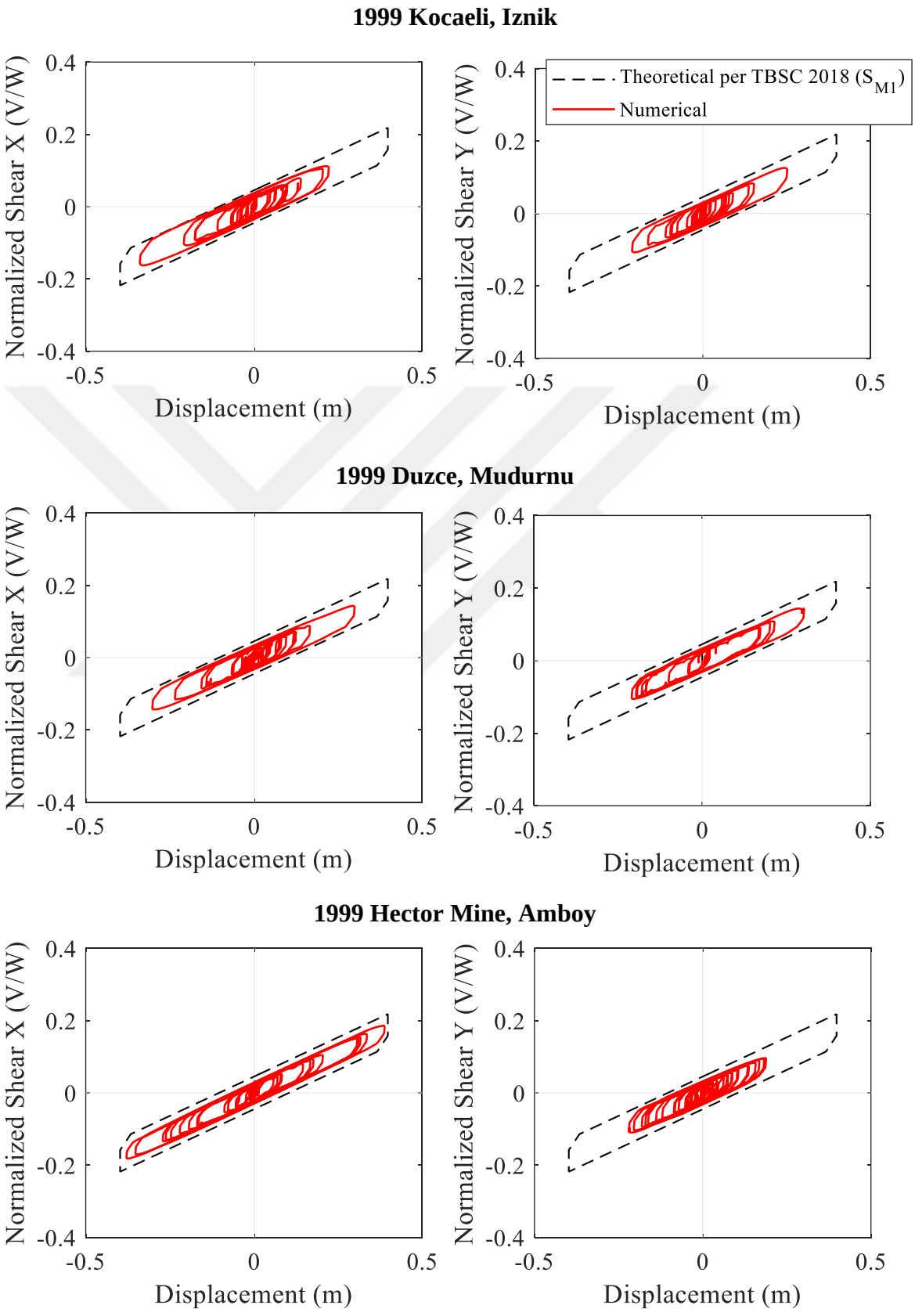

Figure 2.11. X and Y-direction hysteresis loops for the center bearing.

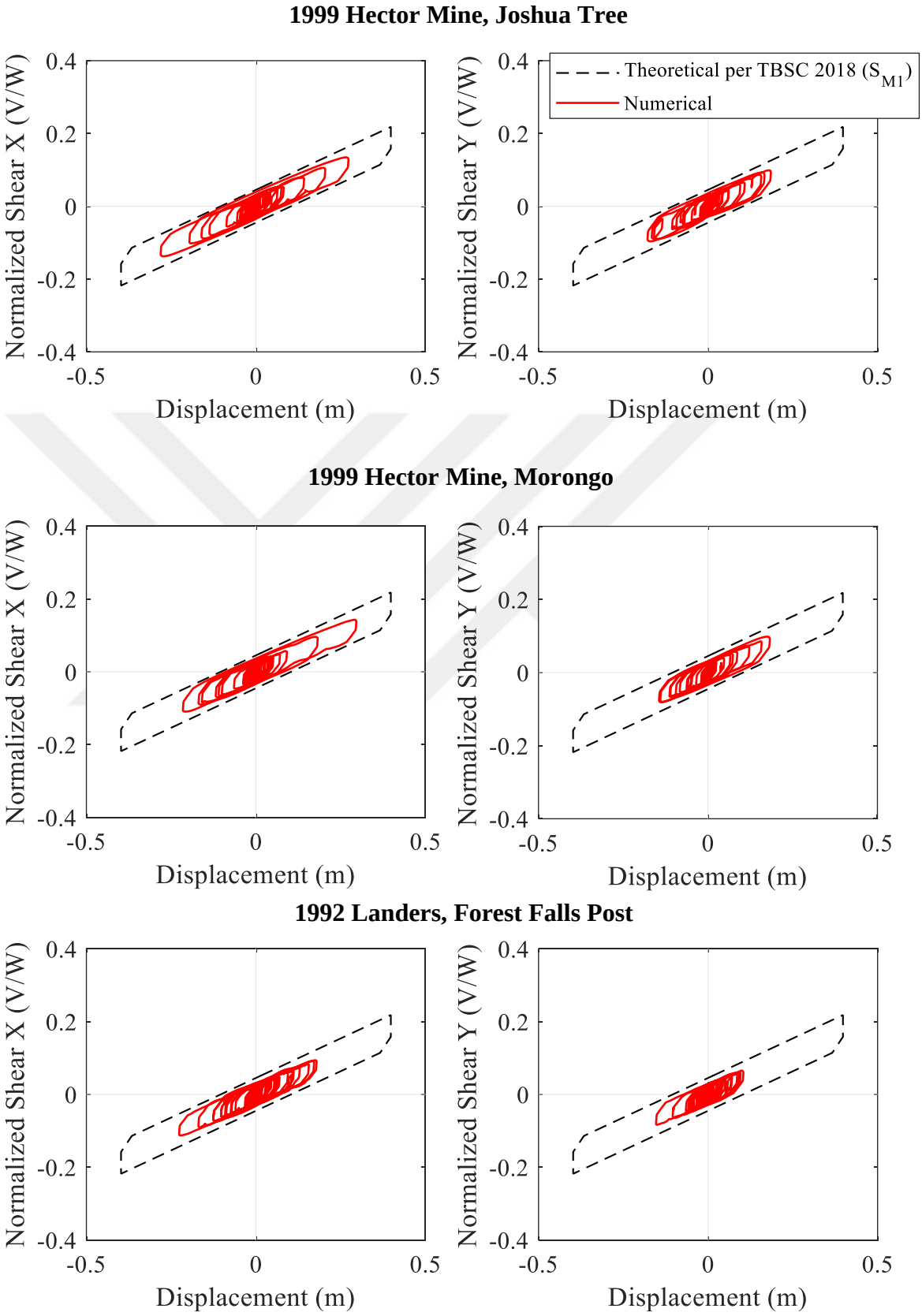

Figure 2.12. X and Y-direction hysteresis loops for the center bearing.

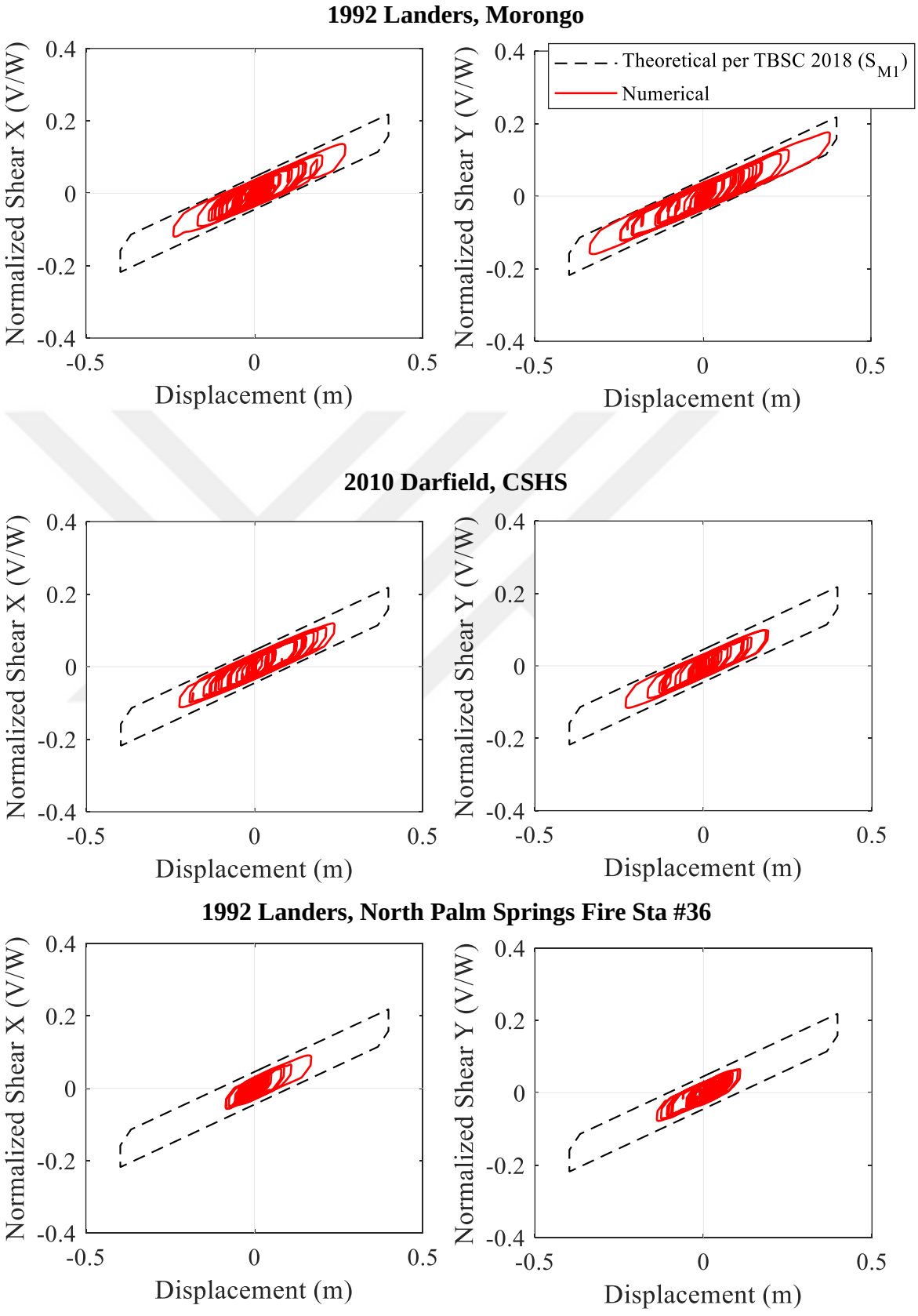

Figure 2.13. X and Y-direction hysteresis loops for the center bearing.

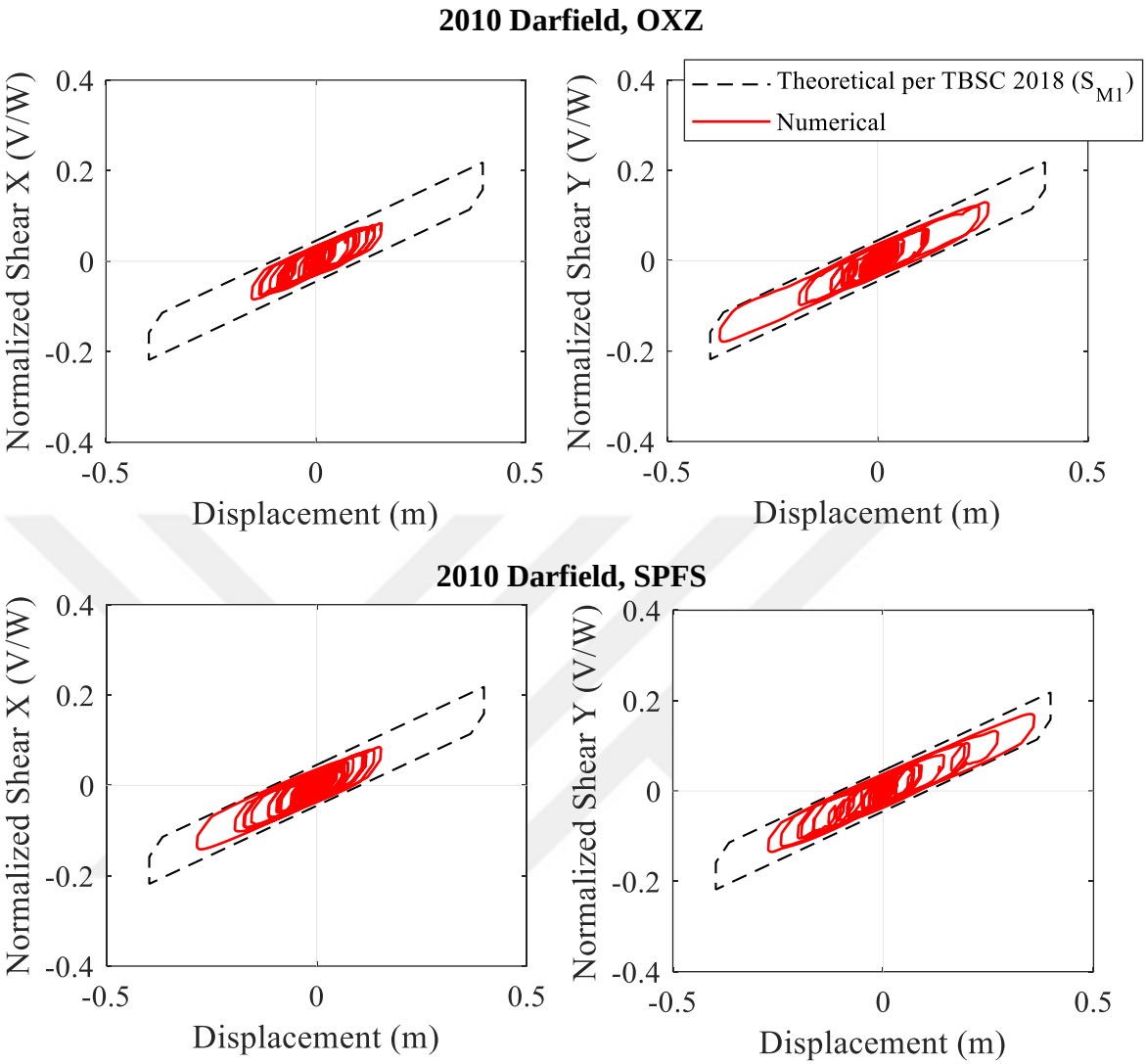

Figure 2.14. X and Y-direction hysteresis loops for the center bearing.

2.7.1. Horizontal and Horizontal-Vertical Coupling Response

In comparison to fixed base equivalents, the base isolation technology in buildings is widely recognized for reducing story drifts, peak floor velocity, and peak floor acceleration (Sato et al., 2011; Ryan et al., 2012). The responses of the TFP base-isolated building subjected to the horizontal components of the ground motions are relatively uniform throughout the superstructure height (Nikfar and Konstantinidis, 2019). Our study also shows that in terms of interstory drifts, the peak absolute PFV and PFA, the mean values of the TFP base-isolated structure response remained to some extent constant over the height of the building subjected to the horizontal ground motions.

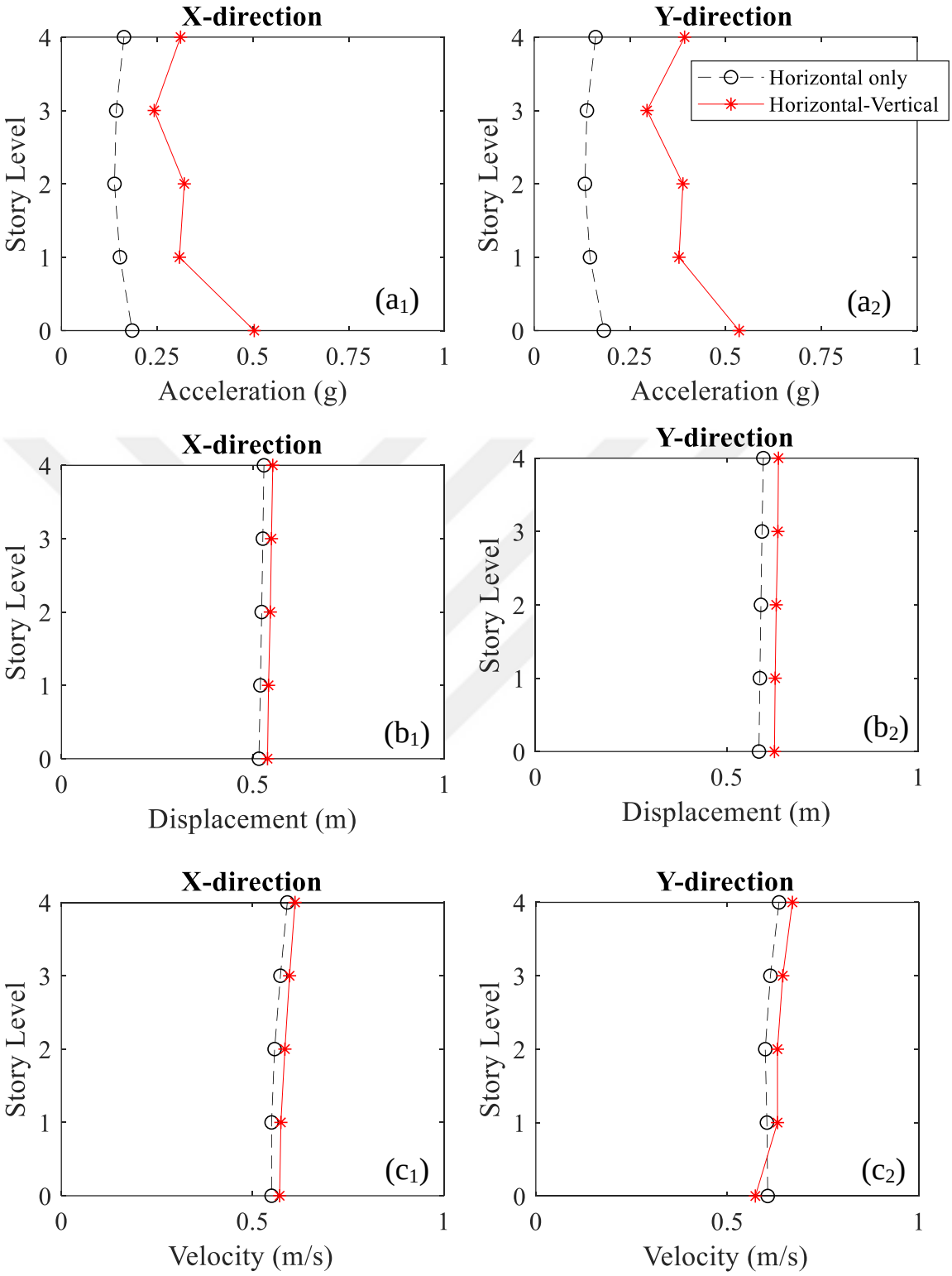

Figure 2.15. Absolute mean peak responses: (a_1) X-direction floor acceleration, (a_2) Y-direction floor acceleration, (b_1) X-direction floor displacement, (b_2) Y-direction floor displacement, (c_1) X-direction floor velocity, (c_2) Y-direction floor velocity.

Although, the inclusion of the vertical ground motion components in the analyses increased the peak floor acceleration demand over the height of the building in the horizontal directions, the changes in the responses of the peak floor displacement and velocity were negligible, as shown in Figure 2.15. The increases in the peak floor acceleration mean response of the building in the X direction were around a factor of 2.0, as Fenz and Constantinou (2008) observed. However, all peak floor accelerations in the horizontal directions were less than 1g under each ground motion.

Table 2.4. Amplification factor for X-direction horizontal acceleration due to the vertical component of ground motions at each floor.

Story Level	Amplification Factor
Roof	1.98
3	1.50
2	2.66
1	2.22
Base	3.00

Table 2.5. Amplification factor for Y-direction horizontal acceleration due to the vertical component of ground motions at each floor.

Story Level	Amplification Factor
Roof	2.90
3	2.28
2	3.86
1	3.19
Base	3.88

Figure 2.16 shows the floor response spectra due to the 11 horizontal ground motions. The first isolation mode in the Y direction appeared on the response in addition to the first mode structural response, T_2 = 2.706 s and T_5 = 0.311, respectively. However, as seen in Figure 2.17, another peak emerged in the response when the vertical component of ground motion pairs was considered in the analyses.

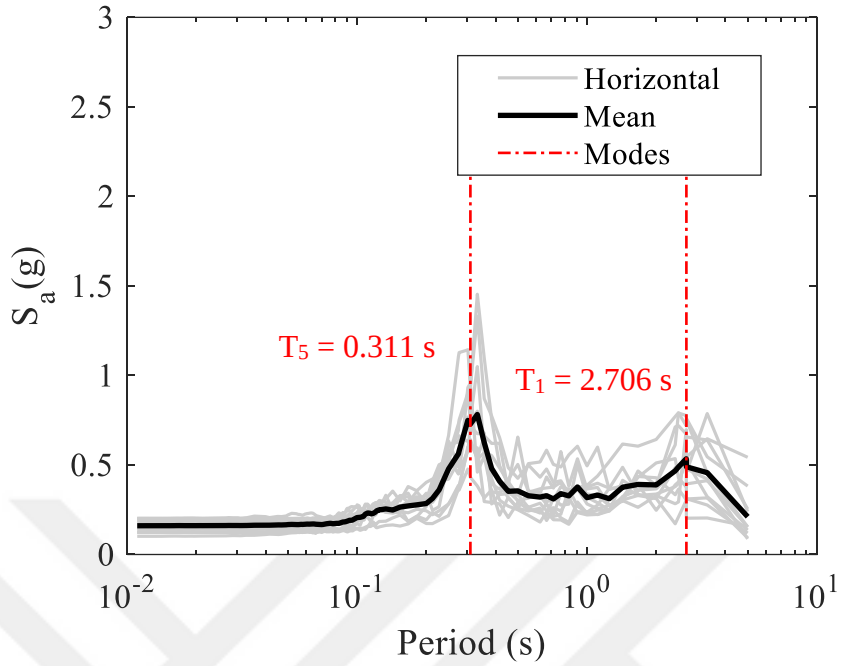

Figure 2.16. Floor response spectra in the Y direction at the roof level under the horizontal ground motions only.

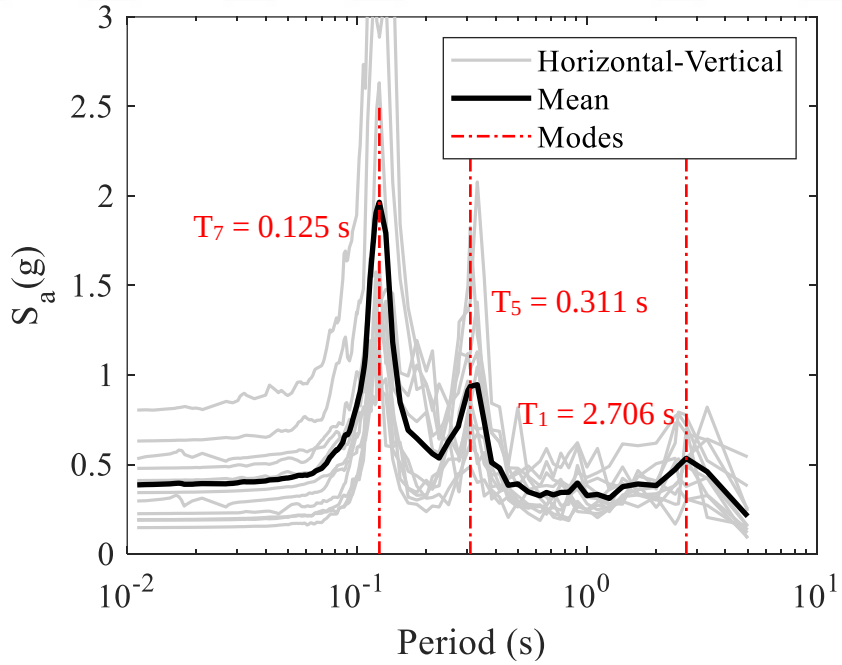

Figure 2.17. Floor response spectra in the Y direction at the roof level under the horizontal and vertical ground motions.

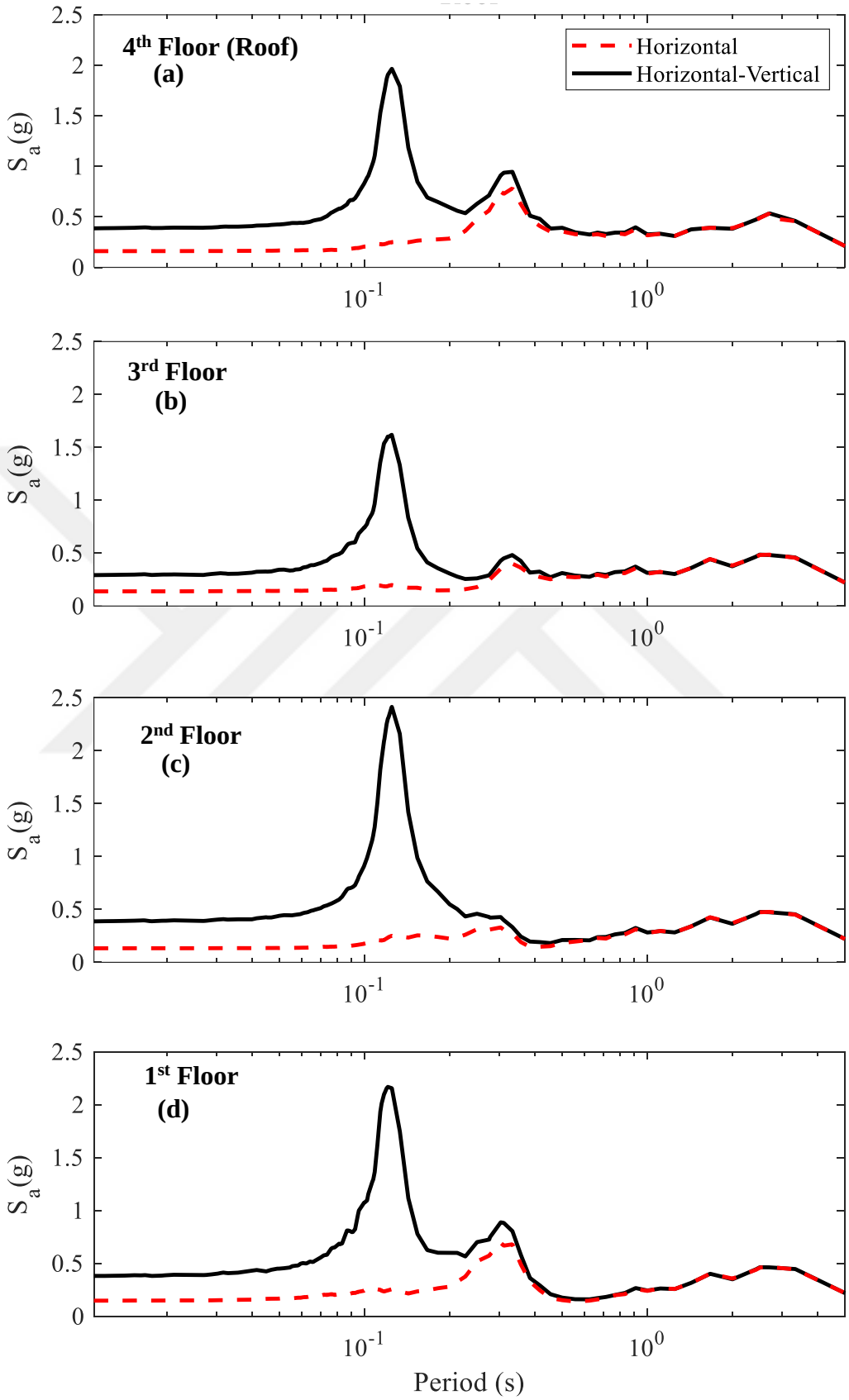

Figure 2.18. Floor response spectra in the Y direction: (a) 4th, (b) 3rd, (c) 2nd, (d) 1st.

2.7.2. Vertical Slab Response

Furukawa et al. (2013) and Ryan et al. (2016) showed that the vertical ground motion can cause damage to nonstructural components, including medical equipment in the base-isolated buildings. Due to the fact that the current ubiquitous base isolation systems usually do not offer vertical isolation, the superstructure undergoes the same vertical excitation as its fixed-base equivalent. These systems may even cause amplification in the vertical response under certain situations, as Furukawa et al. (2013) observed in their full-scale experiments. Therefore, it is critical to determine the vertical seismic demand associated with damage to nonstructural components in base-isolated structures.

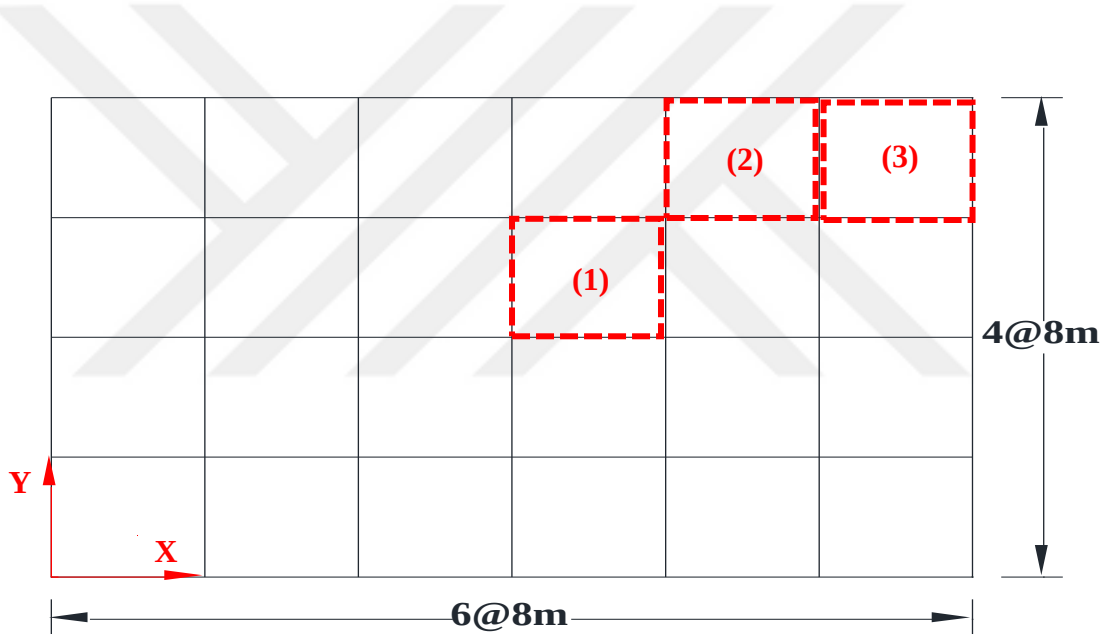

Figure 2.19. Three slabs having different adjacents on the plan view.

Three slabs with varying adjacent boundaries, as indicated in Figure 2.19, were utilized to investigate the vertical floor responses. Under the 11 ground motion pairs, the peak vertical accelerations computed from these slabs were between 0.61g and 3.67g at the roof, which has the highest vertical acceleration among other floors. These values are also within the range of the peak vertical acceleration experimental results (0.41-8.15g) obtained by Furukawa et al. (2013) and Ryan et al. (2016). According to Furukawa et al. (2013), once the vertical floor acceleration exceeded 2g, damage to nonstructural elements occured. Between 1g and 2g, medical equipment and some furniture overturned and showed noticeable movement. Similarly, Ryan et al. (2016) reported that vertical accelerations

between 2 and 3g caused minor damage, whereas those between 3 and 5g cause moderate damage. Additionally, greater than 5g showed extensive damage. Based on these full-scale experimental classifications, Figure 2.20 to Figure 2.22 show that these classifications are Jumping Initiation, Minor Damage, Moderate Damage, and Excessive Damage. For the given location and seismic demand provided by AFAD (2021), our building model, as a hospital, can experience some levels of damage due to the vertical acceleration.

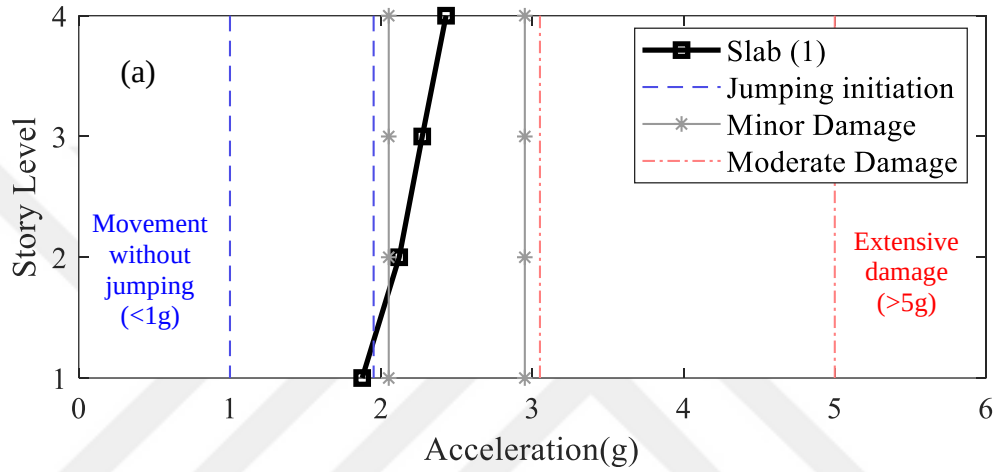

Figure 2.20. Mean values of vertical peak Slab (1) center accelerations under the 11 ground motion pairs.

Although the mean values of the vertical slab acceleration indicate mainly minor damage in Figure 2.20, individual ground motions, such as the 1992 Landers, Morongo Valley Hall (GEOS #58) earthquake, caused the roof slab to accelerate by 3.64g. This result falls within the area of Moderate Damage (3-5g). Additionally, regarding these full-scale testing result classifications, our building model did not sustain excessive damage in the vertical direction when subjected to the ground motions scaled in accordance with TBSC (2018).

Figure 2.21 indicates that the nonstructural contents would start jumping on Slab (2). Regarding individual ground motions slab response, the building model was within the range of the Jumping Initiation region for Slab (2). Figure 2.22 shows that Slab (3) was subjected to vertical ground motions less than 1g in the vertical direction. Below 1g without jumping, rocking, toppling, sliding, or a combination of sliding and rocking govern nonstructural contents' behavior under seismic events. Moreover, slight and moderate damage occur

between 0.4 and 1.25 due to horizontal acceleration, as Furukawa et al. (2013) reported. Therefore, it is crucial to realize that nonstructural contents under the less than 1g vertical acceleration region are critical in terms of their pure planar rocking and overturning behavior when compounded with 0.4g horizontal accelerations, which is the horizontal acceleration range for our building model.

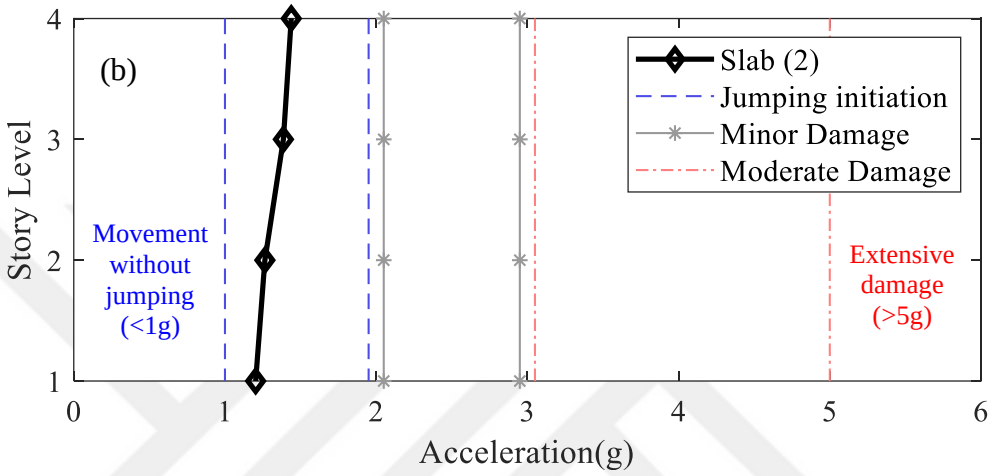

Figure 2.21. Mean values of vertical peak Slab (2) center accelerations under the 11 ground motion pairs.

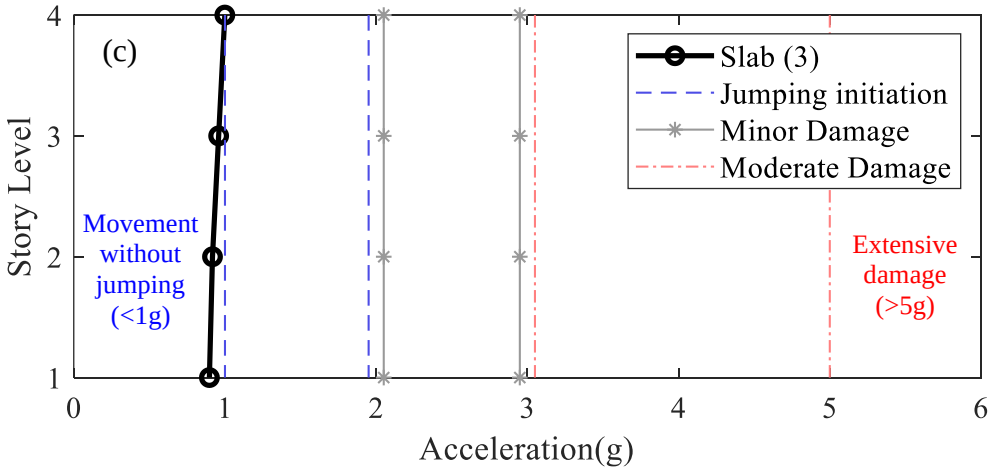

Figure 2.22. Mean values of vertical peak Slab (3) center accelerations under the 11 ground motion pairs.

Additionally, the vertical slab mode and its associated period (T = 0.125 s) were determined using spectral accelerations of the three slabs at the roof level, as shown Figure 2.23. This concluded that regardless of the base isolation vertical period (Tv = 0.08 s), as intended, the predominant vertical period of the building model is governed through slab dynamic characteristics as a single degree of freedom system at the slab center.

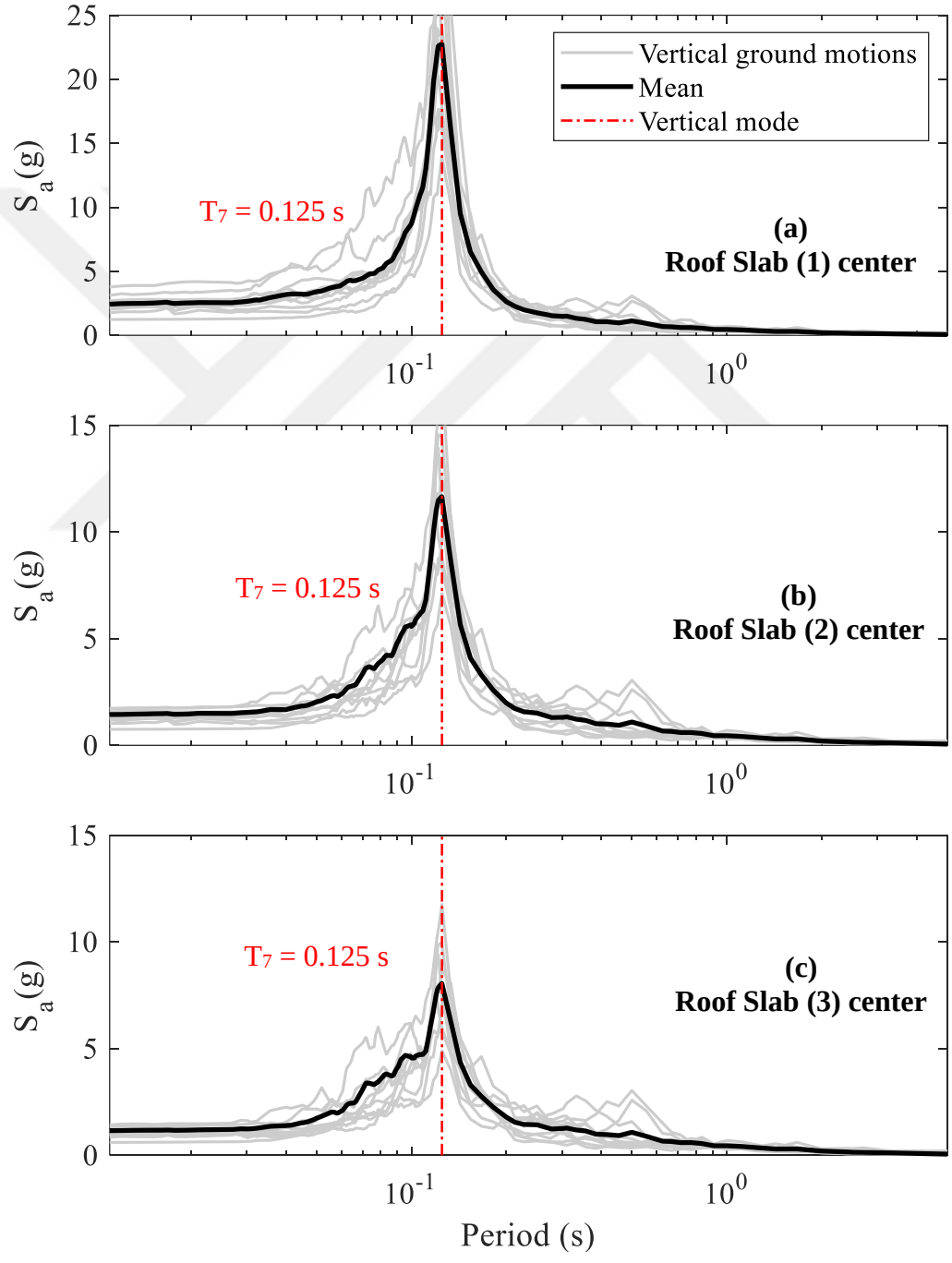

Figure 2.23. Vertical PFA values on the roof: (a) Slab (1), (b) Slab (2), (c) Slab (3).

3. SEISMIC PERFORMANCE OF FREESTANDING CONTENTS

3.1. Introduction

Since Housner's (1963) work on the rocking response of rigid blocks subjected to excitations, many researchers have studied these blocks' complicated behavior under trigonometric motions and earthquakes. The idea of using these rigid blocks was the representation of elements, such as classical columns, electrical equipment, statues, or other nonstructural building items (Makris and Roussos, 2000; Filiatrault et al., 2004; Vassiliou and Makris, 2012). Overturning is an undesirable seismic response of nonstructural elements. Even when no overturning occurs, rocking is an unfavorable type of seismic behavior for medical equipment because it might cause severe damage to the equipment or other acceleration sensitive critical contents in a hospital.

Considering the pure planar rocking motion, as shown in Figure 3.1, a rigid block will firstly rotate in the positive direction, and it will ultimately turn to the negative rotation if it does not overturn. Consequently, it will continue to oscillate while dissipating energy due to the gravitational force and the impact generated by the bottom corners, points *O* and *O*'. In the end, it will stop unless there is further excitation. In this study, nonstructural contents were represented as rigid blocks with uniform mass distribution. Because the mass of the rigid contents was assumed to be negligible in comparison to the mass of the base-isolated building, the dynamic interaction between the building and its contents was ignored.

3.1.1. Review of the Rocking Response of a Rigid Block

The concept of modeling equipment as a rigid block in order to assess its dynamic response due to excitation was validated via shaking table testing using sensitive Direct Current Differential Transformer (DCDT) displacement transducers (Konstantinidis, 2008). Figure 3.1 illustrates the rocking behavior of a rigid block, where h and b denote the height and width of the block, respectively. Since the pure planar rocking behavior is the scope of this study, the friction of the contact between the slabs and rigid blocks was considered high

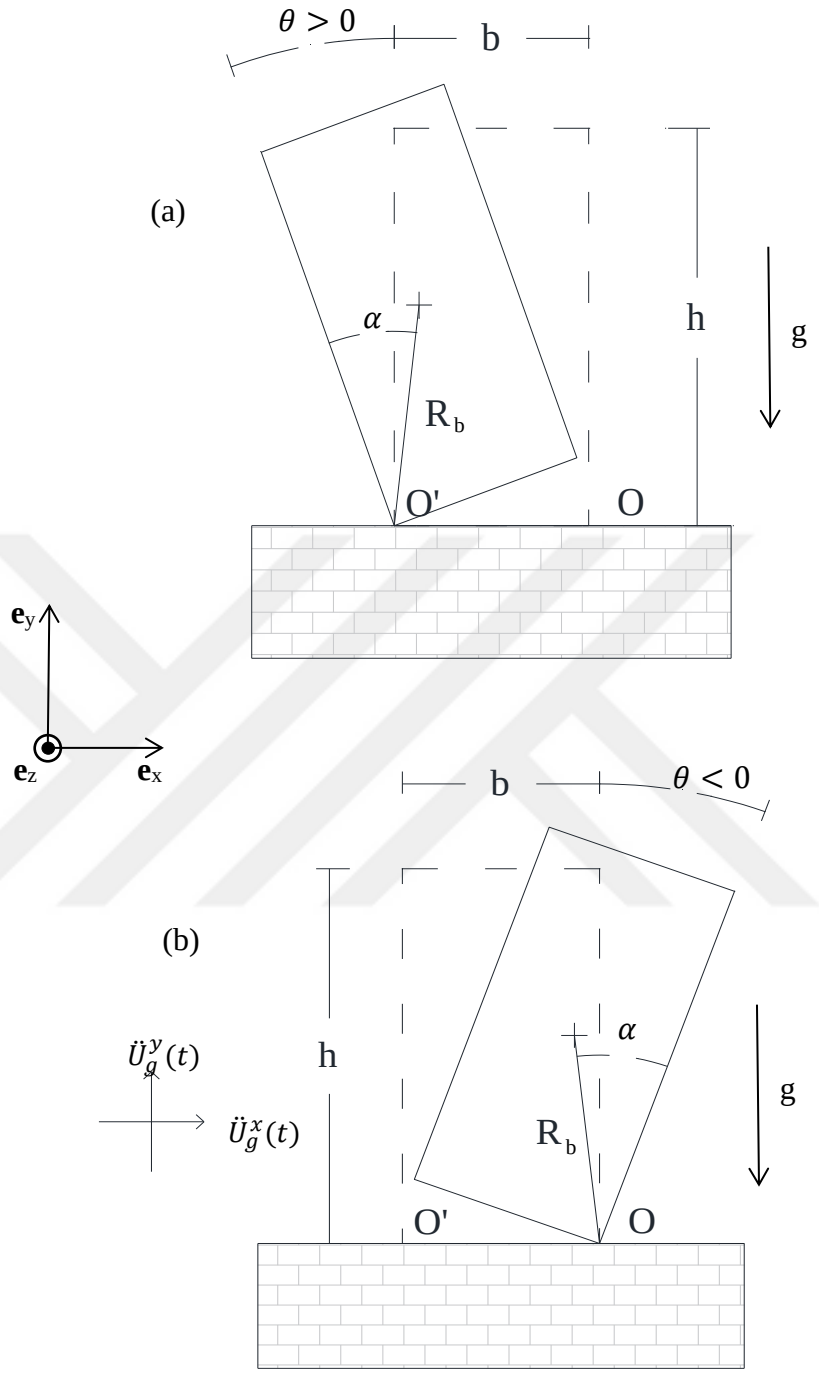

Figure 3.1. Drawing of a rigid block under pure planar rocking motion for two rotational directions: (a) $\theta > 0$, (b) $\theta < 0$.

enough to avoid sliding. The rigid block can rotate around the points *O* and *O*' as rocking initiates. If there is adequate resistance to prevent the rigid block from sliding, the block begins to only rock under excitations. Therefore, the rocking behavior is defined as follows:

$$\left|\ddot{U}_f^x\right| \geq \left(g + \ddot{U}_f^y\right) \tan\alpha \tag{3.1}$$

$$\alpha = \tan^{-1}(b/h) \tag{3.2}$$

where $\ddot{U}_f^x$ and $\ddot{U}_f^y$ denote the absolute lateral and vertical floor accelerations, accordingly.

The dynamics equation of the rigid block considered in the case of the planar rocking motion was obtained as follows (Makris and Roussos, 2000; Konstantinidis, 2008; Linde 2016):

$$\mathbf{M}_O = I_O\ddot{\boldsymbol{\theta}} + \bar{\mathbf{r}} \times m\mathbf{a}_O \tag{3.3}$$

where $\mathbf{M}_O$ is the total moments around the point *O*, I_O is the rigid body moment of inertia around *O*, $\ddot{\boldsymbol{\theta}}$ is the angular acceleration, $\bar{\mathbf{r}}$ is a vector from *O* to the mass, *m*, center, and $\mathbf{a}_O$ is the acceleration corresponding to the horizontal and vertical floor excitations. The moment of inertia for the rectangular rigid block around the corner can be expressed as

$$I_O = \frac{4}{3}mR_b^2. \tag{3.4}$$

By using the standard basis vectors, $\mathbf{e}_x$, $\mathbf{e}_y$, and $\mathbf{e}_z$, in Euclidean space, Equation (3.3) was reorganized with Equation (3.4) to obtain the following equation:

$$\begin{aligned} R_b \sin(\theta-\alpha)\mathbf{e}_x \times \left(-mg\mathbf{e}_y\right) \\ = -\frac{4}{3}mR_b^2\ddot{\theta}\mathbf{e}_z + \left(R_b \sin(\theta-\alpha)\mathbf{e}_x + R_b \cos(\theta-\alpha)\mathbf{e}_y\right) \\ \times m\left(\ddot{U}_f^x\mathbf{e}_x + \ddot{U}_f^y\mathbf{e}_y\right). \end{aligned} \tag{3.5}$$

After calculating the cross product in Equation (3.5), the equation of motion was written as

$$\begin{aligned} -mgR_b \sin(\theta-\alpha)\mathbf{e}_z \\ = \frac{4}{3}mR_b^2\ddot{\theta}\mathbf{e}_z + m\left(R_b \sin(\theta-\alpha)\ddot{U}_f^y - R_b \cos(\theta-\alpha)\ddot{U}_f^x\right)\mathbf{e}_z \end{aligned} \tag{3.6}$$

and then reorganizing Equation (3.6), Equation (3.7) was obtained as

$$\ddot{\theta} = \frac{3}{4R_b^2}\left(\left(g + \ddot{U}_f^y\right)R_b \sin(\theta - \alpha) - \ddot{U}_f^x R_b \cos(\theta - \alpha)\right). \quad (3.7)$$

Next, by rearranging Equation (3.7), the rocking equation of motion became

$$\ddot{\theta} = -p^2\left[\left(1 + \frac{\ddot{U}_f^y}{g}\right)\sin(\alpha - \theta) + \frac{\ddot{U}_f^x}{g}\cos(\alpha - \theta)\right], \quad (3.8)$$

where

$$p = \sqrt{\frac{3g}{4R_b}} \quad (3.9)$$

where

$$R_b = \sqrt{\left(b/2\right)^2 + \left(h/2\right)^2} \quad (3.10)$$

and where p and R_b denote the frequency parameter and the distance from corners to the mass center, respectively.

The frequency parameter indicates that as the block size based on R_b increases, the frequency parameter decreases, and the frequency is also related to the amplitude of the gravitational field, g. As Housner (1963) stated, the vibration frequency of a rigid block subjected to free vibration is not constant because it is proportional to the magnitude of the vibration. Regarding the point *O*, the same derivation can be rewritten as

$$\ddot{\theta} = -p^2\left[\left(1 + \frac{\ddot{U}_f^y}{g}\right)\sin(-\alpha - \theta) + \frac{\ddot{U}_f^x}{g}\cos(-\alpha - \theta)\right]. \quad (3.11)$$

The combination of Equation (3.8) and Equation (3.11) then resulted in the complete equation of motion for a pure planar rocking response of a rigid block as follows:

$$\ddot{\theta} = -p^2\left[\left(1 + \frac{\ddot{U}_f^y}{g}\right)\sin(\mathrm{sgn}(\theta)\alpha - \theta) + \frac{\ddot{U}_f^x}{g}\cos(\mathrm{sgn}(\theta)\alpha - \theta)\right]. \quad (3.12)$$

By using the numerical integration solver, ODE45, with Event Location in MATLAB, the solution of Equation (3.12) was determined through a state-space formulation in which the state vector **x** and the time-derivative vector, **y**(**x**, *t*), are determined with the following expressions:

$$\mathbf{x} = \begin{Bmatrix} \theta \\ \dot{\theta} \end{Bmatrix} \tag{3.13}$$

$$\dot{\mathbf{x}} = \mathbf{y}(\mathbf{x}, t) = \begin{Bmatrix} \dot{\theta} \\ -p^2 \left[\left(1 + \frac{\ddot{U}_f^y}{g} \right) \sin(\text{sgn}(\theta)\alpha - \theta) + \frac{\ddot{U}_f^x}{g} \cos(\text{sgn}(\theta)\alpha - \theta) \right] \end{Bmatrix}. \tag{3.14}$$

3.1.2. Coefficient of Restitution

Assumedly, the rigid block smoothly transitions from O' to O. This requires the block's angular momentum to be conserved both immediately before and after the impact at point *O* and *O*'. Energy loss in the solution of Equation (3.12) was applied due to impact at the bottom corners (point *O* and *O*'). In order to define this energy loss associated with impact at *O* and *O*', the coefficient of restitution, *e*, method was used. Fundamentally, this method asserts that the ratio of the block's angular speed just after impact to its angular speed right before impact can be expressed as

$$e = \frac{\dot{\theta}_2}{\dot{\theta}_1} \tag{3.15}$$

where the subscripts 2 and 1 represent after and before impact, accordingly. However, in accordance with Housner's (1963), we used the coefficient of restitution for a rigid block written as

$$e_{max} = 1 - \frac{3}{2} \sin^2 \alpha. \tag{3.16}$$

The coefficient of restitution defined in Equation (3.16) is the maximum value of *e*, that a block with slenderness, α, would rock. The value of $e_{\max}$ is dependent on the block's slenderness.

3.1.3. Derivation of Vertical Reaction Force on Rocking Response

High vertical floor accelerations can cause the rigid blocks to jump at their corners under rocking motions. In this case, the equation of motion for the pure rocking behavior, Equation (3.12), becomes invalid. Therefore, the vertical force at the bottom corners should be monitored, as Linde et al. (2020) developed. They simply derived the normalized vertical force using dynamic equilibrium by tracking the vertical force at the rocking corner throughout the solution, as follows (Linde, 2016):

$$F_y = m\left(\ddot{\bar{y}} + \ddot{U}_f^y + g\right) \tag{3.17}$$

where F_y denotes the vertical force. Additionally, the vertical distance can expressed as

$$\bar{y} = R_b \cos(\alpha - |\theta|). \tag{3.18}$$

By taking the derivative of Equation (3.18) twice resulted in the vertical acceleration:

$$\ddot{\bar{y}} = R_b \text{sgn}(\theta)\ddot{\theta} \sin(\alpha - |\theta|) - R_b\dot{\theta}^2 \cos(\alpha - |\theta|) \tag{3.19}$$

and substituting Equation (3.19) into Equation (3.17), the force becomes

$$F_y = m\left\{\text{sgn}(\theta)R_b\ddot{\theta} \sin(\alpha - |\theta|) - R_b\dot{\theta}^2 \cos(\alpha - |\theta|)\right\}. \tag{3.20}$$

Then the vertical force normalized by the weight of the rigid block can be written as

$$\overline{f}_y = 1 + \text{sgn}(\theta)\frac{R_b\ddot{\theta}}{g}\sin(\alpha - |\theta|) - \frac{R_b\dot{\theta}^2}{g}\cos(\alpha - |\theta|) + \frac{\ddot{U}_f^y}{g}. \tag{3.21}$$

If the normalized vertical force is a negative value at any instant time, our analysis in MATLAB gives error to inform users that the rigid block has recently jumped; therefore, the pure rocking motion is not valid under this condition.

3.2. Freestanding Contents Rocking Response

Makris and Roussos (2000) investigated that overthrowing of smaller blocks is shown to be more susceptible to the peak ground acceleration, while overturning of larger blocks is reported to be primarily dependent on the long-duration pulse. In other words, high-frequency oscillations, that dominate the long-duration pulse in the excitation, can induce the smaller blocks to overturn, whereas the dynamic characteristic of the long-duration excitation can lead the larger blocks to topple. Motivated by Makris and Roussos's work (2000) and the full-scale TFP base-isolated experiment at E-Defense (Ryan and Dao, 2015), we investigated the effect of high fluctuations generated by the TFP type isolation system due to the inclusion of vertical ground motion in the analyses on the horizontal floor acceleration, which serves as the seismic demand for acceleration-sensitive nonstructural contents.

3.3. Effect of High Frequency Oscillations in Trigonometric Excitation

Under the 1999 Kocaeli, Iznik earthquake, the roof floor acceleration response values of our TFP base-isolated model were utilized to generate excitation through sine functions. In order for evaluating the rocking behavior of a rigid block subjected to high fluctuation, those sine functions included the first isolation mode (T_1 = 2.706 s) and the first structural mode (T_4 = 0.311 s) in addition to the vertical mode (T_7 = 0.125 s). Since it was stated that relatively small rigid blocks are influenced by the high fluctuations (Makris and Roussos, 2000), they were subjected to the sine functions and compared to larger ones with their equivalent slenderness. The toppling criteria was chosen as $\theta/\alpha = 1$ in all rocking analyses.

Figure 3.2 shows that the rocking response of the rigid block content, R_b = 0.268 m, $\alpha \approx 0.175$ rad (10° e.g., bookcase), and $p \approx 5.2$ rad/s, can be significantly affected by the high oscillations in the excitation. Figure 3.2(a) represents the rocking behavior of the block under the floor acceleration of the TFP base-isolated building without the H-V coupling effect. The vertical acceleration is, therefore, taken as zero. The amplitude of the horizontal excitation was adjusted to having a similar value of the roof floor acceleration due to the 1999 Kocaeli, Iznik earthquake. The block did not indicate any rocking behavior. However, as seen in Figure 3.2(b), the block rocked over the period of the excitation and eventually died out without toppling.

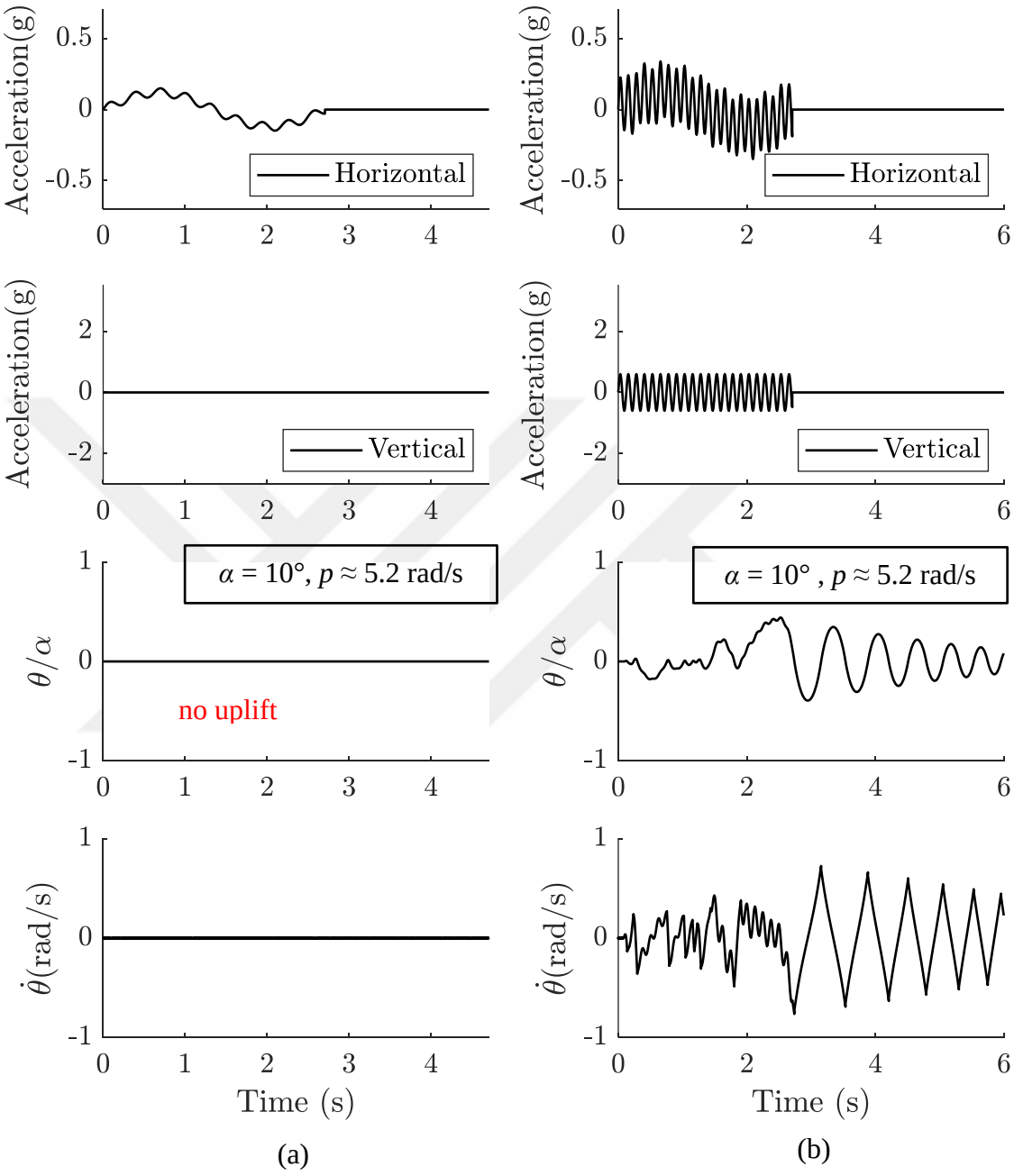

Figure 3.2. Rocking response of a relatively small rigid block (α = 10°, b = 0.093 m, h = 0.528 m, $p \approx 5.2$ rad/s) subjected to: (a) horizontal excitations and (b) highly fluctuated horizontal excitations with vertical components.

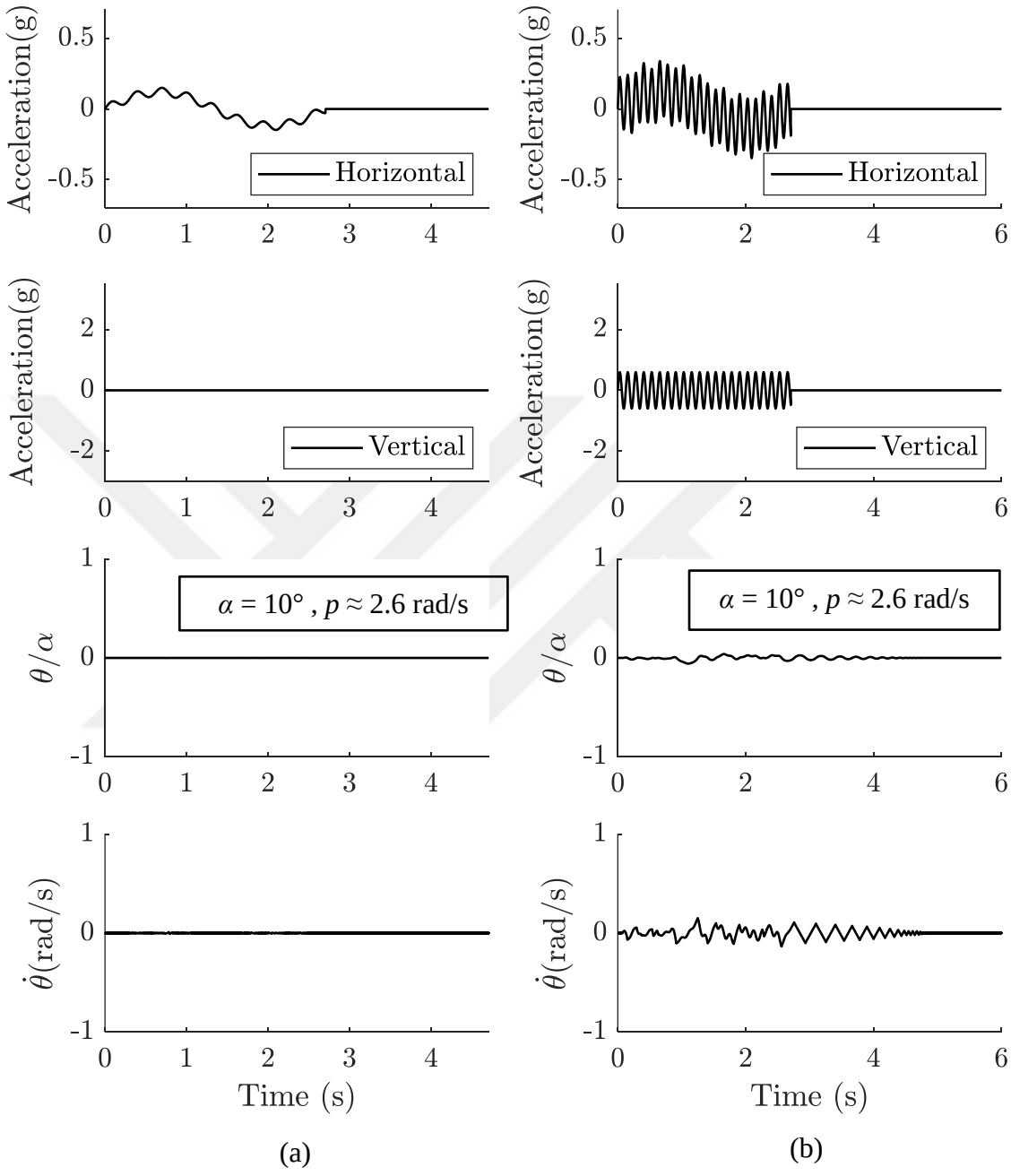

Figure 3.3. Rocking response of a relatively large rigid block (α = 10°, b = 0.372 m, h = 2.113 m, $p \approx 2.6$ rad/s) subjected to: (a) horizontal excitations and (b) highly fluctuated horizontal excitations with vertical components.

In comparison to the smaller rigid block, a larger rigid block with the same slenderness angle but different frequency parameter was chosen to understand the rocking response caused by the high oscillations referring to the base-isolated floor acceleration. Figure 3.3 shows that the long-period excitation governs the rocking behavior of the larger block. The effect of the higher frequency and vertical excitation were negligible, as indicated in Figure 3.3(b) and Linde et al. (2020) reported.

The same small size but slenderer rigid block was also investigated in order to understand how the high fluctuations influence the rocking response. As seen in Figure 3.4(a), the small block having a slenderness of 8.5° did not move throughout the excitation, whereas Figure 3.4(b) indicates that the high fluctuations in the horizontal excitation led the rigid block to overturn. Another rigid block with the same slenderness of 8.5° but a bigger size resulted in very little rocking behavior during the excitation, as shown in Figure 3.5. The vertical excitation and the fluctuations in the horizontal direction showed again negligible effect on the comparatively large rigid block. Moreover, Figure 3.6 to Figure 3.9 also highlighted the same behavior, and increasing the slenderness led rigid blocks to be less affected by the high fluctuations in the excitations.

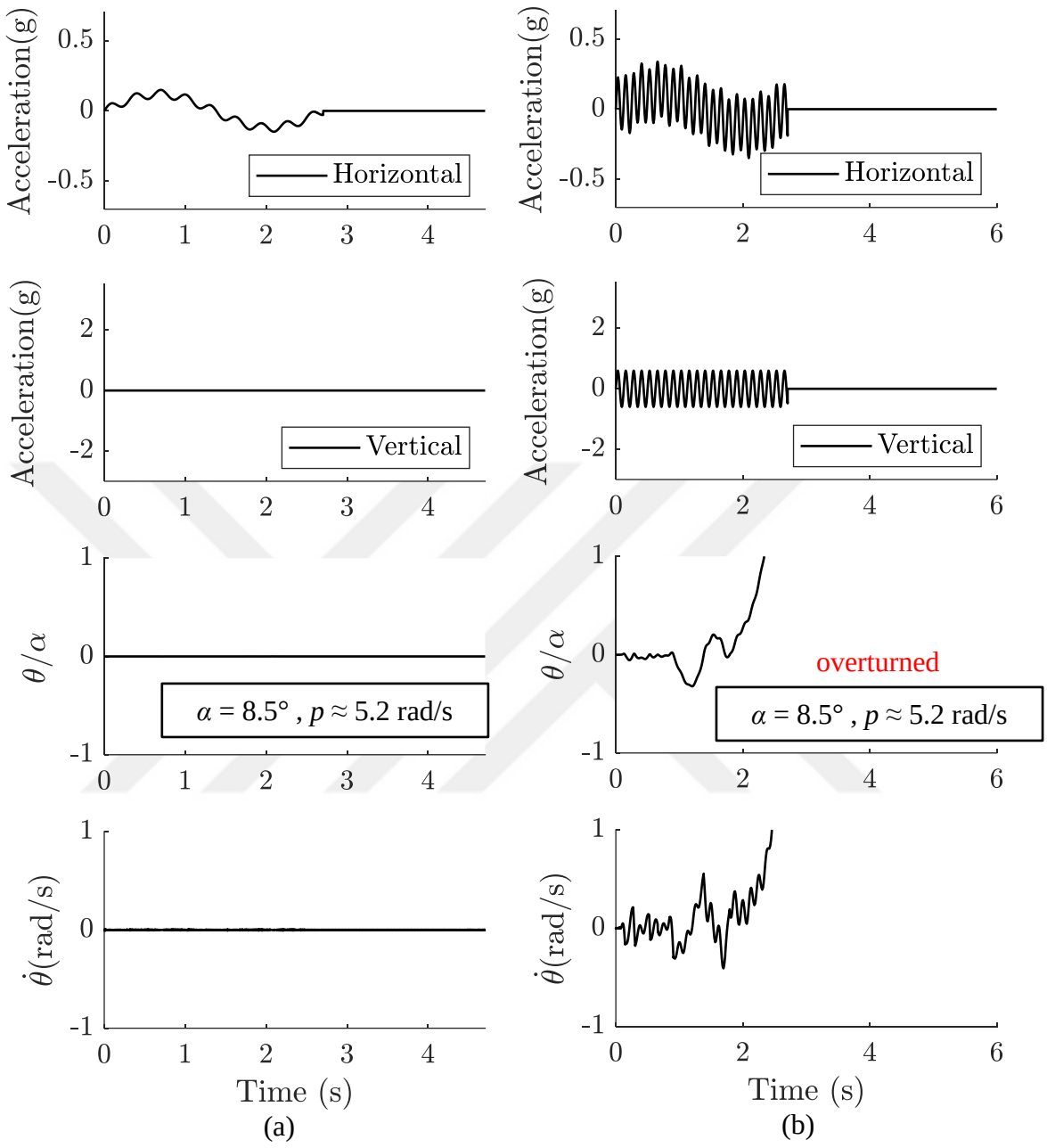

Figure 3.4. Rocking response of a relatively small rigid block (α = 8.5°, b = 0.08 m, h = 0.535 m, $p \approx 5.2$ rad/s) subjected to: (a) horizontal excitations and (b) highly fluctuated horizontal excitations with vertical components.

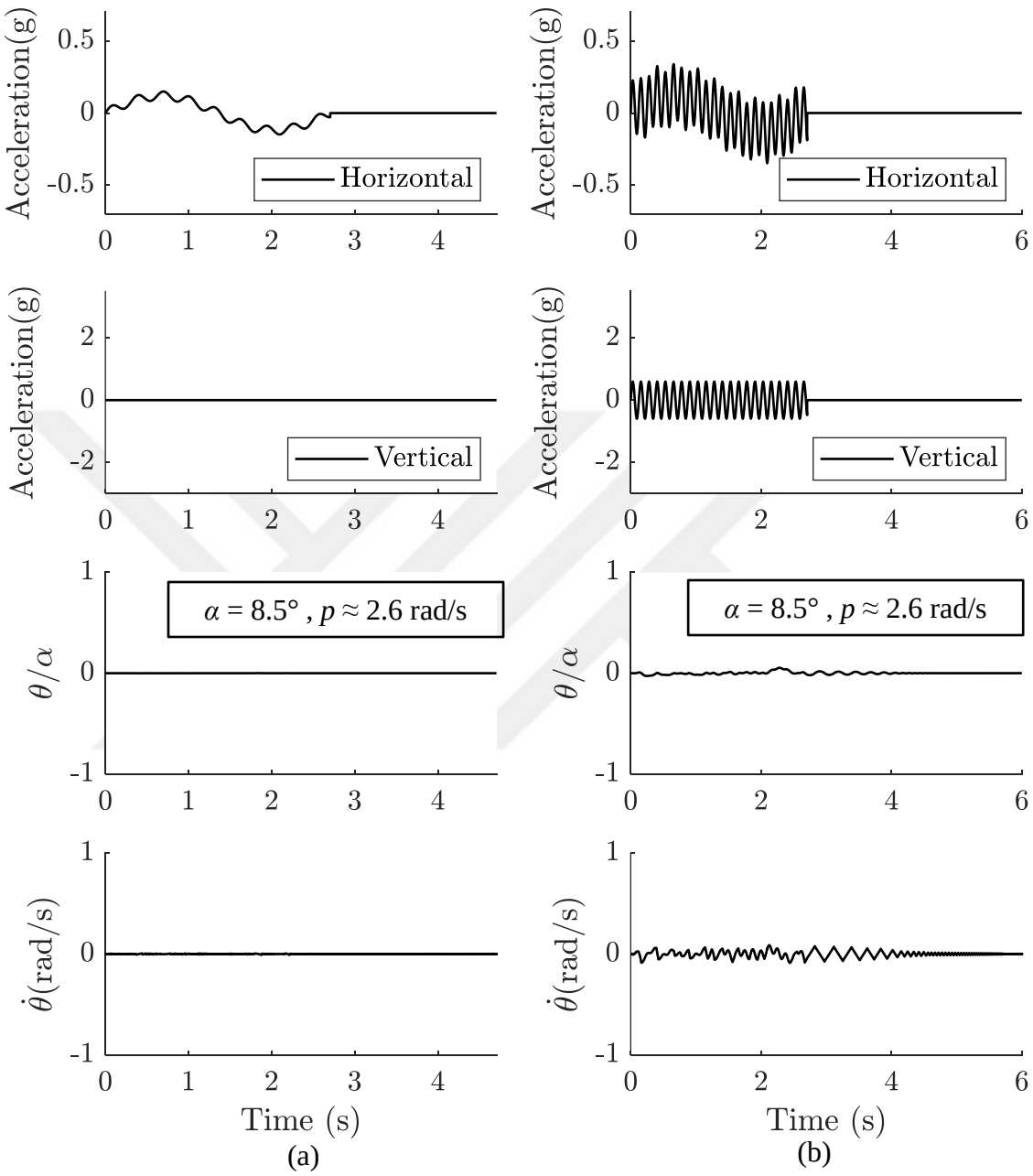

Figure 3.5. Rocking response of a relatively large rigid block (α = 8.5°, b = 0.318 m, h = 2.114 m, $p \approx$ 2.6 rad/s) subjected to: (a) horizontal excitations and (b) highly fluctuated horizontal excitations with vertical components.

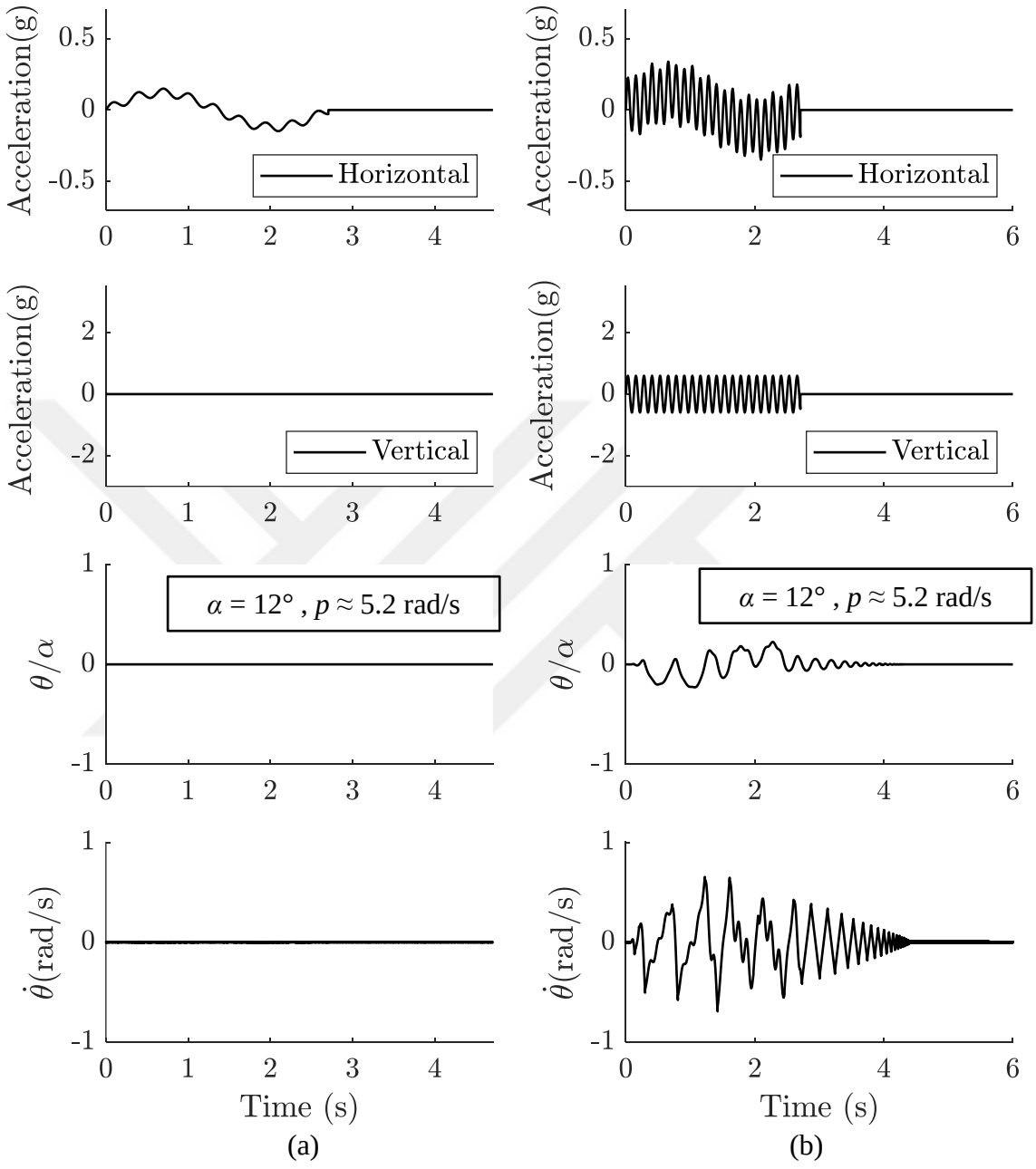

Figure 3.6. Rocking response of a relatively small rigid block (α = 12°, b = 0.113 m, h = 0.53 m, $p \approx$ 5.2 rad/s) subjected to: (a) horizontal excitations and (b) highly fluctuated horizontal excitations with vertical components.

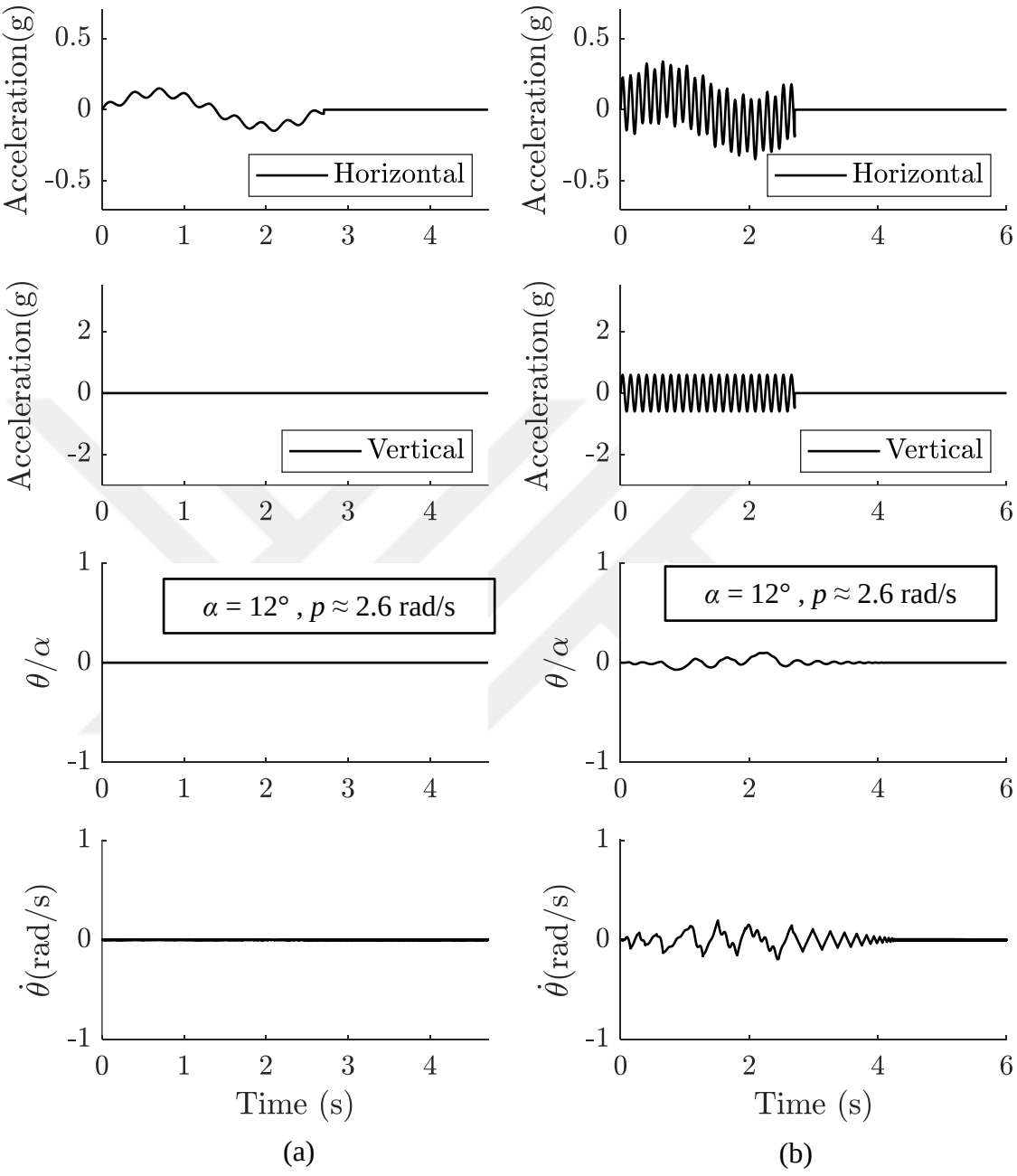

Figure 3.7. Rocking response of a relatively large rigid block (α = 12°, b = 0.448 m, h = 2.1 m, $p \approx$ 2.6 rad/s) subjected to: (a) horizontal excitations and (b) highly fluctuated horizontal excitations with vertical components.

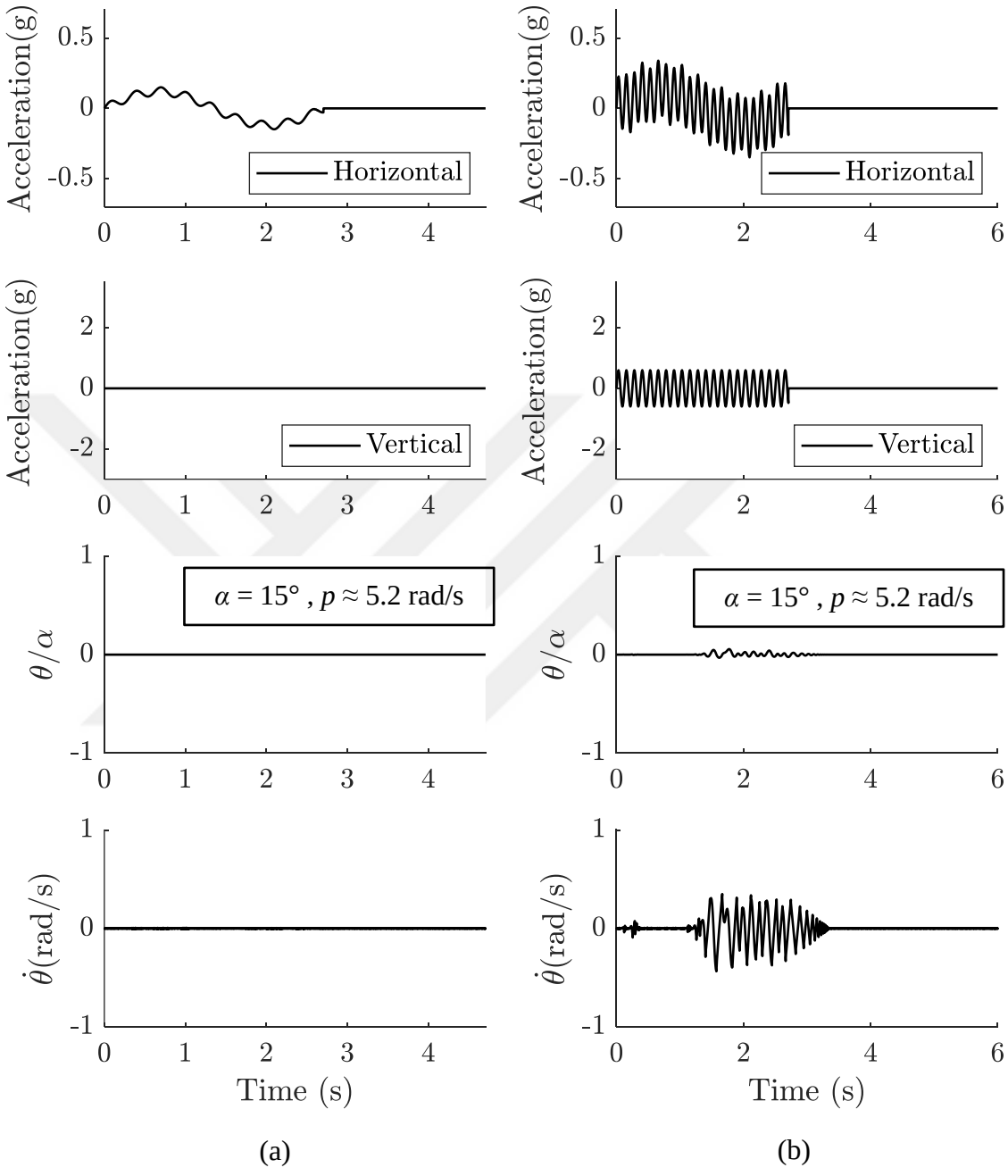

Figure 3.8. Rocking response of a relatively small rigid block (α = 15°, b = 0.142 m, h = 0.53 m, $p \approx$ 5.2 rad/s) subjected to: (a) horizontal excitations and (b) highly fluctuated horizontal excitations with vertical components.

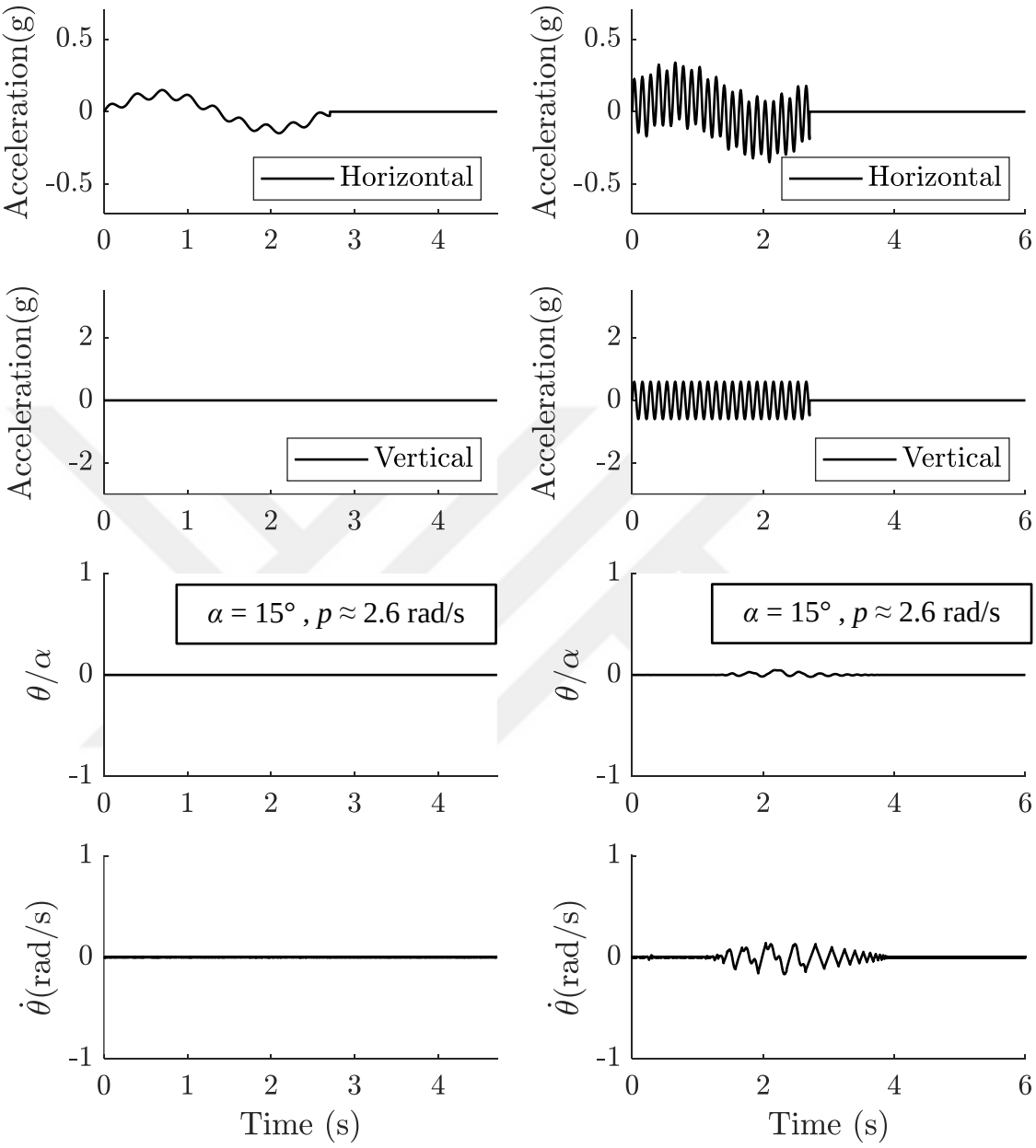

(a) (b)

Figure 3.9. Rocking response of a relatively large rigid block (α = 15°, b = 0.558 m, h = 2.1 m, $p \approx$ 2.6 rad/s) subjected to: (a) horizontal excitations and (b) highly fluctuated horizontal excitations with vertical components.

3.3.1. Effect of Horizontal- Vertical Coupling on Rocking Response

Since Ryan et al. (2012) revealed the H-V coupling phenomenon through their full-scale experimental research at E-Defense, researchers have focused on quantifying the response of buildings, especially base-isolated ones, under the horizontal-vertical ground motions. (Dao and Ryan, 2014; Giammona et al., 2015; Ryan and Dao, 2015; Guzman and Ryan, 2018; Guzman and Ryan, 2020). Additionally, Linde (2016) conducted the first study on the pure planar rocking response of freestanding contents in base-isolated buildings using floor accelerations and taking the H-V effect into account. In that study, the stiffness damping model was used, as Ryan and Polanco (2008) suggested, to perform nonlinear time history analyses of the base-isolated buildings. However, Dao and Ryan (2014) concluded that although the stiffness damping approach matches well with the test data (e.g., floor acceleration) under horizontal ground motions, this approach led the high frequency modes to dampen and thereby considerably underestimating the floor accelerations under 3D earthquakes. They suggested that the constant damping model would be the most appropriate approach for the base-isolated buildings. Then Giammona et al. (2015) used the constant damping method with 0% damping in the first isolation modes and 2% for the rest. However, they obtained that the SAP2000 TFP base-isolated building model with the given damping values overestimate the floor acceleration of the full-scale base-isolated building tested at E-Defense. Guzman and Ryan (2018) and Guzman and Ryan (2020) also applied the constant damping ratio, 2.5%, for all modes but 5% in the first vertical mode by using Modal Damping Overrides in SAP2000. As a consequence of the underestimated and overestimated floor acceleration approaches associated with damping values in the literature, our study selected that the stiffness damping method is used with Modal Damping Overrides at the first vertical mode in order for well capturing the real H-V effect. By doing this, the floor acceleration responses of our TFP base-isolated building model showed similar results that the full-scale experiment at E-Defense experienced under the 3D ground motions (Dao and Ryan 2014).

Figure 3.10 shows that the H-V coupling effect in the floor acceleration caused rocking for the relatively small rigid block, whereas Figure 3.11 indicates that the larger rigid block with the same slenderness resulted in negligible movement.

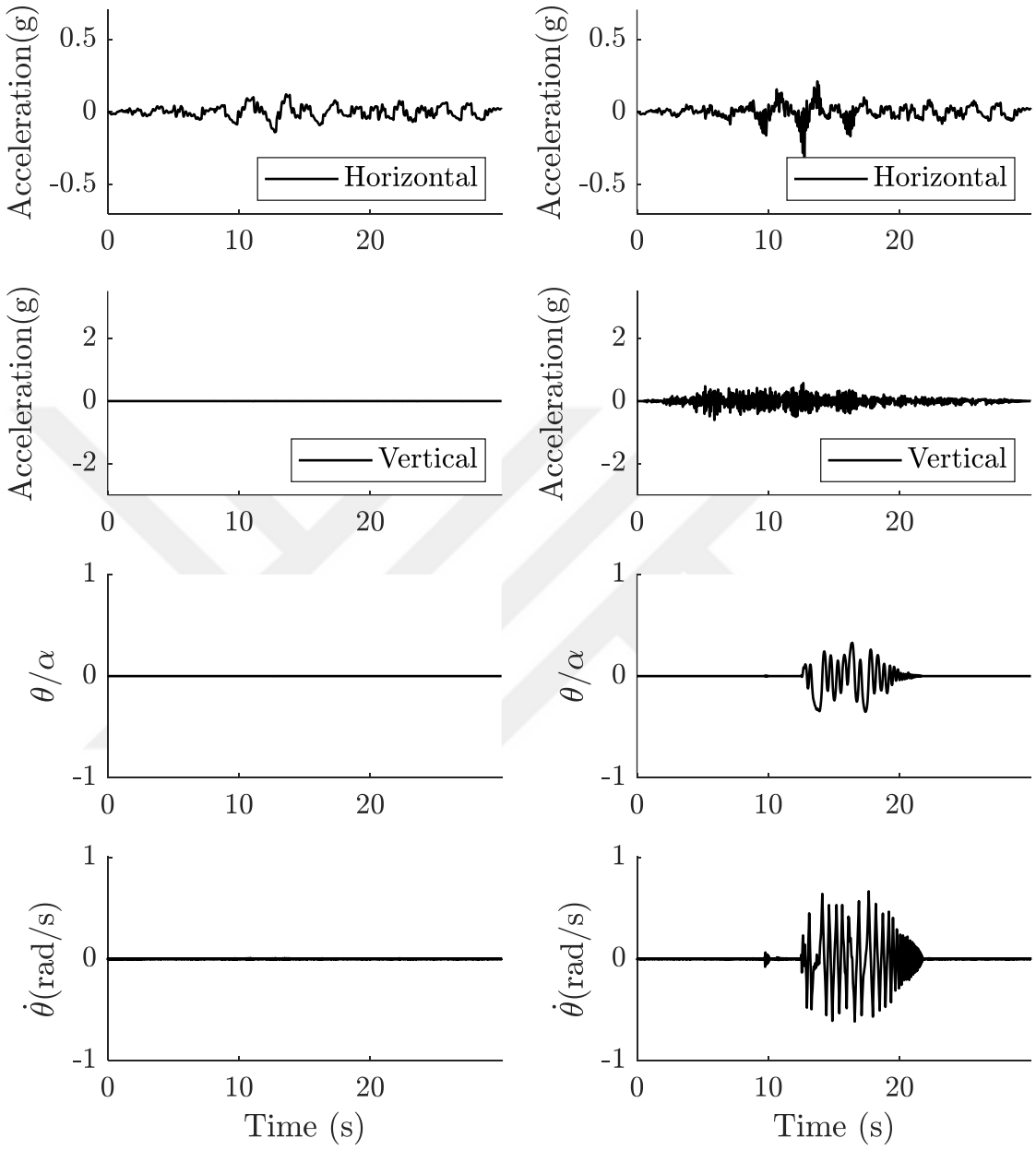

Figure 3.10. Rocking response of a relatively small rigid block (α = 10°, b = 0.093 m, h = 0.528 m, $p \approx 5.2$ rad/s) subjected to: (a) horizontal and (b) the H-V coupled floor accelerations induced by the 1999 Kocaeli, Iznik earthquake.

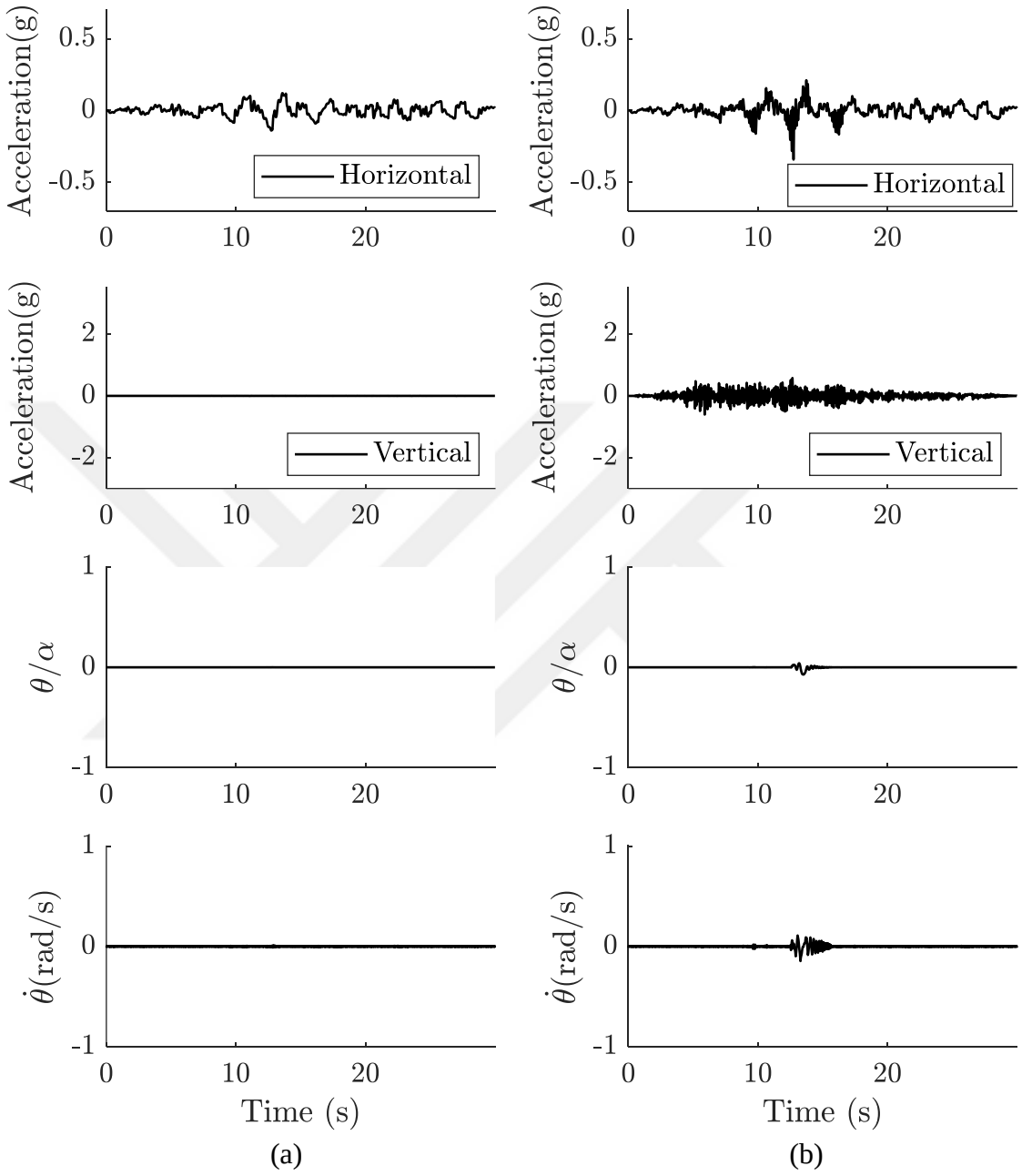

Figure 3.11. Rocking response of a relatively large rigid block (α = 10°, b = 0.372 m, h = 2.113 m, $p \approx 2.6$ rad/s) subjected to: (a) horizontal and (b) the H-V coupled floor accelerations induced by the 1999 Kocaeli, Iznik earthquake.

Figure 3.12 and Figure 3.13 display that the H-V coupling response had a substantial effect on the rocking response of rigid blocks, particularly smaller ones with lower slenderness. Although the difference in the larger blocks' rocking behavior between horizontal only and horizontal-vertical was comparably less, it become considerably greater for small blocks, especially the ones with the so-called frequency of less than 1.5 s. This signicant difference was more pronounced for blocks having a 8.5° slenderness, as seen in Figure 3.12(a).

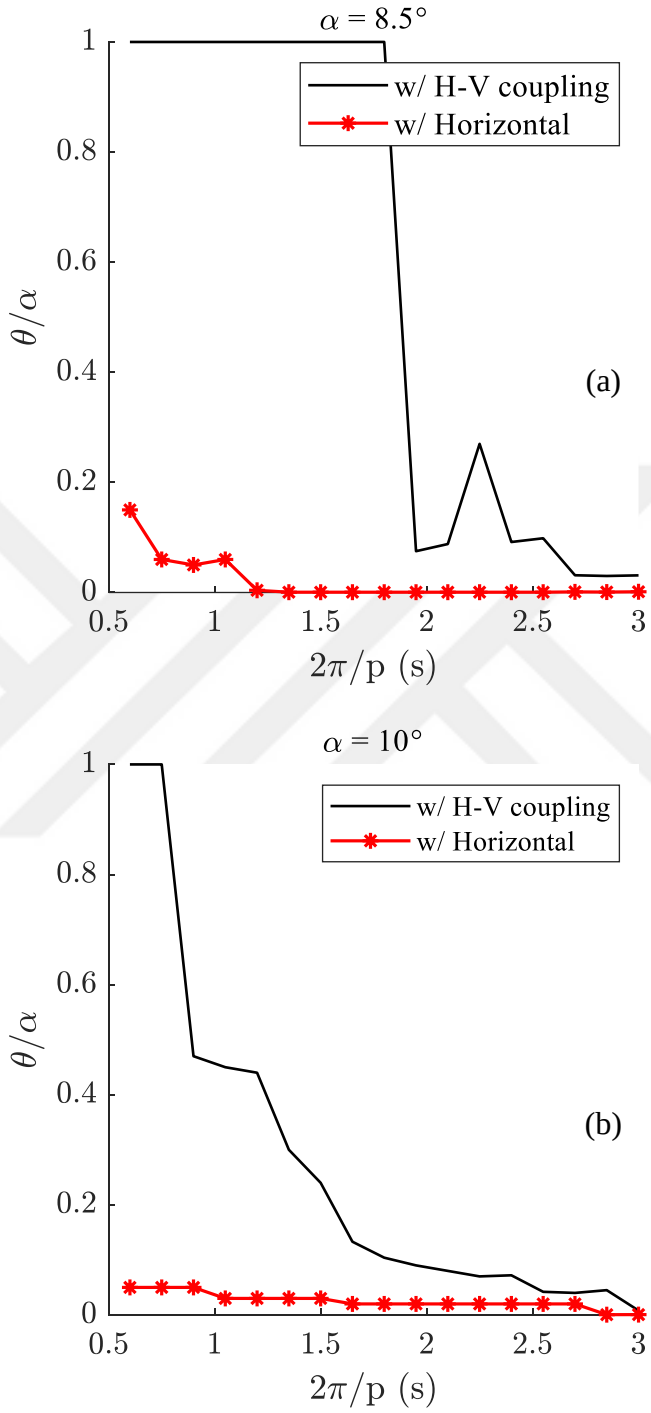

Figure 3.12. Rocking response of rigid blocks: (a) 8.5° and (b) 10° under the Horizontal-Vertical coupling and Horizontal only floor accelerations due to the 1999 Kocaeli, Iznik earthquake.

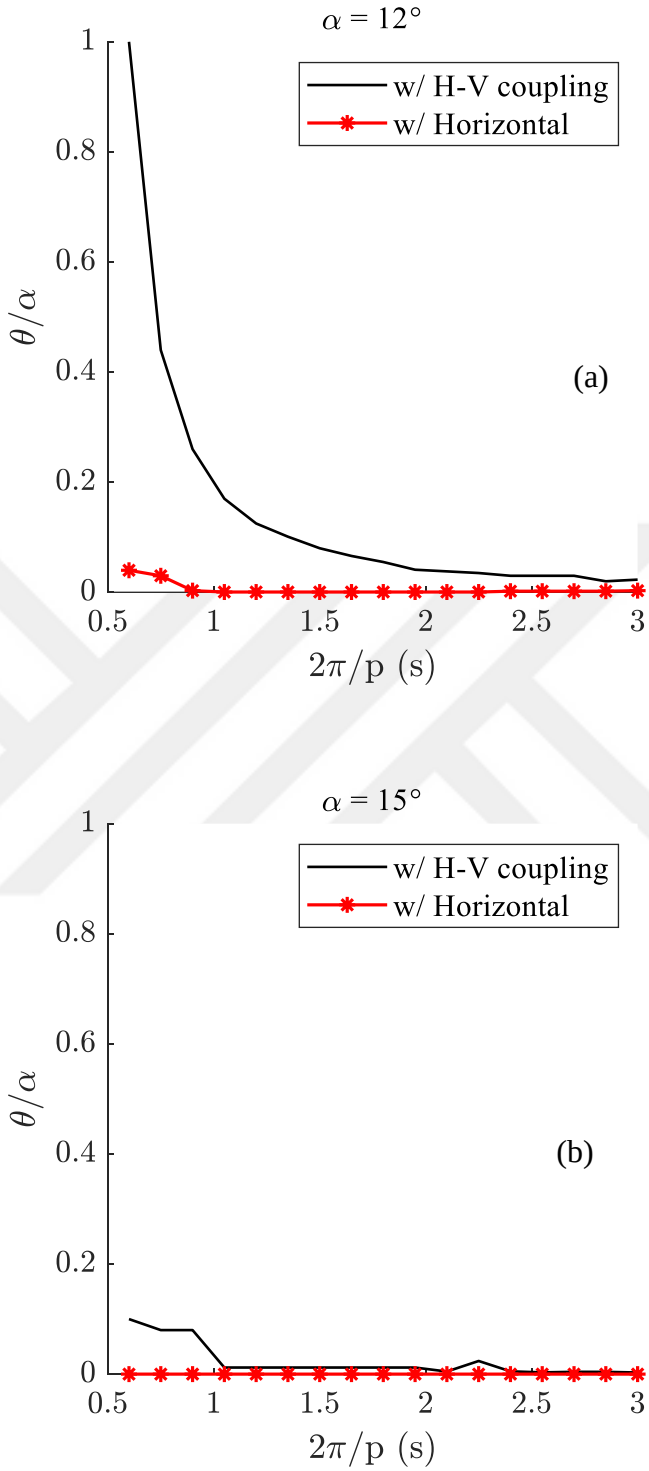

Figure 3.13. Rocking response of rigid blocks: (a) 12° and (b) 15° under the Horizontal-Vertical coupling and Horizontal only floor accelerations due to the 1999 Kocaeli, Iznik earthquake.

Figure 3.12 and Figure 3.13 show the similar behavior of the rigid blocks with the frequency parameters, p = 2.6 rad/s and p =5.2 rad/s under the trigonometric excitations, seen in Figure 3.2 to Figure 3.9, generated using the building response induced by the 1999 Kocaeli, Iznik earthquake. When subjected to horizontal excitations, the majority of blocks did not show considerable rocking and overturning. The H-V coupling effect, however, caused these blocks to rock or even topple, especially the slenderer ones. Moreover, although the H-V response due to the 1999 Kocaeli, Iznik earthquake did not lead the rigid blocks with a 15° slenderness to rock considerably, the H-V response of the 2010 Darfield, SPFS earthquake caused significant rocking motions. Therefore, Figure 3.14 shows that the rocking spectra of the 15° rigid block are more pronounced.

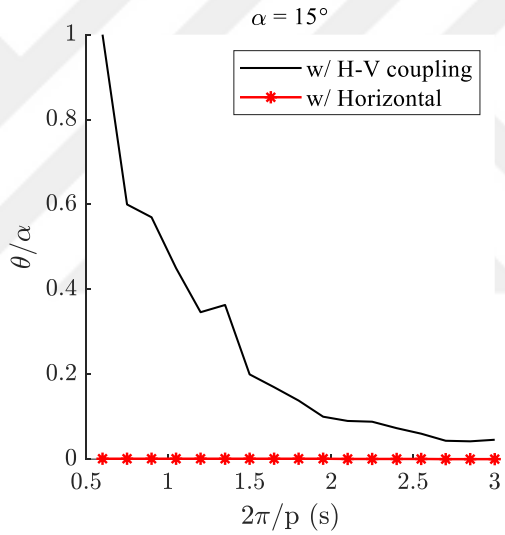

Figure 3.14. Rocking response of rigid blocks with a slenderness of 15° under the Horizontal-Vertical coupling and Horizontal only floor accelerations due to the 2010 Darfield, SPFS earthquake.

Figure 3.15 and Figure 3.16 show that the mean of the 10 ground motions' rocking spectra of the rigid blocks with slenderness of 8.5°, 10°, 12°, and 15°. Apparently, the inclusion of the H-V effect resulted in increasing the seismic demand in terms of rocking for freestanding rigid blocks in a TFP base-isolated building model. The 1992 Landers, Morongo Valley Hall (GEOS #58) was omitted from the rocking response evaluation since the vertical component of this ground motion caused jumping, which made the pure planar rocking response analysis invalid.

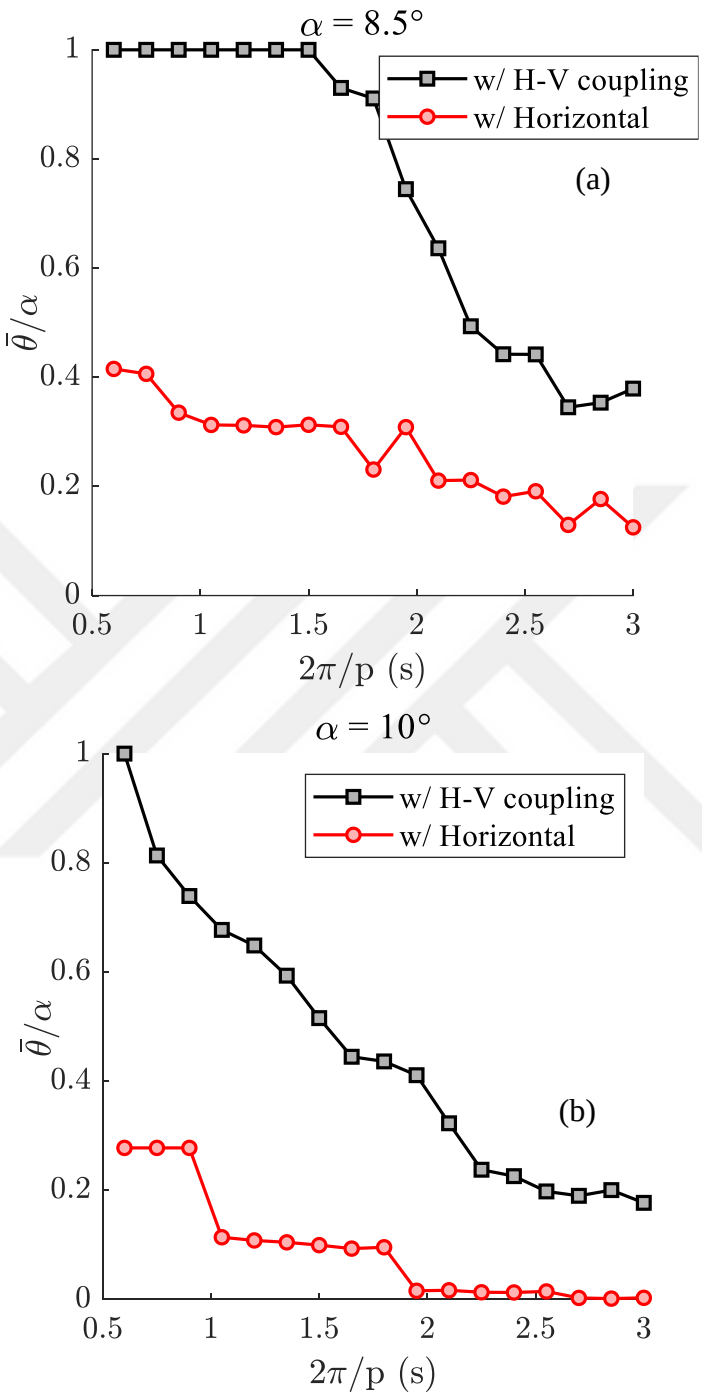

Figure 3.15. Rocking response spectra of the two rigid block types (a) 8.5° and (b) 10° subjected to 10 earthquakes with and without horizontal-vertical (H-V) coupling effect.

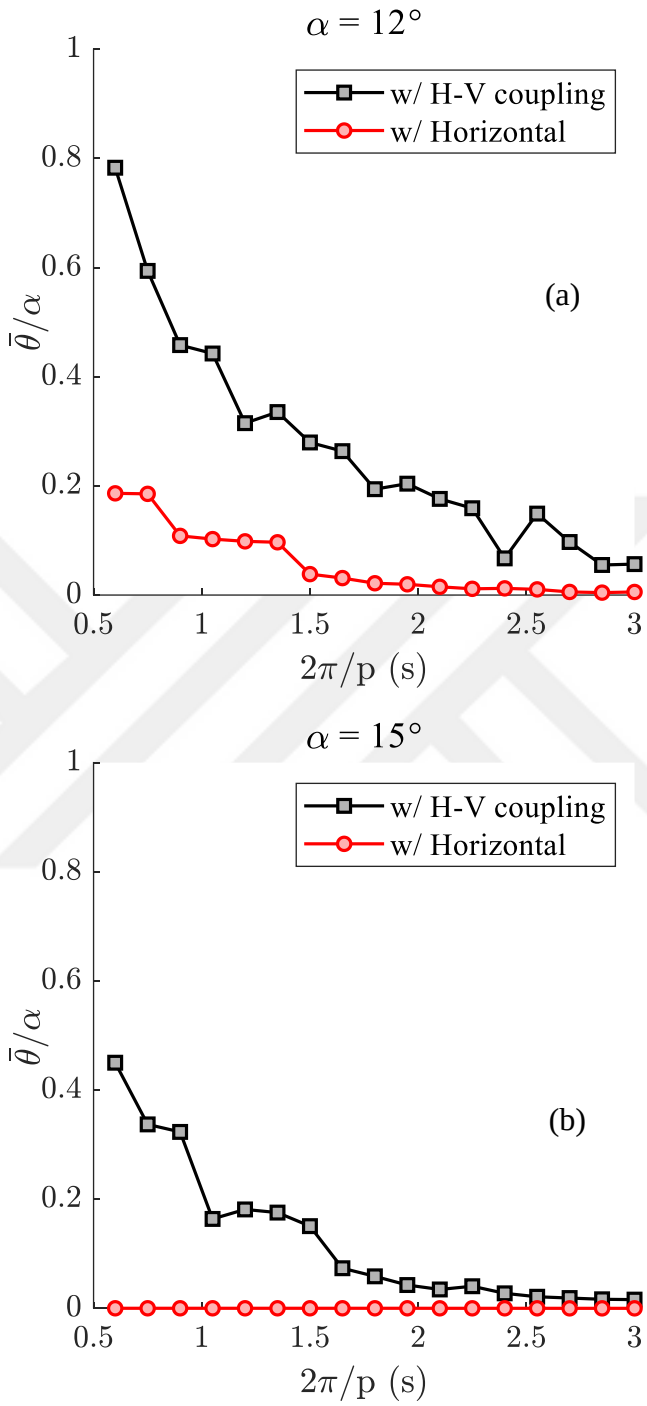

Figure 3.16. Rocking response spectra of the two rigid block types (a) 8.5° and (b) 10° subjected to 10 earthquakes with and without horizontal-vertical (H-V) coupling effect.

3.3.2. Effect of Story Level

As the mean absolute peak floor accelerations of the TFP base-isolated building model were shown in Figure 2.15, the similar highest acceleration values were at the Roof floor and the 2nd floor, except for the base, whereas the 3rd floor had the lowest acceleration values. Therefore, the rigid blocks subjected to the Roof and 2nd floor accelerations were compared. Figure 3.17 indicates that the smaller blocks, especially the ones having less than the so-called frequency of 1.5 s, experienced rocking motion greater than the larger blocks, as expected. Since both the horizontal and vertical accelerations at the 3rd floor were less than the values of the Roof floor, the rigid blocks were less likely to rock. The reason for excluding base floor accelerations from the rocking response analysis in this study is because our base-isolated building model generated higher floor accelerations than the base floor accelerations of the full-scale test building at E-Defense (Dao and Ryan, 2014). Although Dao and Ryan (2014) obtained the test data for the base floor acceleration around 0.4 g, their computer modeling buildings with various damping ratios also overestimated the actual data. In order to avoid this, we omitted the base floor accelerations from rocking response analyses.

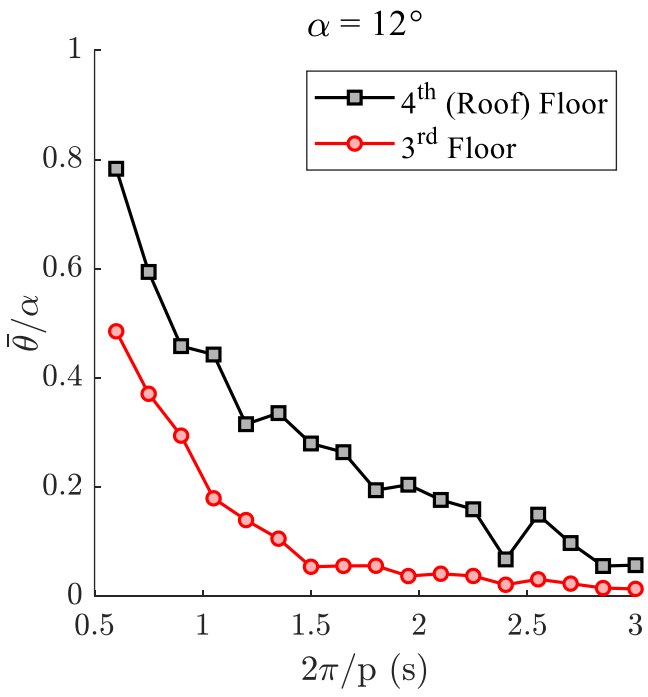

Figure 3.17. Comparison of the rigid blocks with slenderness of 12° under the horizontal and vertical coupled floor accelerations.

3.4. Freestanding Rigid Block Jumping Response

In terms of vertical acceleration on base-isolated structures, Furukawa et al. (2013) observed that, while base isolation systems minimize horizontal floor acceleration, vertical excitation beyond 1g caused jumping in the response of nonstructural contents. Throughout the rocking response analyses, the vertical force was controlled using Equation (3.21), Linde et al. (2020) developed. This equation terminates the analysis if there is jumping, indicated by the first negative value in the force vector, under the horizontal and vertical excitations. Then based on the different slabs locations on the entire building plan in Figure 2.19, the data obtained from the rocking response analyses were rearranged. Figure 3.18 shows that once the vertical seismic demand was beyond 1g, the rigid blocks jumped. As a consequence, the jumping results indicate that the analyses are capable of capturing the actual nonstructural contents' response when the vertical excitation is included.

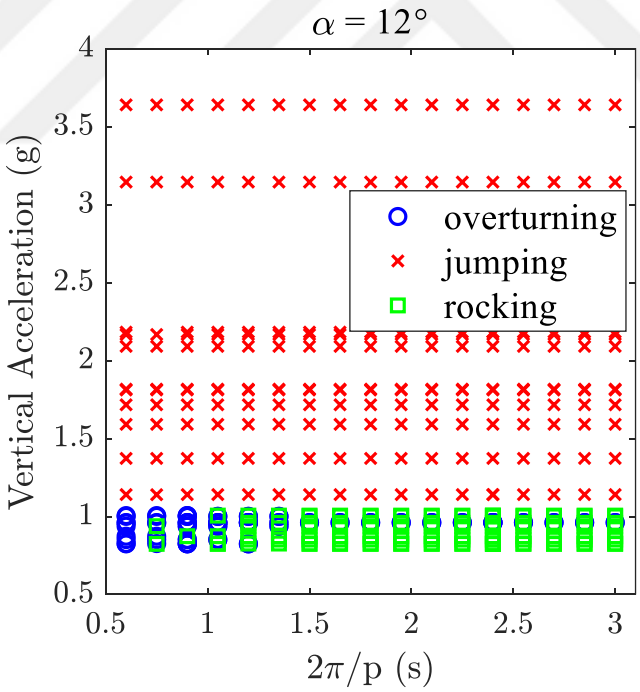

Figure 3.18. Jumping response of the rigid blocks with slenderness of 12° on the various slabs.

4. CONCLUSIONS AND RECOMMENDATIONS

4.1. Summary

The motivation of this research was to investigate the seismic behavior of the nonstructural components in a TFP base-isolated building under the three components of the ground motions. The building model with triple friction bearings was developed in SAP2000. The seismic demand for the design of the TFP bearings were obtained per TBSC (2018), and the geometrical properties of the TFP bearings were determined via an iterative MATLAB code. The base-isolated building model was subjected to the 11 ground motion pairs to determine floor accelerations in the horizontal and vertical direction. The H-V coupling effect in the response was compared to the case, where the building model was solely subjected to the horizontal ground motions. The inclusion of the vertical component in the analysis significantly increased the seismic demand, especially floor accelerations in both directions. Although the building model was sound under the ground motions scaled in accordance with TBSC (2018), the nonstructural components could experience some damage from minor to moderate due to the direct effect of the vertical ground motions above 1-2g. Below this range, the acceleration sensitive freestanding building contents experienced rocking and overturning. The H-V coupling had a significant influence on the rocking analyses. The comparably small and slender contents were greatly affected by the H-V coupling response. The relatively larger and stockier blocks were clearly less influenced by the H-V coupling effect. Since the contribution from the higher mode was predominant in the horizontal response, the 3rd floor experienced the lowest floor acceleration, thereby reducing the rocking and overturning cases, as opposed to the first and 2nd floor. The rocking response analyses were able to capture the jumping response. Once the vertical acceleration demand exceeds 1g, the freestanding rigid blocks began jumping.

Overall, the TFP base isolation system effectively prevented larger and stockier rigid blocks from severe rocking and overturning, whereas this system was less effective for smaller and slenderer rigid blocks when compounded with the H-V coupling effect. The jumping response of the unanchored acceleration-sensitive contents governed the nonstructural components' failure type when the vertical acceleration is above 1g.

4.2. Recommendation and Future Study

The main recommendation of this research is that the H-V coupling effect needs to be carefully evaluated for critical facilities, especially the friction pendulum-type base-isolated buildings, regarding the assessment of their seismic performance of nonstructural components. Due to its axial force dependent frictional system, the horizontal response of the building is affected by the inclusion of the vertical component of ground motions. Omitting the vertical accelerations from the nonlinear time-history analyses resulted in underestimating the horizontal floor accelerations in the TFP base-isolated building model, which is the governing seismic demand parameter for acceleration-sensitive nonstructural components. Although the TFP base-isolated critical buildings, such as hospitals where the medical equipment and contents are essential to keep the facility operational, can be structurally sound under seismic events, its nonstructural components need proper assessment of their seismic performance to remain functional during and after major earthquakes.

In this research, a hypothetical four-story reinforced concrete triple friction pendulum base-isolated hospital building was used to investigate the structural and nonstructural components' response under earthquakes. Further research is clearly required for many types of buildings. The influence of higher modes due to the H-V coupling response may be examined in a TFP base-isolated building with more stories to determine if the horizontal floor acceleration is amplified more. Additionally, near-fault type earthquakes and different soil types can be used to further investigate the seismic response of both structural and nonstructural components in friction-based isolated buildings. Given that the rocking response is highly dependent on the floor acceleration, the floor acceleration obviously has to be quantified more precisely using accelerometer data from actual buildings and full-scale building experiments. For instance, a horizontal and vertical floor acceleration data set from an instrumented real base-isolated hospital with friction bearings, which experienced earthquakes before, can be used for input excitations in rocking response analyses of rigid blocks. Moreover, in addition to symmetrical rigid blocks, nonstructural contents with vertical eccentricities can be analytically modeled and used in rocking response studies under floor accelerations.

REFERENCES

Acikgoz, S. and M. J. DeJong, 2012, "The interaction of elasticity and rocking in flexible structures allowed to uplift", *Earthquake Engineering & Structural Dynamics*, 41(15):2177-2194.

Acikgoz, S., Q. Ma, A. Palermo and M. J DeJong, 2016, "Experimental identification of the dynamic characteristics of a flexible rocking structure", *Journal of Earthquake Engineering*, 20(8), 1199–1221.

AFAD, 2021, *Turkish Earthquake Hazard Map*, Disaster and Emergency Management Presidency, https://tdth.afad.gov.tr/, accessed in June 2021.

Almazan, J. L. and J. C. De La Llera, 2002, "Analytical model of structures with frictional pendulum isolators" *Earthquake Eng. Stmct. Dyn.* 31, 305-332.

ASCE7-16, 2016, *American Society of Civil Engineers (ASCE). Minimum design loads for buildings and other structures*, Reston, VA.

Aslam, M., W. G. Godden and D. Scalise, 1980, "Earthquake Rocking Response of Rigid Bodies", *ASCE Journal of the Structural Division*, 106(ST2), 377–392.

Becker, T., 2011, *Advanced modeling of the performance of structures supported on triple friction pendulum bearings*, University of California, Berkeley.

Bozorgnia, Y., S. A. Mahin and G. Brady, 1998, "Vertical response of twelve structures recorded during the Northridge Earthquake", *Earthquake Spectra*, 41(3):411–432.

Caliò, I. and M. Marletta, 2003, "Passive control of the seismic response of art objects", *Engineering Structures*, 25:1009–1018.

Calvi, G. M., P. Ceresa, C. Casarotti, D. Bolognini and F. Auricchio, 2004, "Effects of axial force variation in the seismic response of bridges isolated with friction pendulum systems", *J. Earthquake Eng.*, 8(1), 187–224.

Çelebi, M., 1996, "Successful performance of a base-isolated hospital building during the 17 January 1994 Northridge earthquake", *The Structural Design of Tall Buildings*, 5, 95-109.

Chen, M. C., E. Pantoli, X. Wang, Astroza, R., H. Ebrahimian, T. C. Hutchinson, J. P. Conte, et al., 2016, "Full-scale structural and nonstructural building system performance during earthquakes: Part I – Specimen description, test protocol and structural response", *Earthquake Spectra*, 32, 737–770.

Chiozzi, A., M. Simoni and A. Tralli, 2014, "Rocking and overturning prevention for non-structural monolithic objects under seismic excitations through base isolation: a case study in ferrara (Italy)", *Proceeding of the 5th European Conference in Civil Engineering, ECCE 2014*, Florence, Italy.

CSI, 2017, *CSI Analysis Reference Manual (For SAP2000, ETABS, SAFE, and CSiBridge)*, Berkeley, California: Computers& Structures, Inc.

Dao, N. D. and K. L. Ryan, 2014, "Computational simulation of a full-scale, fixed-base, and isolated-base steel moment frame building tested at E-Defense", *Journal of Structural Engineering*, 140(8), A4014005.

Dar, A., D. Konstantinidis and W. W. El-Dakhakhni, 2016, "Evaluation of ASCE 43-05 seismic design criteria for rocking objects in nuclear facilities", *Journal of Structural Engineering*, 142 (11): 04016110.

Dimentberg, M., Y. Lin and R. Zhang, 1993, "Toppling of computer-type equipment under base", *Journal of Engineering Mechanics*, 199(1), 145–160.

Dimitrakopoulos, E. G. and M. J. DeJong, 2012, "Revisiting the rocking block: closed-form solutions and similarity laws", *Proceedings of The Royal Society A*, 468, 2294–2318.

Elnashai, A. S., 1997, "Seismic design with vertical earthquake motion", *Seismic Design Methodologies for the Next Generation of Codes*, Balkema Rotterdam: Faifa and Krawinkler (eds).

EPS, 2021, *Earthquake Protection Systems (EPS) Hospitals*. https://www.earthquakeprotection.com/hospitals, accessed on June 1, 2021.

Eröz, M. and R. DesRoches, 2008, "Bridge seismic response as a function of friction pendulum system (FPS) modeling assumptions", *Eng. Struct.*, 30(11), 3204–3212.

Federal Emergency Management Agency, 2012, *Reducing the risks of nonstructural earthquake damage – A practical guide - FEMA E-74*, FEMA, ATC.

Fenz, D. M. and M. C. Constantinou, 2008, *Development, implementation and verification of dynamic analysis models for multi-spherical sliding bearings MCEER-08-0018*, Buffalo, NY: Multidisciplinary Center for Earthquake Engineering Research.

Filiatrault, A. and T. Sullivan, 2014, "Performance-based seismic design of nonstructural building components: The next frontier of earthquake engineering", *Earthq. Eng. Eng. Vib.*, 13, 17–46.

Filiatrault, A., S. Kuan and R. Tremblay, 2004, "Shake table testing of bookcase-partition wall systems", *Canadian Journal of Civil Engineering*, 31 (4): 664–676.

Furukawa, S., E. Sato, Y. Shi, T. Becker and M. Nakashima, 2013, "Full-scale shaking table test of a base-isolated medical facility subjected to vertical motions", *Earthquake Engng Struct. Dyn.*, 42(13), 1931–1949.

Giammona, A. P., K. L. Ryan and N. D. Dao, 2015, "Evaluation of assumptions used in engineering practice to model buildings isolated with triple pendulum isolators in SAP2000", *Earthquake Spectra*, Volume: 31 issue: 2, page(s): 637-660.

Guzman, J. C. and K. L. Ryan, 2020, "Slab Vibration and Horizontal–Vertical Coupling in the Seismic Response of Low-rise Irregular Base-isolated and Conventional Buildings", *Journal of Earthquake Engineering*, 24:1, 1-36.

Guzman, J. C. and K. L. Ryan, 2018, "Computational Simulation of Slab Vibration and Horizontal-Vertical Coupling in a Full-Scale Test Bed Subjected to 3D Shaking at E-Defense", *Earthquake Engng Struct Dyn.*, 47:438–459.

Hogan, S. J., 1989, "On the Dyanmics of Rigid Block Motion under Harmonic Forcing", *Proceedings of the Royal Society of London*, Series A. 425: 441- 476.

Housner, G., 1963, "The behavior of inverted pendulum structures during earthquakes", *Bulletin of the Seismological Society of America*, 53:403–417.

Ibarra, L., 2016, *Seismic Performance of Dry Casks Storage for Long-term Exposure*, NEUP 12-3756 Final Report, Nuclear Energy University Programs/University of Utah, Salt Lake City, UT.

Ishiyama, Y., 1982, "Motions of rigid bodies and criteria for overturning by earthquake excitations", *Earthquake Engineering & Structural Dynamics*, 10(5), 635–650.

Kamil, A. and C. C. Tung, 2001, "Energy balance equation for estimating overturning potential of an unanchored rocking body subjected to earthquake excitation", *Earthquake Spectra*, 17 (2): 209–220.

Khoshnoudian, F. and M. Rabiei, 2010, "Seismic Response of Double Concave Friction Pendulum Base-Isolated Structures Considering Vertical Component of Earthquake", *Advances in Structural Engineering*, 13(1):1-13.

Kircher, A. C., 2003, "It makes dollars and sense to improve nonstructural system performance", *Proceedings of ATC 29-2 Seminar on Seismic Design, Performance and Retrofit of Nonstructural Components in Critical Facilities*, Newport Beach, CA: Applied Technology Council.

Kirkpatrick, P., 1927, "Seismic measurements by the overthrow of columns", *Bulletin of the seismological society of America*, 17 (2):95-109.

Kitayama, S., D. Lee, M. C. Constantinou and K. Kempner Jr., 2017, "Probabilistic seismic assessment of seismically isolated electrical transformers considering vertical isolation and vertical ground motion", *Engineering Structures*, 888–900.

Klaboe, K., S. Pujol and L. Laughery, 2018, "Seismic Response of Rocking Blocks", *Earthquake Spectra*, 1051-1063.

Koh, A., 1986, "Rocking of rigid blocks on randomly shaking foundations", *Nuclear Engineering*, 97, 269–276.

Konstantinidis, D. and N. Makris, 2010, "Experimental and analytical studies on the response of 1/4-scale models of freestanding laboratory equipment subjected to strong earthquake shaking", *Bulletin of Earthquake Engineering*, 8, 1457–1477.

Konstantinidis, D. and N. Makris, 2009, "Experimental and analytical studies on the response of freestanding laboratory equipment to earthquake shaking", *Earthquake Engineering & Structural Dynamics*, 38, 827–848.

Konstantinidis, D., 2008, *Experimental and Analytical Studies on the Seismic Response of Freestanding and Anchored Building Contents*, Berkeley, CA: University of California, Berkeley.

Lin, B. C. and I. Tadjbakhsh, 1986, "Effect of vertical motion on friction-driven isolation systems", *Earthquake Eng. Struct. Dyn.*, 14(4), 609–622.

Linde, S., 2016, *Rocking response of slender free-standing building contents in fixed-base and base-isolated buildings*, Hamilton, ON: McMaster University.

Linde, S., D. Konstantinidis and M. J. Tait, 2020, "Rocking Response of Unanchored Building Contents Considering Horizontal and Vertical Excitation", *J. Struct. Eng.*, 146(9): 04020175.

Makris, N. and D. Konstantinidis, 2001, *The Rocking Spectrum and the Shortcomings of Design Guidelines*, Report No. PEER-01/07 Pacific Earthquake Engineering Research (PEER) Center, University of California, Berkeley, Berkeley, CA.

Makris, N. and D. Konstantinidis, 2003a, "The Rocking Spectrum and the Limitations of Practical Design Methodologies", *Earthquake Engineering and Structural Dynamics*, 32(2): 265-289.

Makris, N. and Y. Roussos, 2000, "Rocking Response of Rigid Blocks under Near Source Ground Motions", *Geotechnique*, 50(3): 243-262.

Makris, N. 2018, "The Dynamics of Rocking Isolation. In: Pitilakis K. (eds) Recent Advances in Earthquake Engineering in Europe. ECEE 2018. Geotechnical", *Geological and Earthquake Engineering*, vol 46. Springer, Cham.

MATLAB, 2002, "High-performance language software for technical computing", *The MathWorks, Inc., Natick.*

MATLAB, 2019, *Version R2019a, The Language of Technical Computing*, Natick, MA: The Mathworks, Inc.

McVitty, W. J. and M. C. Constantinou, 2015, *Propery Modification Factors for Seismic Isolators: Design Guidance for Buildings*, Buffalo, NY: Multidisciplinary Center for Earthquake Engineering Research (MCEER).

Milne, J., 1881, "Experiments in Observational Seismology", *Transactions of the Seismological Society of Japan*, Vol. III., January to December, 12-64.

Milne, J., 1885, "Seismic Experiments", *Transactions of the Seismological Society of Japan*, 1-82.

Miranda, E., G. Mosqueda, R. Retamales and G. Pekcan, 2012, "Performance of nonstructural components during the 27 February 2010 Chile earthquake", *Earthquake Spectra*, 28(S1): S453-S471.

Morgan, T. A. and S. A. Mahin, 2011, *The use of innovative base iso- lation systems to achieve complex seismic performance objectives. Rep. No. PEER-2011/06*, Univ. of California, Berkeley, CA: Pacific Earthquake Engineering Research Center.

Mosqueda, G., A. S. Whittaker and G. L. Fenves, 2004, "Characterization and modeling of friction pendulum bearings subjected to multiple components of excitation", *J. Struct. Eng.*, 130:433-442.

Motosaka, M. and K. Mitsuji, 2012, "Building damage during the 2011 off the Pacific coast of Tohoku Earthquake", *Soils and Foundations*, 52(5), 929-944.

Nagarajaiah, S. and X. Sun, 2000, "Response of base-isolated USC hospital building in Northridge earthquake", *Journal of Structural Engineering (ASCE)*, 126(10):1177–1186.

Nikfar, F. and D. Konstantinidis, 2019, "Experimental study on the seismic response of equipment wheels and casters in base-isolated hospitals", *J. Struct. Eng.*, 145(3): 04019001.

Panchal, V. R., R. S. Jangid, D. P. Soni and B. B. Mistry, 2010, "Response of the double variable frequency pendulum isolator under triaxial ground excitations", *J. Earthquake Eng.*, 14(4), 527–558.

Pantoli, E., M. C. Chen, T. Hutchinson, R. Astroza, J. Conte, H. Ebrahimian, J. Restrepo and X. Wang, 2016b, "Landmark data set from the Building Nonstructural Components and Systems (BNCS) project", *Earthquake Spectra*, 32, 1239–1259.

Pantoli, E., M. C. Chen, X. Wang, R. Astroza, H. Ebrahimian, T. C. Hutchinson, J. Conte, et al., 2016a, "Full-scale structural and nonstructural building system performance during earthquakes: Part II - NCS damage states", *Earthquake Spectra*, 32, 771–794.

PEER, 2021, *Pacific Earthquake Engineering Research Center (PEER) Strong Ground Motion Databases*, https://ngawest2.berkeley.edu/, accessed on January 10, 2021.

Peña, F., F. Prieto, P. Lorenço, A. C. Costa and J. Lemos, 2007, "On the dynamics of rocking motion of single rigid-block structures", *Earthquake Engineering & Structural*, 36, 2382–2399.

Perry, J., 1881, "Note on the Rocking of a Column", *Transactions of the Seismological Society of Japan*, Vol. III., January to December, 103-106.

Phipps, M., 1997, *The impact of nonstructural damage on building performance: reflections on the 1994 Northridge earthquake*, University of California, Berkeley, California: Report UCB/EERC- 97/05, The EERC-CUREE Symposium in Honor of Vitelmo V. Bertero, Earthquake Engineering Research Center.

Politopoulos, I. and N. Moussallam, 2012, "Horizontal floor response spectra of base-isolated buildings due to vertical excitation", *Earthquake Eng. Struct. Dyn.*, 41(3), 587–592.

Priestley, M .J., R. J. Evison and A. J. Carr, 1978, "Seismic response of structures free to rock on their foundations", *Bulletin of the New Zealand National Society for Earthquake Engineering*, 11(3), 141–150.

Psycharis, I. N. and P. C. Jennings, 1983, "Rocking of slender rigid bodies allowed to uplift", *Earthquake Engineering & Structural Dynamics*, 11(1), 57–76.

Reitherman, R. and T. Sabol, 1995, "Northridge earthquake of January 17, 1994: reconnaissance report -nonstructural damage", *Earthquake Spectra, EERI*, 453-514.

Roussis, P., E. Pavlou and E. Pisiara, 2008, "Base Isolation technology for earthquake protection of art objects", *The 14th World Conference on Earthquake Engineering*, Beijing, China.

Ryan, K. and J. Polanco, 2008, "Problems with Rayleigh damping in base-isolated buildings", *J. Struct. Eng. 134*, 134 (11): 1780–1784.

Ryan, K. L., C. B. Coria and N. D. Dao, 2013, *Large Scale Earthquake Simulation of a Hybrid Lead Rubber Isolation System Designed under Nuclear Seismicity Considerations, Report No. CCEER-13-09*, University of Nevada, Reno, Nevada: Center for Civil Engineering Earthquake Research, Department of Civil and Environmental Engineering.

Ryan, K. L, N. D. Dao, E. Sato, T. Sasaki and T. Okazaki, 2012, "Aspects of isolation device behavior observed from full-scale testing of an isolated building at E-Defense", *Proc., ASCE Structures Congress, 20th Analysis and Computation Specialty Track*, Reston, VA: American Society of Civil Engineers.

Ryan, K. L., S. Soroushian, M. Maragakis, E. Sato, T. Sasaki and T. Okazak, 2016, "Seismic Simulation of an Integrated Ceiling-Partition Wall-Piping System at E-Defense. I: Three-Dimensional Structural Response and Base Isolation", *J. Struct. Eng.* (J. Struct. Eng.), 142 (2): 04015130.

Ryan, K. L. and N. D. Dao, 2015, "Influence of vertical ground shaking on horizontal response of seismically isolated buildings with friction bearings", *Journal of Structural Engineering*, 142(1), 04015089.

SAP2000, 2021, *SAP2000 Integrated Software for Structural Analysis and Design Version 20.2.0.* Berkeley, California: Computers & Structures, Inc.

Sarlis, A. A. and M. C. Constantinou, 2010, *Modeling of Triple Friction Pendulum Isolators in Program SAP2000, Supplement to MCEER Report 05-009*, University at Buffalo,

Buffalo, NY: Multidisciplinary Center for Earthquake Engineering Research (MCEER).

Sarlis, A. A. and M. C. Constantinou, 2010, *Modeling triple friction pendulum isolators in program SAP2000*, Buffalo, NY.

Sarlis, A. A., M. C. Constantinou and A. Reinhorn, 2013, *Shake table testing of triple friction pendulum isolators under extreme conditions MCEER-13-0011*, Buffalo, NY: Multidisciplinary Center for Earthquake Engineering Research.

Sato, E., S. Furukawa, A. Kakehi and M. Nakashima, 2011, "Full-scale shaking table test for examination of safety and functionality of base-isolated medical facilities", *Earthquake Engng Struct. Dyn*, 40:1435–1453.

Scheller, J. and M. C. Constantinous, 1999, *Response history analysis of structures with seismic isolation and energy dissipation systems: Verification examples for program SAP2000*, University at Buffalo, State University of New York School of Civil, Structural and Environmental Engineering, Buffalo, New York: Multidisciplinary Center for Earthquake Engineering Research (MCEER).

Shakib, H. and A. Fuladgar, 2003, "Effect of vertical component of earthquake on the response of pure-friction base-isolated asymmetric buildings", *Eng. Struct.*, 25(14), 1841–1850.

Shenton, H.W. III., 1996, "Criteria for Initiation of Slide, Rock, and Slide-Rock Rigid-Body Modes", *Journal of Engineering Mechanics (ASCE)*, 122(7): 690-693.

Skinner, R. I., W. H. Robinson and G. H. McVerry, 1993, *An Introduction to Seismic Isolation*, NY, USA: John Wiley & Sons Inc.

Soong, T., 1990, "Seismic performance of nonstructural elements during the Loma Prieta earthquake", *Report NIST SP 796, Proceedings of the 22nd Joint Meeting U.S.-Japan Cooperative Program in Natural Resources Panel on Wind and Seismic Effects*, Gaithersburg, Maryland: National Institute of Standards and Technology. 331-336.

Soong, T. T., G. Chen, Z. Wu, R. Zhang and M. Grigoriu, 1993, *Assessment of the 1991 NEHRP provisions for nonstructural components and recommended revisions*,

Buffalo, N.Y.: Report NCEER-93-0003, National Center for Earthquake Engineering Research.

Soroushian, S., K. L. Ryan, M. Maragakis, E. Sato, T. Sasaki, T. Okazaki, L. Tedesco, A. E. Zaghi, G. Mosqueda and A. Dennis, 2012, "Seismic Response of Ceiling/Sprinkler Piping Nonstructural Systems in NEES TIPS/NEES Nonstructural/NIED Collaborative Tests on a Full Scale 5-Story Building", *In: Proceedings of the 2012 ASCE Structures Congress*, p. 1315–1326.

Taghavi, S. and E. Miranda, 2003, *Response assessment of nonstrucutral building elements*, PEER Report 2003/05, Berkeley, CA: Pasific Earthquake Engineering Research Center.

TBSC, 2018, *Turkish Building Seismic Code*, Ankara: Disaster and Emergency Management Presidency.

TS498, 1997, *Design Loads for Buildings*, Ankara: Turkish Standards Institute.

TS500, 2000, *Turkish Standards Institute, Requirements for Design and Construction of Reinforced Concrete Structures*, Ankara: Turkish Standards Institute.

Vassiliou, M., R. Truniger and B. Stojadinovic, 2015, "An analytical model of a deformable cantilever structure rocking on a rigid surface: Development and verification", *Earthquake Engineering and Structural Dynamics*, 44, 2775–2794.

Vassiliou, M. and N. Makris, 2012, "Analysis of the rocking response of rigid blocks standing free on a seismically isolated base", *Earthquake Engineering and Structural Dynamics*, 41: 177–196.

Wilson, E., 2004, *Static and Dynamic Analysis of Structures*, Berkeley, CA: Computers and Structures Inc.

Wong, M. and W. Tso, 1989, "Steady state rocking response of rigid blocks. Part 2: Experiment", *Earthquake Engineering & Structural Dynamics*, 18, 107–120.

Yim, S. C. S., A. K. Chopra and J. Penzien, 1980, "Rocking Response of Rigid Blocks to Earthquakes", *Earthquake Engineering and Structural Dynamics*, 8(6): 565-587.

Zayas, V., S. Low and S. Mahin, 1987, *The FPS Earthquake Resisting System, Technical Report UCB/EERC-87/01*, CA, USA: Earthquake Engineering Research Center, University of California, Berkeley.

Zayas, V. A., S. S. Low and S. A. Mahin, 1987, *The FPS earthquake resisting system. Rep. No. UCB/EERC-87/01*, Univ. of California, Berkeley, CA: Earthquake Engineering Research Center.

Zhang, J. and N. Makris 2001, "Rocking Response of Free-Standing Blocks under Cycloidal Pulses", *Journal of Engineering Mechanics (ASCE)*, 127(5): 473-483.

APPENDIX A:

Table A.1. Ground motions for scaling according to TBSC (2018)

No.	Year	Earthquake Name	Station	Magnitude	R_{jb} (km)	V_{s30} (m/s)	Scale Factor
1	1999	Kocaeli	Iznik	7.51	30.73	476.62	2.8
2	1999	Duzce	Mudurnu	7.14	34.3	535.24	5.9
3	1999	Hector Mine	Amboy	7.13	41.81	382.93	2.73
4	1999	Hector Mine	Joshua Tree	7.13	31.06	379.32	3.9
5	1999	Hector Mine	Morongo Valley Fire Station	7.13	53.21	396.41	4.12
6	1992	Landers	Forest Falls Post Office	7.28	45.34	436.14	5.6
7	1992	Landers	Morongo Valley Hall (GEOS #58)	7.28	40.67	368.2	4.52
8	1992	Landers	North Palm Springs Fire Sta #36	7.28	26.95	367.84	3.2
9	2010	Darfield	CSHS	7	43.6	638.39	3.9
10	2010	Darfield	OXZ	7	30.63	481.62	5.37
11	2010	Darfield	SPFS	7	29.86	389.54	4.25

APPENDIX B:



Performance of Nonstructural Components during the 27 February 2010 Chile Earthquake

Author:
Eduardo Miranda, Gilberto Mosqueda, Rodrigo Retamales, et al

Publication: Earthquake Spectra

Publisher: SAGE Publications

Date: 06/01/2012

Copyright © 2012, © SAGE Publications

Gratis Reuse

Permission is granted at no cost for use of content in a Master's Thesis and/or Doctoral Dissertation, subject to the following limitations. You may use a single excerpt or up to 3 figures tables. If you use more than those limits, or intend to distribute or sell your Master's Thesis/Doctoral Dissertation to the general public through print or website publication, please return to the previous page and select 'Republish in a Book/Journal' or 'Post on intranet/password-protected website' to complete your request.

APPENDIX C:

JOHN WILEY AND SONS LICENSE TERMS AND CONDITIONS

Jul 03, 2021

This Agreement between Mr. Goktug Tufekci ("You") and John Wiley and Sons ("John Wiley and Sons") consists of your license details and the terms and conditions provided by John Wiley and Sons and Copyright Clearance Center.

License Number	5101531385047
License date	Jul 03, 2021
Licensed Content Publisher	John Wiley and Sons
Licensed Content Publication	Earthquake Engineering and Structural Dynamics
Licensed Content Title	Full-scale shaking table test of a base-isolated medical facility subjected to vertical motions
Licensed Content Author	Masayoshi Nakashima, Tracy Becker, Yundong Shi, et al
Licensed Content Date	May 20, 2013
Licensed Content Volume	42
Licensed Content Issue	13
Licensed Content Pages	19
Type of Use	Dissertation/Thesis
Requestor type	University/Academic
Format	Print and electronic
Portion	Figure/table
Number of figures/tables	2
Will you be translating?	No
Title	Performance of Nonstructural Components in Triple Friction Pendulum Base-isolated Buildings
Institution name	Bogazici University
Expected presentation date	Jul 2021
Portions	Figure 1., Figure 10.
Requestor Location	Mr. Goktug Tufekci Bebek, Besiktas Istanbul, 34342 Turkey Attn: Mr. Goktug Tufekci
Publisher Tax ID	EU826007151
Total	**0.00 USD**
Terms and Conditions	

APPENDIX D:

JOHN WILEY AND SONS LICENSE TERMS AND CONDITIONS

Jul 03, 2021

This Agreement between Mr. Goktug Tufekci ("You") and John Wiley and Sons ("John Wiley and Sons") consists of your license details and the terms and conditions provided by John Wiley and Sons and Copyright Clearance Center.

License Number	5101580560375
License date	Jul 03, 2021
Licensed Content Publisher	John Wiley and Sons
Licensed Content Publication	Earthquake Engineering and Structural Dynamics
Licensed Content Title	Full-scale shaking table test for examination of safety and functionality of base-isolated medical facilities
Licensed Content Author	Eiji Sato, Sachi Furukawa, Atsuo Kakehi, et al
Licensed Content Date	Jan 18, 2011
Licensed Content Pages	10
Type of Use	Dissertation/Thesis
Requestor type	University/Academic
Format	Print and electronic
Portion	Figure/table
Number of figures/tables	1
Will you be translating?	No
Title	Performance of Nonstructural Components in Triple Friction Pendulum Base-isolated Buildings
Institution name	Bogazici University
Expected presentation date	Jul 2021
Portions	Figure 3
Requestor Location	Mr. Goktug Tufekci Bebek, Besiktas Istanbul, 34342 Turkey Attn: Mr. Goktug Tufekci
Publisher Tax ID	EU826007151
Total	**0.00 USD**
Terms and Conditions	

APPENDIX E:



Full-Scale Structural and Nonstructural Building System Performance during Earthquakes: Part I – Specimen Description, Test Protocol, and Structural Response

Author: Michelle C. Chen, Elide Pantoli, Xiang Wang, et al

Publication: Earthquake Spectra

Publisher: SAGE Publications

Date: 05/01/2016

Copyright © 2016, © SAGE Publications

Gratis Reuse

Permission is granted at no cost for use of content in a Master's Thesis and/or Doctoral Dissertation, subject to the following limitations. You may use a single excerpt or up to 3 figures tables. If you use more than those limits, or intend to distribute or sell your Master's Thesis/Doctoral Dissertation to the general public through print or website publication, please return to the previous page and select 'Republish in a Book/Journal' or 'Post on intranet/password-protected website' to complete your request.

APPENDIX F:

SAGE Publishing

Full-Scale Structural and Nonstructural Building System Performance during Earthquakes: Part II – NCS Damage States

Author: Elide Pantoli, Michelle C. Chen, Xiang Wang, et al

Publication: Earthquake Spectra

Publisher: SAGE Publications

Date: 05/01/2016

Copyright © 2016, © SAGE Publications

Gratis Reuse

Permission is granted at no cost for use of content in a Master's Thesis and/or Doctoral Dissertation, subject to the following limitations. You may use a single excerpt or up to 3 figures tables. If you use more than those limits, or intend to distribute or sell your Master's Thesis/Doctoral Dissertation to the general public through print or website publication, please return to the previous page and select 'Republish in a Book/Journal' or 'Post on intranet/password-protected website' to complete your request.